Spring 2021

Computational intelligent impact force modeling and monitoring in HISLO conditions for maximizing surface mining efficiency, safety, and health

Danish Ali

Department: Mining Engineering

COMPUTATIONAL INTELLIGENT IMPACT FORCE MODELING AND MONITORING IN HISLO CONDITIONS FOR MAXIMIZING SURFACE MINING EFFICIENCY, SAFETY, AND HEALTH

by

DANISH ALI

A DISSERTATION

Presented to the Faculty of the Graduate School of the

MISSOURI UNIVERSITY OF SCIENCE AND TECHNOLOGY

In Partial Fulfillment of the Requirements for the Degree

DOCTOR OF PHILOSOPHY

in

MINING ENGINEERING

2021

Approved by:

Dr. Samuel Frimpong, Advisor
Dr. Lana Z. Alagha
Dr. Grzegorz Galecki
Dr. K. Chandrashekhara
Dr. Sanjay Madria

ABSTRACT

Shovel-truck systems are the most widely employed excavation and material handling systems for surface mining operations. During this process, a high-impact shovel loading operation (HISLO) produces large forces that cause extreme whole body vibrations (WBV) that can severely affect the safety and health of haul truck operators. Previously developed solutions have failed to produce satisfactory results as the vibrations at the truck operator seat still exceed the "Extremely Uncomfortable Limits". This study was a novel effort in developing deep learning-based solution to the HISLO problem.

This research study developed a rigorous mathematical model and a 3D virtual simulation model to capture the dynamic impact force for a multi-pass shovel loading operation. The research further involved the application of artificial intelligence and machine learning for implementing the impact force detection in real time.

Experimental results showed the impact force magnitudes of 571 kN and 422 kN, for the first and second shovel pass, respectively, through an accurate representation of HISLO with continuous flow modelling using FEA-DEM coupled methodology. The novel 'DeepImpact' model, showed an exceptional performance, giving an R^2, RMSE, and MAE values of 0.9948, 10.750, and 6.33, respectively, during the model validation.

This research was a pioneering effort for advancing knowledge and frontiers in addressing the WBV challenges in deploying heavy mining machinery in safe and healthy large surface mining environments. The smart and intelligent real-time monitoring system from this study, along with process optimization, minimizes the impact force on truck surface, which in turn reduces the level of vibration on the operator, thus leading to a safer and healthier working mining environments.

ACKNOWLEDGMENTS

I am thankful to my advisor, Dr. Samuel Frimpong, for his help, inspiration, guidance, and encouragement throughout the course of this work.

I also appreciate the guidance and encouragement of my advisory committee members. Their contributions have improved my work. My gratitude also goes to Ms. Tina Alobaidan and Ms. Judy Russell, and Mr. Stephen Casey for their assistance. I thank Sharon Matson, my Graduate Advisor, for her assistance. I would also like to mention my friends Atta-ur-Rehman, Bruno Kansake, Bharath Ballamudi, Ashraf Alsafasfeh, Rasaan Syed, Mohammad Roman, Waqas-ur-Rehman, Muhammad Waqas, and Badar Hayat for their encouragement and assistance.

I am indebted to my parents, Waqar Ali and Mehreen Chaudhary, for their prayers, guidance, and an endless support throughout my life. I am also grateful to the love of my life Fatima Sajjad, for her patience, support, and encouragement throughout this endeavor, and for being always there for me.

I am thankful to my sister and my brother for their endless support during my academic pursuit.

TABLE OF CONTENTS

Page

LIST OF FIGURES

Page

LIST OF TABLES

Page

NOMENCLATURE

Symbol	Description
g	Acceleration due to gravity (m/s^2)
H	Heaviside step function
H_t	Dumping distance (Distance b/w truck body surface and tip of the shovel dipper door as the material is released for dumping into the truck) (m)
ϵ	Time for which the impulse acts (sec)
M + 1	No. of sub-passes in which a particular shovel ore-pass is divided
a	Time at which shovel starts dumping
m_1	Mass of the rock/soil material (kg)
m_2	Mass of the truck body (kg)
m_3	Mass of the chassis (kg)
m_4	Mass of the front tire assembly (kg)
m_5	Mass of the rear tire assembly (kg)
C_1	Damping coefficient of the rock/soil material (Ns/m)
C_2	Damping coefficient of the truck body (Ns/m)
C_{3f}	Damping coefficient for the front tire and sprung mass connectivity (Ns/m)
C_{3r}	Damping coefficient for the rear tire and sprung mass connectivity (Ns/m)
C_4	Damping coefficient for the front tire and ground surface connectivity (Ns/m)
C_5	Damping coefficient for the rear tire and ground surface connectivity (Ns/m)
K_1	Stiffness constant of the rock/soil material (N/m)

K_2	Stiffness constant of the truck body (N/m)
K_{3f}	Stiffness constant for the front tire and sprung mass connectivity (N/m)
K_{3r}	Stiffness constant for the rear tire and sprung mass connectivity (N/m)
K_4	Stiffness constant for the front tire and ground surface connectivity (N/m)
K_5	Stiffness constant for the rear tire and ground surface connectivity (N/m)
A	Distance from body connection location to the center of mass of the chassis
B	Distance from front suspension system to the center of mass of the chassis
D	Distance from rear suspension system to the center of mass of the chassis
t	Time component (sec)
$\theta(t)$	Pitch angle for chassis
T	Kinetic Energy of the HISLO Vibration System
V	Potential/Strain Energy of the HISLO Vibration System
R	Dissipation Energy of the HISLO Vibration System
$z_i(t)$	Displacement of ith component of the system where i = 1..5
$F_i(t)$	External force acting on the ith component of the system where i = 1..6
$\vec{M}$	Mass matrix for the complete system (6 x 6)
$\vec{C}$	Damping matrix for the complete system (6 x 6)
$\vec{K}$	Stiffness matrix for the complete system (6 x 6)
$\vec{P}$	Mass modal matrix for the complete system (6 x 6)
$q_i(t)$	Modal participation coefficient for ith component of the system where i = 1..6
$\vec{u}_i(t)$	Normal mode for the ith component of the system where i = 1..6
ω_{ni}	Natural frequency of ith component of the system where i = 1..6

ω_{di}	Damped natural frequency of ith component of the system where i = 1..6
ζ_i	Damping ratio of ith component of the system where i = 1..6
α, β	Rayleigh model's damping coefficients
$F_{TB}(t)$	Resulting force on truck body surface due to shovel material dumping
I	Area moment of inertia for the chassis (m^4)

1. INTRODUCTION

1.1. BACKGROUND OF THE RESEARCH PROBLEM

Surface mining operations account for the extraction of almost 97% of non-fuel minerals and 66% of coal production [1, 2]. The shovel-truck system (in Figure 1.1) is the most flexible, economic, and productive method for surface mining operations, over the years, resulting from technological advances. For any shovel-truck system in surface mining operations, truck loading and haulage are two main operations that affect the overall mine productivity. Therefore, it is imperative that these operations are efficient, effective, safe, and economic.

Studies have shown that there is a quadruple increase in productivity for a 380-ton dump truck, compared with the productivity of a 120-ton truck [3]. Thus, one can easily achieve higher economic advantages by matching ultra-large shovels with ultra-large dump trucks. The ultra-large shovels load these dump trucks with over 100-ton passes under gravity, creating large impact forces and high frequency shockwaves. This phenomenon is termed high impact shovel loading operations (HISLO), which ultimately causes the high frequency shockwaves. The shockwaves propagate through the truck body and chassis to the operator's cabin and seat, thus exposing their feet, legs, lower back, hands, spine, and neck to these high frequency shockwaves. The combined effect of this experience and exposure is termed as whole-body vibrations (WBV) phenomenon.

The WBV levels, in excess of the 'Extremely Uncomfortable' limits, under ISO standards [4], have severe impacts on the operator's health and safety, especially long-term lower-back problems and other musculoskeletal diseases [5]. Previous research has developed limited solutions to WBV problems associated with these ultra-large machines

[6–10]. Thus, advanced research is required to address fundamental challenges in this research space. The scope of the existing research is mostly limited to relatively small equipment units in industries, such as agriculture, military, aerospace, commercial transport, and automotive [11–17]. This research was a pioneering effort to provide solutions to the WBV problems under HISLO conditions, and to provide safe and healthy environments for truck operators in surface mining operations.

1.2. STATEMENT OF THE RESEARCH PROBLEM

Haul trucks contribute significantly to injuries and accidents in surface mining operations. According to MSHA, out of 250 fatalities that occurred from 1990 to 2001 in surface mining, 40% were attributed to powered haulage. An average of 675 accidents and 21 powered haulage fatalities occur each year in surface mining, and 20% of these injuries and fatalities involve dump trucks [18]. Approximately 46.3 % of accidents involving haul truck occur during operations, and 37.7% of these accidents are due to jarring, which causes operator back injuries [19]. Based on 2000 and 2007 data, Ruff et al. [20] show that 33% of the most severe equipment accidents in mines are from dump trucks, and 44% of fatal accidents in surface mines among mobile machines are caused by dump trucks. According to a 2019 MSHA report, 39.5% of powered haulage accidents involved dump trucks resulting in severe injuries to operators [21]. Therefore, there was a strong need for advanced research initiatives that provide the basis for technological innovations and improvements in truck technology for controlling injuries and ensuring safe operations.

Figure 1.1. High Impact Shovel Loading Operations (HISLO) in Surface Mining [8]

The International Standards Organization (ISO) has provided the recommendations on safe limits, beyond which long-term exposure could cause severe lower-back, neck, and other physical disorders and disabilities. The applicable ISO standards in vehicular vibrations include Sections 1, 2, 4 and 5 of ISO 2631 [4, 5, 22, 23]. These sections provide specific threshold limits in order to comply with the safe standards for any vibrating equipment. Table 1.1 shows the WBV levels and their corresponding effects on operators during an 8-hour interval. Whenever operators are exposed to WBV (RMS) levels equal or in excess of 1 m/sec^2, during an 8-hour duration, they become vulnerable to experiencing sacrum, lumbar, and cervical problems [5].

Even though Aouad and Frimpong [24] have characterized the types of vibrations generated in ultra-large mining trucks, there was still a lack of insight into controlling the impact of these vibrations.

Table 1.1. Expected Comfort Zones to Vibration [4]

Acceleration Value (RMS)	**Comfort Zone**
Less than 0.315 m/sec^2	Not Uncomfortable
0.315 – 0.63 m/sec^2	A little Uncomfortable
0.5 – 1 m/sec^2	Fairly Uncomfortable
0.8 – 1.6 m/sec^2	Uncomfortable
1.25 – 2.5 m/sec^2	Very Uncomfortable
Greater than 2 m/sec^2	Extremely Uncomfortable

Considering that a dump truck is stationary and the excitation force introduced by the material being dumped into the truck body is dynamic, the WBV phenomenon under HISLO conditions, is different from those in military applications from Friedmann [12], Moses [16], Cowings et al. [25], Wickramasinghe et al. [15], Rozali et al. [26], Khan et al. [27], and Ha et al. [28]. Since HISLO vibrations are forced vibrations, they are induced from the generated impact force as materials fall from the dipper or bucket of a large-capacity shovel from a specific dumping height into the dump truck. The main determining factors of the dynamic impact force include the mass of the falling material (which also depends on density, porosity, moisture content, angle of repose, cohesion, and shovel dipper size), the dumping characteristics (including height/distance of dumping, the time which the material takes during dumping, and the shovel dumping/loading mechanism), the truck body material characteristics (stiffness and damping of the truck parts), and environmental factors (including terrain conditions and space limitations) [6]. Since the

dynamic impact force is the main cause of the HISLO vibration problem, it is extremely crucial that such force is modeled with utmost precision.

A thorough literature survey has been conducted for evaluating the contributions to the body of knowledge regarding impact force modeling. Iverson [29] and Metz [30] used impact testing or virtual simulation experiments to determine the impact force on a single body. Neither of the aforementioned researchers focused on determining the impact force generated by material flowing under gravity. Aouad and Frimpong [24] provided the very first mathematical model for the impact force generated by the soil or broken rock material flowing under gravity, given by equation (1.1). However, the model lacked critical parameters, over which the impact force in HISLO should depend, including height of dumping. During any shovel loading operation in surface mining, the dumping height is defined as the distance between the floor of the truck bowl and the lowest tip of the shovel dipper door. The model also did not consider the impact duration, which is defined as the time the material remains in contact initially. The impact forces generated in the model by Aouad and Frimpong [24] were greatly overestimated because the soil/rock material was always calculated with the assumption that the material was dumped all at once. In reality, the material is generally well fragmented either during the direct shovel excavation or due to pre-fragmentation by drilling and blasting in hard rock materials. In such cases, the material consists of small size particles, and it is dumped into the truck with only a small portion making initial contact, followed by a series of chunk of dumped material. This means the material remains in contact for a limited time, and does not hit the truck bed surface all at once.

Latter, Ali and Frimpong [9], provided a more comprehensive and realistic mathematical model for capturing the impact force during shovel loading operation, given by equation (1.2). However, this model also lacks essential parameters underlying the impact force in a HISLO scenario, including truck body material characteristics. The model was limited due to the single shovel pass limitation.

Typically, a shovel in any surface mining operation fully loads a dump truck using 3 or 4 passes. In order to execute the second pass, the shovel swings back, digs, and dumps another 100 tons of material into the dump truck. The impact force for subsequent passes is reduced because of the 'cushioning effect' provided by the previously dumped material. Any useful mathematical model that captures the dynamic impact force must consider this cushioning effect.

Previous studies have assumed the impact force from the second shovel pass is equivalent to the first shovel pass [24]. Few studies have conducted vibration analysis for evaluating the operator health risk using only the first shovel pass [31], thus rendering the analysis and the work limited in its scope and application. This research formulated a more comprehensive, realistic, and generalized dynamic impact force under HISLO conditions.

Moreover, the structural material, through which the high frequency shockwaves propagate, has a very important role in determining the magnitude of vibration and selection of the component of vibration for effective transference. In HISLO, the impact force due to dumping material under gravity produces high frequency shockwaves that pass through the truck body and expose the operator to whole body vibrations (WBV). Therefore, the material characteristic of truck body should be considered in modelling the impact force for accurate response of the truck body to impact excitation.

Since the external impact force is the major cause of WBV, research has demonstrated that the impact force can be reduced by 17.34% for the first shovel pass. According to Ali and Frimpong [6], the resulting vibration levels at the operator seat are reduced by 19.61% [8]. The solution framework provided by Ali and Frimpong [6] reduces the vibrations levels at the operator seat from 3.56 m/s^2 to 2.86 m/s^2. According to the specified ISO safety limits, this value still exceeds the maximum limit of the 'Extremely Uncomfortable Zone', which can still cause permanent and life threatening injuries to operators. Advanced research initiatives were thus required to provide solutions to the HISLO problems and their impact on operator safety and health.

A 3D virtual simulation of the shovel dumping process, using Finite Element Analysis - Discrete Element Method (FEA-DEM) technique in ABAQUS, was used to improve multi-shovel-pass impact force mathematical model. It also tested the viability of the WBV solutions with continuous flow modelling of rock/soil material. The virtual FEA-DEM simulator considered the cushioning effect in subsequent passes. It also considered the effect of truck material characteristics on the impact force generation and high frequency shockwaves progression. The virtual simulator examined the impact force generation and progression within the modified model to provide a comprehensive solution to the WBV problem.

This research also applied artificial intelligence and machine learning to implement the impact force detection in real time. The research developed a smart modelling algorithm to receive information using perceptrons to predict the resulting impact force before every shovel pass. The mathematical models and offline simulation system require significant computational time, specialized software platform, and a certain level of

expertise, which can be extremely difficult on any mine site. The novel intelligence-based system allowed an operator to examine the impact forces and the resulting vibration levels even before the shovel has dumped the material in the truck bowl. The system also predicted the optimum height for shovels to dump materials into the truck to minimize the impact force for HISLO conditions. This artificial intelligence system further assists the shovel operators during the shovel dumping process and improve the overall efficiency of the system along with the health and safety of the mine site.

$$F_1(t) = \begin{cases} F_0 \int_0^{\infty} \delta(t - t_0)dt & \forall t = t_0 \\ 0 & \forall t \neq t_0 \end{cases} \tag{1.1}$$

$$\begin{aligned} F(t) = \frac{\sqrt{2gH_t}\, m}{\epsilon^2 (M+1)} \sum_{j=0}^{M} \Bigg[& 2\left(t - \left(j\left(\frac{\epsilon}{a}\right)a\right)\right) H\left(t - \left(j\left(\frac{\epsilon}{a}\right)a\right)\right) \\ & - 4\left(t - \left(j\left(\frac{\epsilon}{a}\right)a\right) - \frac{\epsilon}{2}\right) H\left(t - \left(j\left(\frac{\epsilon}{a}\right)a\right) - \frac{\epsilon}{2}\right) \\ & + 2\left(t - \left(j\left(\frac{\epsilon}{a}\right)a\right) - \epsilon\right) H\left(t - \left(j\left(\frac{\epsilon}{a}\right)a\right) - \epsilon\right) \Bigg] \end{aligned} \tag{1.2}$$

1.3. OBJECTIVE AND SCOPE OF WORK

The primary research objective was to provide safe and healthy working environments by reducing the dynamic impact force through continuous dumping process

and intelligent monitoring of dump height reduction and dipper-truck interactions. The elements for this primary objective include:

(i) developing a rigorous, continuous shovel material dumping system;

(ii) simulating a virtual prototype of the HILSO process to optimize the dynamic impulse force;

(iii) modelling the cushioning effect during the subsequent passes;

(iv) verifying the model results by comparing the results from the simulation and the mathematical model;

(v) running detailed experiments using the verified model for varying operating conditions and material properties;

(vi) investigating and exploring the forces/stresses generation on truck bed surface with proper continuous flow modeling for the shovel dumping process; and

(vii) developing a methodology for real-time implementation of impact force monitoring system using artificial intelligence and machine learning algorithms.

This study has formulated a generalized impulse force model for the HILSO process. A practical solution to the WBV problem using a continuous flow modelling technique was developed. It created a 3D virtual simulation model for the HISLO dumping process for process optimization. The effectiveness, applicability and viability of the continuous flow model was also examined via virtual simulation in DEM-FEA integrated platform within ABAQUS. The virtual simulator tested the efficiency, effectiveness, and accuracy of the new mathematical model. Detailed experimentation was conducted to investigate the impact force dynamics under varying operating conditions and material properties. A framework for real-time implementation of impact force monitoring was

developed using AI and machine learning for any shovel-truck system under HISLO conditions. The generic intelligent algorithm, using state-of-the-art artificial neural deep learning algorithm, is applicable to any ultra-large dump truck, matched with any ultra-large shovel, in any surface mining operation around the globe.

1.4. PROPOSED RESEARCH METHODOLOGY

This research developed an analogic mathematical model of the system to demonstrate the concept of material flow under gravity. The model yielded the impulse force resulting from the HISLO process for any number of shovel passes. An impulse force model was developed using truck responses from Lagrangian mechanics.

A 3D virtual simulation model was designed to simulate the HISLO process. This process simulated the P&H 4100XPC shovel loading the CAT 793D dump truck with 100-ton material passes, within a DEM-FEA integrated platform in ABAQUS. The study verified the 3D simulation model to ensure accuracy and validity of the model using real-world data. The study used the validated model to examine the impact force generation and progression for any HISLO process. The cushioning effect and continuous material flow were modeled and examined, which will intuitively reduce the impulse force at the truck bed surface. The study then provided a rationale for studying the effects of impulse force.

Deep learning (DL) algorithm was used to develop an intelligence-based framework for real-time implementation of the impact force monitoring system. Detailed experiments were designed and conducted using the validated mathematical and simulation models for different material types with regard to varying operating conditions during HILSO processes. The results were used to train the AI model using the deep learning algorithm, and optimizing the architecture and the hyper-parameters. Model evaluation

first involved testing the final architecture using the held-out testing experimental dataset. The second phase involved the process of evaluating the model performance against other machine learning algorithms to ensure state-of-the-art performance. The final optimized deep learning architecture was then used to develop the final model for monitoring the impact force in real-time and to optimize the HISLO process for any shovel-truck system to maximize workplace safety and health.

1.5. ORIGINALITY OF THE PHD RESEARCH

This research was a pioneering effort towards improving the existing knowledge and frontier advances for shovel dumping operations. The study developed a comprehensive model for dynamic impact force generation and progression during any HISLO process. The study also developed a novel algorithm and framework to address the WBV problem under HISLO conditions and addressed the real-time HISLO process observation and optimization problems to provide safe and healthy environments for the shovel-truck method in surface mining operations.

This study provided new data and strides for developing robust mathematical models for capturing the dynamic impact force HISLO process for any shovel pass for dumping materials into trucks. The study included novel models that considered the cushioning effect from previous passes. This study also advanced original and practical solutions to the existing WBV problem, under HISLO conditions, within varying operating conditions and material properties. The research also pioneered the development of real-time intelligent system for monitoring the dynamic impact force and optimizing the dumping process for solving the WBV problem. The solution to this problem addresses a

monumental challenge in the use of heavy mining machinery for achieving economic bulk production in surface mining operations.

1.6. EXPECTED RESEARCH CONTRIBUTIONS

This research aimed to advance knowledge and frontiers in HISLO, whole body vibration exposure and their impact on haul truck operators along with efficiency and effectiveness of shovel loading operations. In particular, the expected contributions from this research include:

- Scientific progress and deeper understanding of the dynamic impulse force for multiple shovel passes in HISLO process;
- Mathematical formulation for characterizing and optimizing the shovel dumping process;
- A practical and effective solution to the WBV problem during HISLO;
- Minimizing and possibly eliminating the impact of WBV exposures on dump truck operators under HISLO conditions;
- Providing a means for operators to monitor the impact force and the resulting vibrations along with modifying the shovel dumping process by optimizing the dumping height to minimize the impact force in real-time for each shovel pass;
- Developing an intelligent algorithm for automated impact force monitoring;
- Implementing AI based system for smart real-time monitoring of impact force for every shovel pass and optimizing the dumping operation; and
- Improving workplace safety, health and the efficiency and effectiveness economic bulk production capacities in surface mining operations.

1.7. STRUCTURE OF THE PHD DISSERTATION

A nomenclature section provides the definitions and explanations of variables and acronyms used in this research study. Section 1 contains an introduction to the PhD dissertation. The introduction lays the foundation for the study by discussing the HISLO vibration problems in large scale surface mining operations, followed by the objectives and scope of the study, the proposed research methodology. The introduction also discusses the novelty of the study and its contribution to the industry and to the body of knowledge. Section 2 provides a thorough review and analysis of all the relevant literature and shows the progression of knowledge, contributions by researchers and limitations of the current studies. Section 3 contains detailed procedural information for the development of the mathematical model to capture the dynamic impact force during a multi-pass shovel loading operation. Section 4 presents the detailed 3D virtual prototype model along with the complete simulation design procedure in ABAQUS. Section 5 provides detailed experimental design set up and procedures to investigate the impact force dynamics under varying operating conditions and material properties. Section 6 presents the detailed procedures adopted for the data transformation and intelligence-based framework for real-time implementation of the impact force monitoring using AI and machine learning algorithm. Section 7 presents the experimental, virtual prototype simulation and AI model results with detailed discussions. Section 8 summarizes the findings, presents the conclusions, provides contributions for this PhD research, and makes recommendations for future research. All the references used as bases for carrying out this research study are listed under the reference section.

2. LITERATURE REVIEW

A comprehensive review of the relevant literature examined the current body of knowledge, contributions from researchers and the outstanding problems within the research frontier. It covered the significant work done in the field of machine vibration, whole body vibration (WBV), impact force modelling, material dynamic simulation, discrete element analysis, artificial intelligence, and machine learning for smart operations.

2.1. WBV CHARACTERIZATION, INVESTIGATION, AND CONTROL

Two of the main components for any shovel-truck operation include truck loading and haulage. Efficiency and effectiveness of the operations along with operators' health and safety are the most important considerations for both operations. During shovel loading operations, ultra-large shovels load ultra-large trucks with over 100-ton passes under gravity, creating large impact forces and high frequency shockwaves. The shockwaves generated, under HISLO conditions, propagate through the truck body, chassis and to the cabin and the seat of the operator, thus exposing the operator's feet, legs, lower back, hands, spine, and neck to these high frequency shockwaves. This experience and exposure is termed as the WBV phenomenon.

In earth moving operations, WBV has a significant impact on human health. Adlinger et al. [19] conducted a study on surface coal mining accidents and found out that equipment operation was the most common category of accident for haulage truck (46.3%) and jarring is the most common type of equipment operation accidents (about 37.7%), which results in operator back injuries. Given the vibration problems and their effects on

human operators, research must provide solutions to control and minimize the impact of vibrations to improve the health and safety of heavy earthmoving equipment operators.

A truck operator can experience vibrations through jolting and jarring while being loaded by a shovel, driving truck over obstacles or unintentionally striking a berm on haul roads. Miller et al. [32] devised a method for installing "black boxes" called Shox Boxes onboard equipment that already has a GPS system onboard for assessing jolting and their root causes. That Shox Box system reviews data in real-time and sends pertinent information via radio to a central database. The Shox Box prototype was developed in a surface mining environment and it is a useful tool for assessing and recommending proactive actions towards maintaining jolting within an acceptable range.

Kittusamy [33] investigated the vibration exposure at the seat/operator interface, transmissibility of vibration in z-axis, and the psychological ratings of vibration discomfort level and evaluated the postural requirements of the job. A tri-axial piezo-resistive seat pad accelerometer (Model VT-3) and a single axis piezo-resistive accelerometer (Model 7265A-HS) were used to assess WBV at the seat/operator interface and at the floor level, respectively. The results from that study revealed that the operators were exposed to WBV levels significantly above the allowable limits established by the European Commission. The study recommended that the design of the seats should be such that the vibrations at the lower frequencies (1 – 8 Hz) are attenuated appropriately. Kittusamy [34] further extended the research and formulated a checklist to evaluate the cab design of heavy construction equipment. Different loaders and excavators were evaluated using the formulated checklist and it was found that majority of the vibration could be felt through

the floor and at the seats. Therefore, these heavy equipment units do contribute to high WBV levels that could cause musculoskeletal symptoms and injuries among the operators.

Kittusamy et al. [35] conducted a study to compare the NIOSH seat design with a design that was already in existence on underground haulage vehicles. Accelerometers gathered objective data and a visual analog scale (VAS) and a questionnaire gathered subjective data. Based on the results, the researchers concluded that the NIOSH seat design was better in providing comfort and reducing vibration as compared to the existing seat design. Kittusamy [36] also conducted a study using a questionnaire to assess demographics, work information, job history, and musculoskeletal symptoms in operators of heavy earthmoving equipment. The study focused on the neck, middle/upper back, lower back, shoulder and upper-arm, elbow and forearm, wrist and hand, hip, knee, and ankle and foot areas. The results indicated that the workers were at risk for developing musculoskeletal disorders. Furthermore, Kittusamy et al. [37] conducted a study to determine the effectiveness of a continuous passive lumbar motion system in reducing lower back discomfort among operators of heavy earthmoving equipment. The results indicated that the use of a continuous passive lumbar motion system could effectively reduce the low back discomfort, normally experienced by heavy earthmoving equipment operators.

Eger et al. [38], during the small and large load haul dump (LHD) vehicles operation, measured WBV exposures at the vehicle and operator seat interfaces. They used tri-axial seat-pad and tri-axial accelerometers mounted with a large magnet, respectively, to measure WBV exposures at the seat pad/operator interface and vehicle floor/seat base interface. They compared the results from those tests to the ISO 2631-1 health caution

zones in order to determine safe exposure durations. Those results indicated that LHD operators were exposed to WBV levels, which exceeded the ISO 2631-1 exposure guidelines, putting them at risk of injuries. In larger LHDs, the highest magnitudes of vibrations were observed within a range between 0.89 and 1.18 m/s^2 in the z-axis. For smaller LHDs, the highest magnitude of vibration was observed within 0.55 and 0.64 m/s^2 in the x-axis.

Hoy et al. [39] investigated the risk from WBV exposures and postures for low back pain (LBP) among forklift truck (forklift) drivers. Vibrations at the seat were measured in all the three axes (x, y and z), under actual working conditions, and compared with ISO 2631-1 limits. The results indicated that LBP is more prevalent among the forklift truck drivers as compared to the non-drivers and that WBV exposures contribute, among other factors, to cause LBP. It was also shown that the WBV exposures in the x and y directions are well within the acceptable limits (below 0.5 m/s^2) based on the ISO 2631-1 limits. However, the vibration levels in the z-axis direction (0.73 m/s^2), with a peak ranging between 1.24 and 24.46 m/s^2, exceeded the ISO 2631-1 limits.

Wenzhang [40] used MSC. ADAMS to build a vehicle dynamic simulation model and studied the non-linear dynamic characteristic of its rubber component. It showed that one could consider the effect of linear and non-linear dynamic characteristics of the rubber component in a vehicle using vehicle dynamic analysis. The dynamic stiffness of the rubber component was 14 kN/mm based on exciting frequency, component mass and damping ratio of 11 Hz, 245 kg and 0.2, respectively. The results showed that the corresponding single DOF system vibrates with the natural frequency of 11 Hz. For non-linear stiffness

characteristics of rubber component, it showed that the peak response frequency was 12 Hz with a displacement of 0.1mm.

Kim et al. [41] modeled a vehicle with flexible body frame and active height control (AHC) system using MSC.ADAMS with 86-DOF. The proposed AHC system consisted of an automatic air leveling and semi-active suspension system for sport utility vehicles. They simulated the virtual prototype model to analyze the vehicle control and handling performances for various driving conditions. Eight (8) mode shapes were observed ranging from 26.9 HZ for the 1^{st} mode to 54.4 Hz for the 8^{th} mode. The simulation results indicated that the AHC system automatically responded to the additional 200 kg on the rear side of the SUV and the spring was compressed by 25 mm due to this extra load. The spring was leveled back by the AHC system to its normal position after 19.62 seconds by the compressed air that was supplied for 4.03 seconds. The leveling speed was 1.6 mm/second and did not cause passenger discomfort.

Chang et al. [42] investigated ten dump trucks driven by domestic truck driver at the sandstone field for the preliminary vibration determination. Tolerable exposure time per day for drivers was evaluated using the ISO 2631 – 1 [4] and article 301 in Taiwan's regulation "Rules of Equipment and measures for Protecting Laborers' Safety and health". The health risk was also assessed using ISO 2631 – 5 [5] for dump truck drivers. Using ISO 2631 – 1 [4], it was found out that the tolerable exposure time of these dump trucks were all being exceeded in the study. Based on ISO 2631 – 5 [5], the study showed that the dump truck drivers had a high probability of experiencing an adverse health effect.

The very first fundamental research in terms of whole body vibration (WBV) and its impact on dump truck's operator was carried out by Frimpong et al. [43]. A simplistic

model was developed to capture the vibration response of an integrated operator–machine–material system under high-impact shovel loading operations (HISLO). The study used MSC.ADAMS to develop the virtual prototype models to simulate the response of the integrated system suspension to vibrations. The results showed that the shockwaves, during dumping, which are being propagated into the operator's cabin are not being effectively attenuated, or reduced to a satisfactory level, by the current suspension mechanisms resulting in an adverse impact on operator's safety and health.

Aouad and Frimpong [24] also developed comprehensive mathematical models and a 3D virtual prototype simulator for truck vibrations under HISLO conditions. Aouad and Frimpong [44] carried out a fundamental research to model the HISLO during the shovel dumping process. They formulated the equations of motions, governing the HISLO problem, using the Lagrangian formulation. The Fehberg 4^{th}-5^{th} order Runge–Kutta (RKF45) numerical method was used to solve the equations of motion in the MAPLE environment. The results showed that the vertical root mean square (RMS) accelerations were 3.56, 1.12, and 0.87 m/s^2, respectively, for the operator's seat, lower back and cervical regions. Comparing these vibration levels to the ISO 2631-1 limits (less than 0.315 m/s^2), they concluded that these levels fall beyond or within the extremely uncomfortable zone. This exposure poses severe health threats including severe long-term lower back, neck and other disorders to truck operators over long exposure period.

Ali and Frimpong [6] presented the novel idea of controlling the WBVs by optimizing the shovel dumping operation. Their research achieved a reduction of 17.34% during the first shovel pass by optimizing the dumping height during truck loading. That reduction in the impact force resulted in the reduction of vibrations levels at the operator's

seat by 19.61% [8]. The solution framework from Ali and Frimpong [6] reduces the vibrations levels at the operator's seat from 3.56 m/s^2 to 2.86 m/s^2. However, based on the specified ISO safety limits, this value still exceeds the upper limit of the 'Extremely Uncomfortable Zone' [4]. Thus, the current optimized process could still expose operators to high WBV levels that could cause permanent life threatening injuries to vehicle operators. Therefore, there is a strong need to develop improved solutions to bring the vibration levels to within the comfortable category via advanced research initiatives.

2.2. IMPACT FORCE AND DYNAMIC LOAD MODELLING

Discrete element method (DEM) has been used extensively for solving a diverse range of scientific and engineering problems in physical media. These media include soil and rock behavior, slope stability, rockfall hazard mitigation, hydraulic fracturing, material impact modelling, soil and flow-surface interaction, bulk material flow, mixing and transportation of aggregates, and rock/soil fragmentation (Itasca, 2011).

Doktan [45] studied the effect of blast fragmentation on the performance of shovel-truck fleet. Numerical models were developed using DEM to improve the particle to surface interaction for a better understanding of digging and loading operations. The results showed that shovel digging and loading time could reduce by 35% and 22%, respectively, with improved blast fragmentation. However, the model was limited to mixtures with uniform and small size particulate material, thus not applicable for any large scale mining excavation.

Iverson et al. [29] evaluated the usefulness of computer simulation models for improving ore pass designs. DEM was used to simulate the gravity induced rock flow for studying rock particle interaction and impact forces on the bottom end structure. The results

showed that with the application of dogleg transition, the dynamic loads at the chute gate could be significantly reduced. The results could be used to improve chute design, thus reducing the risk of structural damage and improving the overall safety of operation. However, authors used a 2D model for simulating the rock flow, which impose strict limitations in terms of dynamic load modelling, therefore cannot be rendered as an accurate representation of material flow.

Teufelsbauer [46] investigated material flow patterns and generation of impact forces on rigid incline surfaces. Simulation experiments were conducted for granular and 3D free-surface flows at inclined rigid chutes using DEM. The results emphasized the importance of rotational control for a successful DEM-based modelling of granular particle flow, thus allowing an accurate capturing of the resulting impact forces on critical portions of the structure. The model was developed for laboratory scale experimentation performed under controlled environment, therefore lacks applicability for any real-world material flow process.

Hosseininia [47] studied the effect of anisotropy of the granular particles and the resulting voids on overall mechanical behavior of the granular material assemblies. The research used DEM to simulate several biaxial compression tests for the granular assemblies with convex polygonal geometries. The results showed highest shear strengths for assemblies having particles with least change in inclination and with large voids causing dilatancy of the granular material. The 2D numerical model developed in this study was a simplistic approach for modelling the mechanical behavior of granular assemblies because in reality granular particles are always 3D.

Law et al. [48] investigated the dynamic process of granular material flow through a row of baffles to model the resulting impact forces. A virtual simulation model was designed using DEM to capture the hot spots and force magnitudes during the impact process. The results showed that the impact force magnitude decreased with the upstream distance along with a uniform deceleration of discrete particles at the point of impact. The DEM simulation experiments used the linear contact model for capturing the interaction between the particles and the structural surfaces. The findings of this study are, thus, limited in scope as the linear contact model used for the DEM simulation is a simplistic assumption as it neglects consideration of the contact stiffness when updating the contact forces and the particle movement.

Albaba et al. [49] then presented the clump model for an accurate representation of impact forces using DEM. Numerical experiments were conducted involving dry granular material flow impacting the rigid surface while flowing through an inclined chute. Comparison between the simulation and the experimental results, with regards to total normal forces and the bending moment, showed the effectiveness and accuracy of the designed simulation model. However, the overall force distributions were different for each test, which could be due to the sensitivity of the DEM model to the particle position and orientation at the impacting wall, or limitation of the DEM method in modelling the interaction of discrete particles with deformable bodies and rigid surfaces. Thus, using the FEA-DEM coupled methodology would improve the shortcomings and allow for an accurate impact force modelling.

Bruno [50] examined the haul road response to the dynamic loads imposed by the large capacity dump truck. FEA was used to model the truck-haul road interaction for

capturing the stress, strain, and deformation of the road in response to the truck tire dynamic forces generated during haulage for ultra-large trucks. However, the road layers were modelled as continuum with C3D8R finite elements even though the haul roads consists of rock/soil material. FEA-DEM coupled methodology should be applied with using DEM to model the road surface which would allow for an accurate capturing of haul road response with a proper particle-to-particle contact definition for road rock/soil material.

Bobaru et al. [51] investigated the interaction between a granular material layer and an elastic foundation. FEA-DEM coupled methodology was used to simulate the bending of the granular particles and to capture the resulting structural change. The computed values of Young's modulus and the bending stiffness of the granular layer showed strong agreement with the previously conducted experiments, which can be further used to analyze the forced vibration case. The two-dimensionality of the FEA-DEM model puts significant limitations in terms of accurate dynamic modelling attempted in this study.

Leonardi et al. [52] presented a computational framework for a rational design of flexible barriers. The designed framework utilized the FEM to model the flexible barrier and DEM to govern the motion of debris flow as a fluid-grain mixture. The study showed the advantage of the flexibility of the designed barriers towards reducing the risk of structural collapse, by capturing the stress distribution on its fabric. However, the work can be greatly improved by relaxing the ideal flow assumption during the FEA-DEM simulation design.

Ur-Rehman et al. [53] studied the load haul dump (LHD) bucket-muckpile interaction. FEA-DEM coupled methodology was used to investigate the effect of different

attack angles on initial penetration. Experimental results of the simulation study showed a strong dependence of resistive forces on the cutting tool attack angle. In another study, Ur-Rehman and Awuah-Offei [54] examined the effect of bucket orientation and operating parameters – rake angle, tractive effort, speed, and digging height – on the resistive forces and penetration for the LHD loaders. It was found that the loader's penetration and resistive forces are better explained by the speed and tractive effort as compared to the digging height and rake angle. However, in both the studies, the LHD bucket was a scaled model thus significantly limiting the study results in terms of scope and applicability.

Fundamental research for modelling HISLO impact force was carried out by Ali and Frimpong [9]. A mathematical model was developed to capture the dynamic impact force for the first shovel pass of material under gravity into a truck. The research advanced the frontier of the existing knowledge. However, the model had significant limitations, including its inability to (i) model impact forces for subsequent passes after the first shovel pass; (ii) capture the cushioning effect of material from previous passes; and (iii) capture truck physical properties, which can have significant effect on the behavior of generated impact force.

2.3. INTELLIGENCE-BASED SOLUTIONS USING AI AND ML

Artificial intelligence (AI) is a field of computer science that deals with transforming and developing machines capable of performing certain tasks without requiring any specific instruction. The ultimate goal of AI is for machines to achieve human-level of intelligence. Deep learning and machine learning are the subfields or particular applications of AI, which deal with designing algorithms capable of educating machines by helping them recognize patterns and extract knowledge from previous cases.

AI is useful and more efficient in recognizing cancer tissue faster than human experts, finding criminal patterns in tons of financial transactions, doing speech and video recognition to converting huge video banks into structured information, creating chatbots that speak and understand speech to become better assistants.

Machine learning and AI can be applied from the beginning of mining to the end of the mine life-cycle, from prospecting to production to closure and mine reclamation. However, according to a recent white paper by Narendran and Weinelt [55] at the World Economic Forum, compared to other industries, especially customer-oriented ones, the mining and metals sector is considered to have least levels of digital utilization. Progress on machine and operation advancement with intelligent technology development has been extremely slow [56, 57] in this sector. However, the mining industry is beginning to recognize and understand the importance of AI and has recently started to explore the development and applicability of these technologies to enhance safety and productivity in mining operations.

Researchers have used AI and machine learning to develop frameworks for intelligence-based process advancement in a variety of fields in the mining sector, including mineral resource mapping/exploration, mineral processing, and rock mechanics.

Al-Alawi and Tawo [58] developed an ANN-based model for mineral resource evaluation for a bauxite deposit and compared the results with the geostatistical kriging technique which showed close agreement. Brown et al. [59] built a multilayer perceptron neural network model using GIS data from various exploration projects in an attempt to prepare a mineral prospectivity map for a gold deposit. Later, Brown et al. [60] used the neural network model to exhibit improved performance as compared to Bayesian and fuzzy

logic models for gold deposit mineral prospectivity mapping. Rigol-Sanchez [61] used the back propagation ANN to identify mineral rich zones using GIS data containing remote sensing and exploration data for a gold field. Nykanen et al. [62] developed a fuzzy logic model to locate favorable areas for iron oxide, copper, and gold deposits in Finland using geological, geophysics, geochemistry, and mineral occurrence data. Bokhari et al. [63] used the fuzzy logic model for mineral potential predictions of various commodities in southwestern China. Lee and Oh [64] built an artificial neural network to generate a mineral potential map for thirty-two different deposits using the collected geochemical and geophysical data. Setyadi et al. [65] used the fuzzy logic approach to process site geophysical data to understand the geological feature for mineral resource mapping. The fuzzy logic application was also used by Kashani et al. [66] with geological, geochemistry, and mineralogical data to build fuzzy logic models for copper deposits in Iran. Zhang and Zhou [67] and Tabaei [68] introduced specific fuzzy-based models to produce a mineral prospectivity map in order to identify new targets in any area using geochemical and geological data, for mapping mineralization, for gold deposits and using magnetic, geological, and satellite data for the Mississippi valley-type (MVT) deposits, respectively.

Researchers have also used artificial and computational intelligence for smarter mine planning and operations. Karadogan et al. [69] demonstrated the application of the fuzzy set approach for mining method selection using geological, geotechnical, economic, and environment data for an underground mine in Turkey. Smart algorithms can assist the mining engineers during such a complex multi-variant decision-making process. Bascetin et al. [70] demonstrated the application of a computer software named equipment selection (EQS) for automating the mining equipment selection process based off of the fuzzy set

theory. Bazzazi et al. [71] introduced a multi-criterion decision-making process, based on fuzzy sets, to select mining equipment for a particular operation. Hosseini et al. [72] proposed a fuzzy logic model to investigate the potential of an Iranian coal mine mechanization for decreasing the cost and increasing the overall profitability of the project. Ozkan et al. [73] successfully applied the fuzzy logic-based model for resource classification when solving previously encountered problems in the conventional method for lignite basin reserves.

Reclamation is an important part of mining process with proper selection of post-mining land use based on multiple factors, thus making it a complex decision-making process. Bandopadhyay and Chattopadhyay [74] introduced the idea of using the fuzzy logic approach to optimize the post-mining land use. Kommadath et al. [75] demonstrated the efficiency and effectiveness of the fuzzy logic based model to assess sustainability for the mining sector. Bangian et al. [76] built a fuzzy logic model to optimize the reclamation process of an open pit copper mine in Iran to justify the associated cost. Anis et al. [77] demonstrated the application of the GIS-based fuzzy logic model for an optimized utilization of land at the end of mining process for an Indonesian coal mine.

Assessment of risky situations during mining operations is important to create a safe working environment. An intelligent system is essential to overcome the associated uncertainties during each process [78]. Iphar and Cukurluoz [79] introduced a fuzzy logic-based model for risk assessment and safety evaluation that is more effective than the conventional decision matrix methods at an underground coal mine in Turkey.

Drilling and blasting are important unit mining operation, and thus, modelling the performance of any drill and blast operation requires special attention. Artificial neural

network (ANN) has been widely used to evaluate and analyze the blast performance. Monjezi et al. [80] evaluated various training algorithms used for ANN when predicting muck pile ratio, fly rock expectation, and the explosive amount being utilized. Khandelwal and Singh [81] and Khandelwal et al. [82] showed the effectiveness of using ANN for predicting the peak particle velocity for the blast-induced ground vibrations. Zhongya and Xiaoguang [83], demonstrating the superiority of ANN combined with factor analysis and mean value-based optimization over the non-optimized ANN for the same application of blast-induced ground vibrations. Proper rock fragmentation is essential for a successful blasting operation, as the material handling equipment and processing plant are designed for a specific degree of fragmentation. Bahrami et al. [84] and Sayadi et al. [85] have both shown acceptable results for predicting rock fragmentation using ANN for iron ore and limestone mining operations, respectively. Recently, Ebrahimi et al. [86] displayed improved accuracy of an ANN model by employing an artificial bee colony algorithm to optimize the blasting input parameters and predict the rock fragmentation in comparison to the empirical model. Tiile [87] has also demonstrated the effectiveness of ANN over empirical models and conventional statistical techniques for predicting the blast performance, that is characterized by both the degree of resulting vibrations and rock fragmentation for a gold mining operation.

Researchers have also used fuzzy logic, which is the most popular AI methodology for mechanical control systems, to characterize the blasting performance. Ghasemi et al. [88] developed a Mamdani-based fuzzy logic model for predicting the peak particle velocity during blasting operation for a copper surface mine. Monjezi et al. [89], Monjezi et al. [90], and Rezaei et al. [91] designed a fuzzy logic-based predictive system for rock

fragmentation, back break, and fly rock estimation, respectively, for an iron ore mining operation, which performed better than the regression, statistical, and empirical methods. Shams et al. [92] recently introduced a fuzzy inference-based system for rock fragmentation prediction for a copper mining operation as well.

Drilling is an extremely cost-intensive process in terms of both capital and operating costs, and thus, requires efficient design and real-time performance evaluation for a successful application. Karri [93] proposed a neural network model with a radial-basis function to predict the drilling performance characterized by drilling thrust and torque. Desai and Shaikh [94] demonstrated the effectiveness of ANN in combination with evolutionary-techniques-based model training for predicting the drill wear. Torno et al. [95] designed a fuzzy logic model for the continuous prediction of the geological properties of the rock mass and optimization of drilling parameters during the excavation process for sandstone, gypsum, and igneous rocks in Spain. Jang and Topal [96] developed an ANN-based prediction system with the capability of serving as an overbreak warning and prevention system during drill and blast operation. Elkatatny et al. [97] developed a mathematical model using ANN for predicting the emulsion based (oil-based mud) drilling fluid properties. Recently, Lashari et al. [98] introduced a multi-layered ANN model capable of predicting the rate of penetration along with bit malfunction identification, during the drilling process for shale rock.

Majority of the aforementioned work within the mining sector involved either the artificial neural network or fuzzy logic approach. Artificial neural network lacks the ability to handle complex problems requiring extensive computational units. Fuzzy logic lacks pattern recognition ability – a key element in data-based machine learning and artificial

intelligence – thus limiting its learning capabilities. None of the existing work involves deep-learning-based model development, which is a cutting-edge knowledge extraction technique with exceptional self-learning capabilities. Modern technologies use data-based intelligent monitoring and control systems for real-time implementation and processing in order to ensure both quality and safety of the process [78]. Such technologies have the power to learn and adjust as the process changes, making them effective and applicable in any scenario. Therefore, it is of immense importance that any technology developed should focus on modern data-driven implementation to ensure self-sustainability in a dynamic environment.

As mentioned previously, during truck loading an operator experiences severe whole body vibrations, which can cause long-term disabilities if it continues for an extended period of time. The implementation of the solution for HISLO WBV problem is another issue that has to be addressed. The mathematical model and offline simulation system not only require significant amount of time and specialized software platform but also extraordinary amount of expertise on the subject for it to be used, which is extremely difficult on any mine site, especially for such a dynamic problem. Therefore, a framework for intelligently processing the solution implementation is required in order to assist the shovel operators in real-time. Machine learning and artificial intelligence, particularly deep learning, can be used to develop such a smart framework which enables the solution implementation in the most effective and efficient manner [99].

Hydro-pneumatic suspension struts are most commonly used in large dump trucks as the vibration attenuation system. With aging, the suspension system deteriorates and loses its capability to effectively attenuate the impact of vibrations produced by the

dumping process under gravity. This is due to the contamination of hydraulic oil, mixing of the oil and nitrogen, or rupturing of the gas accumulator diaphragm [10]. The effectiveness of any suspension system is evaluated by determining the output vibration levels. In the case of the dump truck, it is important to determine the vibration levels at the operator's seat for evaluating the effectiveness of the hydro-pneumatic suspension struts as the truck ages. AI models have been used for suspension system modeling and performance prediction as demonstrated by Ali and Frimpong [100]. They used three state-of-the-art artificial intelligence and machine learning models, including ANN, MFL, and HyFIS for developing and training an intelligence-based framework in the study to model and predict the performance of the hydro-pneumatic suspension system in the large capacity dump trucks. RMS accelerations in vertical and horizontal direction at the operator's seat were used to capture the performance of the suspension system. These intelligent and self-learning models should now be implemented in the truck control system in order to autonomously evaluate the performance of the suspension system in real-time, throughout the machine operation. This will allow the operator or the maintenance crew to have a precise idea of the condition of the suspension system and when to implement preventive maintenance of the suspension system. With efficient performance tracking and just-in-time maintenance, the suspension system performance will be maximized to attenuate the impact of vibrations due to gravity dumping.

This research initiative is a pioneering effort toward advancing knowledge and frontiers in impact force modeling and WBV attenuation using AI and machine learning algorithms. This pioneering effort will develop and implement intelligent monitoring of impact force generation and progression, dump height reduction and dipper-truck

interactions under HISLO conditions. The successful implementation of such a system will maximize workplace safety and health and surface mining productivity and economic benefits.

2.4. SUMMARY

A critical review of all the relevant literature was carried out to evaluate the contributions and existing frontiers of the body of knowledge in the areas of whole body vibrations, impact force modeling, discrete element analysis, dynamic virtual simulation systems, and smart solution development using artificial intelligence and machine learning.

Majority of the research on WBV phenomenon and its control solutions has been carried out in the area of military applications [12, 15, 16, 25–28]. While dump trucks are stationary elements under HISLO conditions, the external excitation force generated during a WBV exposure of operators in mining operations is dynamic. Thus, military applications are starkly different from mining in terms of HISLO WBV phenomenon. Aouad and Frimpong [24] studied HISLO dynamic vibration problem through a virtual simulator to quantify the vibrational levels for dump truck. Apart from the works of Ali and Frimpong [6, 9], where mathematical and virtual models for optimizing the shovel dumping operations were developed, few or no work has been devoted to developing solutions for HISLO vibration problem. Ali and Frimpong [6, 9] discovered that the external impact force generated through gravity dumping of material from shovels was the major cause of whole body vibrations.

Previous researchers, in terms of intelligence-based solution development, have used machine learning and artificial intelligence in a variety of fields in the mining sector, including mineral resource mapping/exploration, mineral processing, and rock mechanics.

No work has been carried out to develop intelligent monitoring systems for impact force generation and progression at the truck bed surface. This research study was a pioneering effort towards developing artificial intelligence and machine learning algorithms for solving the problems associated with real-time monitoring of the dynamic impact force, optimization of the dumping process and the resulting WBV levels.

3. MATHEMATICAL MODELLING OF HISLO IMPULSE FORCE

A robust mathematical pass model was developed for capturing the dynamic impact force on truck surface during multi- shovel loading process. The section includes detailed step-by-step process for the model formulation. This section also contains the governing equations of the complete system.

3.1. MATHEMATICAL MODEL FORMULATION

The impact force resulting from the gravity dumping of material into a truck body is dynamic. Therefore, the response of the truck body was used to develop a rigorous dynamic model for capturing the resulting impact force as material is dropped from the shovel dipper/bucket onto the truck bed. The following assumptions were used to develop the model from the HISLO vibration system:

- Back end assembly of the truck, consisting of truck body, chassis, pitch of truck with respect to ground, and both frontal/rear tire/wheel assemblies, were considered along with the ground surface for analysis. The components were selected because they define the portion where material is dropped and where impact force is generated.
- Each truck component was a discretized rigid body element of the whole system.
- The connections between each truck component were modelled via using spring and damper mechanism.
- The impulse force remained dynamic throughout the shovel dumping process.
- The z-direction represented the vertical (up-down) movement of the truck.

Figure 3.1 shows the structural model of the truck for the HISLO vibration system. It is a 6-DOF system where each component is a discretized rigid mass connected with the other essential components of the truck via spring and damper mechanism. The external excitation force due to the shovel dumping was modelled using equation (3.1). The excitation force acts directly on the truck body for the first shovel pass, but for any subsequent shovel pass it acts through the material in the truck from previous shovel pass(es). For the second shovel pass, the external force is transferred to the truck body after passing through the material from the first pass. Spring and damper component between the masses 'm1' and 'm2' models the energy dissipation due to the material in the truck body from previous shovel pass(es). A portion of the force gets dissipated, and the remaining portion gets transmitted, first, to the truck body, and then, to other truck components. Each component generates reactive forces in response to the external force, which is modelled from the reactions of the spring and dampers. The reaction forces act in the z-direction because all the connections are pinned in vertical position.

$$F(t) = \frac{\sqrt{2gH_t}\, m}{\epsilon^2(M+1)} \sum_{j=0}^{M} \left[2\left(t - \left(j\left(\frac{\epsilon}{a}\right)a\right)\right) H\left(t - \left(j\left(\frac{\epsilon}{a}\right)a\right)\right) \right.$$
$$- 4\left(t - \left(j\left(\frac{\epsilon}{a}\right)a\right) - \frac{\epsilon}{2}\right) H\left(t - \left(j\left(\frac{\epsilon}{a}\right)a\right) - \frac{\epsilon}{2}\right) \qquad (3.1)$$
$$\left. + 2\left(t - \left(j\left(\frac{\epsilon}{a}\right)a\right) - \epsilon\right) H\left(t - \left(j\left(\frac{\epsilon}{a}\right)a\right) - \epsilon\right) \right]$$

Lagrangian formulation was used to resolve the HISLO vibration system and develop the set of equation of motions for the system. The equation of motions (EOMs) of

a vibration system developed using the Lagrangian mechanics are commonly known as Euler-Lagrange equation [101]. Any component of the system can have a total of six variables describing that capture its complete motion at any given instance of time. Lagrangian equations for any system using the energy approach have three main components: kinetic, potential/strain, and dissipation energies.

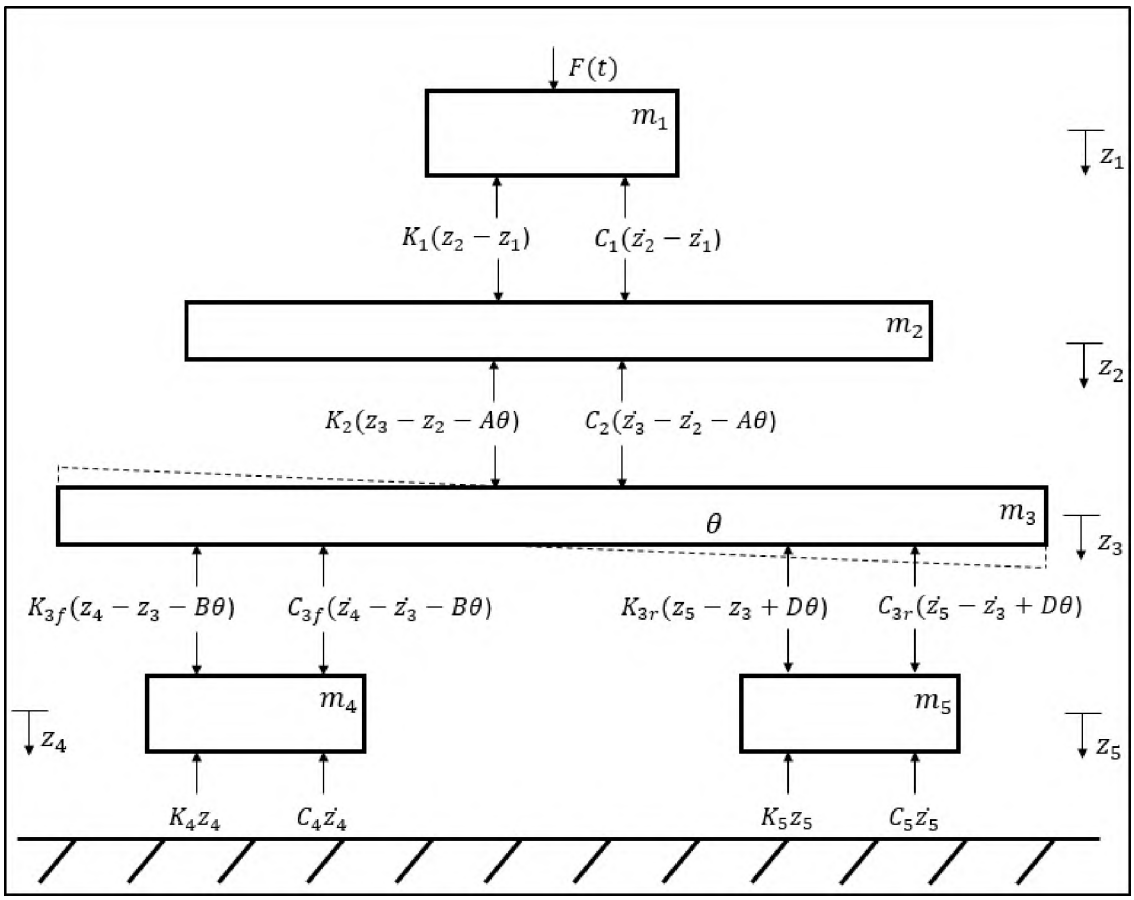

Figure 3.1. Free Body Diagram of each Component in HISLO Vibration System

Equations (3.2), (3.3), and (3.4) are the three energy components representing the kinetic, potential/strain, and dissipation energies, respectively, for the complete HISLO vibration system (Figure 3.1).

$$\mathrm{T} = \frac{1}{2}\left(m_1\dot{z}_1{}^2 + m_2\dot{z}_2{}^2 + m_3\dot{z}_3{}^2 + m_4\dot{z}_4{}^2 + m_5\dot{z}_5{}^2 + I\dot{\theta}^2\right) \tag{3.2}$$

$$\begin{aligned}\mathrm{V} = \frac{1}{2}\big(&K_1(z_2 - z_1)^2 + K_2(z_3 - z_2 - A\theta)^2 + K_{3f}(z_4 - z_3 - B\theta)^2 \\ &+ K_{3r}(z_5 - z_3 + D\theta)^2 + K_4 z_4{}^2 + K_5\, z_5{}^2\big)\end{aligned} \tag{3.3}$$

$$\begin{aligned}R = \frac{1}{2}\big(&C_1(\dot{z}_2 - \dot{z}_1)^2 + C_2(\dot{z}_3 - \dot{z}_2 - A\dot{\theta})^2 + C_{3f}(\dot{z}_4 - \dot{z}_3 - B\dot{\theta})^2 \\ &+ C_{3r}(\dot{z}_5 - \dot{z}_3 + D\dot{\theta})^2 + C_4\dot{z}_4{}^2 + C_5\,\dot{z}_5{}^2\big)\end{aligned} \tag{3.4}$$

Equation (3.5) is the Lagrangian equation in its generalized form for a non-conservative forced system. Since L = T – V, the generalized Lagrangian formulation can be expanded to include the system kinetic and potential energies, as given by equation (3.6). Due to the independence of $\dot{q}_i$ and q_i, the terms $\frac{\partial V}{\partial \dot{q}_i}$ and $\frac{\partial T}{\partial q_i}$ did not play any role in the overall dynamics of the system. Hence, the final form of Lagrange's equation for the system is formulated as equation (3.7).

$$\frac{d}{dt}\left(\frac{\partial L}{\partial \dot{q}_i}\right) - \frac{\partial L}{\partial q_i} + \frac{\partial R}{\partial \dot{q}_i} = Q_i(t) \tag{3.5}$$

$$\frac{d}{dt}\left(\frac{\partial T}{\partial \dot{q}_i}-\frac{\partial V}{\partial \dot{q}_i}\right)-\frac{\partial T}{\partial q_i}+\frac{\partial V}{\partial q_i}+\frac{\partial R}{\partial \dot{q}_i}=F_i(t) \tag{3.6}$$

$$\frac{d}{dt}\left(\frac{\partial T}{\partial \dot{q}_i}\right)+\frac{\partial V}{\partial q_i}+\frac{\partial R}{\partial \dot{q}_i}=F_i(t)\ \ \forall\, i=1,2,..,6 \tag{3.7}$$

The final Lagrange's equation, equation (3.7), computes the equation of motion for each of the displacement variables z_1, z_2, z_3, z_4, and z_5 and the pitch angle θ. Equations (3.2), (3.3), and (3.4) compute the kinetic, potential, and dissipation energy terms, respectively, in the transformed equations. A set of 6 equations of motion (EOM) was obtained, as given by equations (3.8), (3.9), (3.10), (3.11), (3.12), and (3.13), to describe the complete HISLO system. The force vectors $F_2(t)$, $F_3(t)$, $F_4(t)$, $F_5(t)$, and $F_5(t)$ were all assigned zero due to the absence of any external force on the corresponding sprung masses.

$$m_1\ddot{z}_1+C_1(\dot{z}_1-\dot{z}_2)+K_1(z_1-z_2)=F_1(t) \tag{3.8}$$

$$m_2\ddot{z}_2+C_2\left(\dot{z}_2-\dot{z}_3+A\dot{\theta}\right)-C_1(\dot{z}_1-\dot{z}_2)++K_2(z_2-z_3+A\theta)-K_1(z_1-z_2)=0 \tag{3.9}$$

$$m_3\ddot{z}_3 + C_{3f}(\dot{z}_3 - \dot{z}_4 + B\dot{\theta}) - C_2(\dot{z}_2 - \dot{z}_3 + A\dot{\theta}) - C_{3r}(\dot{z}_5 - \dot{z}_3 + D\dot{\theta}) + K_{3f}(z_3 - z_4 + B\theta) - K_2(z_2 - z_3 + A\theta) - K_{3r}(z_5 - z_3 + D\theta) = 0 \quad (3.10)$$

$$m_4\ddot{z}_4 + C_4\dot{z}_4 - C_{3f}(\dot{z}_3 - \dot{z}_4 + B\dot{\theta}) + K_4z_4 - K_{3f}(z_3 - z_4 + B\theta) = 0 \quad (3.11)$$

$$m_5\ddot{z}_5 + C_5\dot{z}_5 + C_{3r}(\dot{z}_5 - \dot{z}_3 + D\dot{\theta}) + K_5z_5 + K_{3r}(z_5 - z_3 + D\theta) = 0 \quad (3.12)$$

$$I\ddot{\theta} + AC_2(\dot{z}_2 - \dot{z}_3 + A\dot{\theta}) + BC_{3f}(\dot{z}_3 - \dot{z}_4 + B\dot{\theta}) + DC_{3r}(\dot{z}_5 - \dot{z}_3 + D\dot{\theta}) + AK_2(z_2 - z_3 + A\theta) + BK_{3f}(z_3 - z_4 + B\theta) + DK_{3r}(z_5 - z_3 + D\theta) = 0 \quad (3.13)$$

Equations (3.8), (3.9), (3.10), (3.11), (3.12), and (3.13), in a matrix form, are shown in equation (3.14), with a 6 x 6 mass, damping and stiffness matrices and 6 x 1 acceleration, velocity, displacement, and force matrices. Equation (3.16) is formulated as equation (3.14) in a vector-compact form.

$$\begin{bmatrix} m_1 & 0 & 0 & 0 & 0 & 0 \\ 0 & m_2 & 0 & 0 & 0 & 0 \\ 0 & 0 & m_3 & 0 & 0 & 0 \\ 0 & 0 & 0 & m_4 & 0 & 0 \\ 0 & 0 & 0 & 0 & m_5 & 0 \\ 0 & 0 & 0 & 0 & 0 & I \end{bmatrix} \begin{Bmatrix} \ddot{z}_1 \\ \ddot{z}_2 \\ \ddot{z}_3 \\ \ddot{z}_4 \\ \ddot{z}_5 \\ \ddot{\theta} \end{Bmatrix} + \quad (3.14)$$

$$\begin{bmatrix} C_1 & -C_1 & 0 & 0 & 0 & 0 \\ -C_1 & C_1+C_2 & -C_2 & 0 & 0 & AC_2 \\ 0 & -C_2 & a* & -C_{3f} & -C_{3r} & b* \\ 0 & 0 & -C_{3f} & C_{3f}+C_4 & 0 & -BC_{3f} \\ 0 & 0 & -C_{3r} & 0 & C_{3r}+C_5 & DC_{3r} \\ 0 & AC_2 & b* & -BC_{3f} & DC_{3r} & d* \end{bmatrix} \begin{Bmatrix} \dot{z}_1 \\ \dot{z}_2 \\ \dot{z}_3 \\ \dot{z}_4 \\ \dot{z}_5 \\ \dot{\theta} \end{Bmatrix} +$$

$$\begin{bmatrix} K_1 & -K_1 & 0 & 0 & 0 & 0 \\ -K_1 & K_1+K_2 & -K_2 & 0 & 0 & AK_2 \\ 0 & -K_2 & e* & -K_{3f} & -K_{3r} & \text{f*} \\ 0 & 0 & -K_{3f} & K_{3f}+K_4 & 0 & -BK_{3f} \\ 0 & 0 & -K_{3r} & 0 & K_{3r}+K_5 & DK_{3r} \\ 0 & AK_2 & \text{f*} & -BK_{3f} & DK_{3r} & \text{g*} \end{bmatrix} \begin{Bmatrix} z_1 \\ z_2 \\ z_3 \\ z_4 \\ z_5 \\ \theta \end{Bmatrix} =$$

$$\begin{Bmatrix} f(t) \\ 0 \\ 0 \\ 0 \\ 0 \\ 0 \end{Bmatrix}$$

Where,

$$\left.\begin{aligned} a* &= C_{3f}+C_2+C_{3r} \\ b* &= BC_{3f}-AC_2-DC_{3r} \\ d* &= B^2C_{3f}+A^2C_2+D^2C_{3r} \\ e* &= K_{3f}+K_2+K_{3r} \\ f* &= BK_{3f}-AK_2-DK_{3r} \\ g* &= B^2K_{3f}+A^2K_2+D^2K_{3r} \end{aligned}\right\} \qquad (3.15)$$

$$\vec{M}\,\ddot{\vec{z}}(t) + \vec{C}\,\dot{\vec{z}}(t) + \vec{K}\,\vec{z}(t) = \vec{F}(t) \tag{3.16}$$

EOMS for the complete system, as shown in equation (3.14), are a set of 2nd order coupled differential equations (DEs). For decoupling these DEs, modal analysis methodology was used in this study to solve these complex EOMs.

3.2. MODAL ANALYSIS FOR FORCED DAMPED VIBRATION SYSTEM

Damping is an important phenomenon in any real world structure. It is responsible for bringing any object and/or structure, after the dissipation of oscillation energy, to complete rest. Thus, any modelling approach that does not include the damping phenomenon does not represent a real world scenario. However, it should be noted that the inclusion of damping in modelling introduces complexity and coupling of EOMs and thus, tedious to solve.

To decouple EOMs for HISLO vibration system, the Rayleigh method was used. This method involved approximating the damping matrix in the EOM using the Rayleigh proportional damping model, as defined by equation (3.17).

$$\vec{C} = \alpha\vec{M} + \beta\vec{K} \tag{3.17}$$

Modal analysis was used to extract the response of a system to the excitation caused by an externally applied force to the system. The methodology works on the assumption that the solution of the system consists of a combination of normal modes '$\vec{u}_j(t)$', obtained

by solving the Eigen value problem, along with generalized coordinates '$q_i(t)$', also known as modal participation coefficients, as given by equation (3.18).

$$\vec{z}_i(t) = \vec{P}\,\vec{q}(t) = \sum_{j=1}^{6} \vec{u}_j(t)\, q_i(t) \;\forall\; i = 1,2,..,6 \tag{3.18}$$

Substitution of equation (3.18) in the generalized version of EOMs, given by equation (3.16), yielded equation (3.19) in the vector form, where each term represented a particular matrix, as explained in Section 3.1. Multiplying equation (3.19) with the transposed normal modes '$\vec{P}^T$' generated equation (3.20).

$$\vec{M}\vec{P}\,\ddot{\vec{q}} + \vec{C}\vec{P}\,\dot{\vec{q}} + \vec{K}\vec{P}\,\vec{q} = \vec{F}(t) \tag{3.19}$$

$$\vec{P}^T\vec{M}\vec{P}\,\ddot{\vec{q}} + \vec{P}^T\vec{C}\vec{P}\,\dot{\vec{q}} + \vec{P}^T\vec{K}\vec{P}\,\vec{q} = \vec{P}^T\vec{F}(t) \tag{3.20}$$

Where,

$$\left.\begin{aligned} \overline{P}^T\overline{M}\overline{P} &= \overline{I}(\text{IdentityMatrix}) \\ \overline{P}^T\overline{K}\overline{P} &= \overline{\Omega}(\text{Diagonalof } \omega_i^{\,2}) \end{aligned}\right\} \tag{3.21}$$

Equation (3.22) gave the Rayleigh proportional damping model using equations 3.17 and 3.20 with equation (3.21). Decoupling the governing EOMs of the 6 DOF system (in equation (3.16)) yielded equation (3.23).

$$\vec{P}^T\vec{C}\vec{P}\,\dot{\vec{q}} = \alpha\vec{I} + \beta\vec{\Omega}\,\dot{\vec{q}} = (\alpha\ +\ \beta\,\omega_{ni}^2)\dot{q}_i\ \ \forall\, i = 1,2,..,6 \tag{3.22}$$

$$\ddot{q}_i + 2\zeta_i\omega_{ni}\dot{q}_i + \omega_{ni}^2\,q_i = N_i(t) \quad \forall\, i = 1,2,..,6 \tag{3.23}$$

Where,

$$\left.\begin{aligned} 2\zeta_i\omega_{ni} &= \alpha\ +\ \beta\,\omega_{ni}^2 \\ N_i(t) &= \sum_{j=1}^{6} u_{ji}F_j(t) \end{aligned}\right\} \tag{3.24}$$

Equation (3.23) gave the decoupled six DEs for the HISLO system, which could then be solved analytically or numerically.

3.3. SOLVING THE DECOUPLED EOMS OF THE SYSTEM

Laplace transformation was applied to equation (3.23) to find the solution to the six DEs corresponding to the HISLO vibration system, given by equation (3.25). The simplification of equation (3.25) and solving for '$q_i(s)$' yielded equation (3.26).

$$\begin{aligned} &s^2q_i(s) - sq_i(0) - \dot{q}_i(0) + 2\zeta_i\omega_{ni}q_i(s) - 2\zeta_i\omega_{ni}q_i(0) + \omega_{ni}^2\,q_i(s) \\ &= \int_0^{\infty} e^{-st}N_i(t)dt \quad \forall\, i = 1,2,..,6 \end{aligned} \tag{3.25}$$

$$q_i(s) = \frac{\int_0^\infty e^{-st} N_i(t)dt}{(s+\zeta_i\omega_{ni})^2 + \omega_{di}^2}$$
$$+ q_i(0)\left[\frac{s+\zeta_i\omega_{ni}}{(s+\zeta_i\omega_{ni})^2 + \omega_{di}^2}\right.$$
$$\left. + \frac{\zeta_i\omega_{ni}\sqrt{1-\zeta_i^2}}{\sqrt{1-\zeta_i^2}[(s+\zeta_i\omega_{ni})^2 + \omega_{di}^2]}\right] \quad (3.26)$$
$$+ \dot{q}_i(0)\left[\frac{1}{(s+\zeta_i\omega_{ni})^2 + \omega_{di}^2}\right] \quad \forall\, i = 1,2,..,6$$

Where,

$$\omega_{di} = \omega_{ni}\sqrt{1-\zeta_i^2} \;\; (Damped\ Frequency) \quad \forall\, i = 1,2,..,6 \qquad (3.27)$$

By applying Laplace inverse to equation (3.26) and using the convolution integral concept, equation (3.28) was derived.

The terms $q_i(0)$ and $\dot{q}_i(0)$ were the initial conditions pertaining to the initial displacement and velocity of the system, respectively. The initial conditions ($q_i(0)$ and $\dot{q}_i(0)$) for the HISLO system were equivalent to zero. Applying those initial conditions to equation (3.28), the equation for generalized displacements '$q_i(t)$' for the modal coordinates was derived, as given by equation (3.29).

$$q_i(t) = \frac{1}{\omega_{di}} \int_0^t N_i(t-\tau) e^{-\zeta_i \omega_{ni}(t-\tau)} \sin[\omega_{di}(t-\tau)] dt$$

$$+ q_i(0) e^{-\zeta_i \omega_{ni} t} \left[\cos(\omega_{di} t) + \frac{\zeta_i}{\sqrt{1-\zeta_i^2}} \sin(\omega_{di} t) \right] \tag{3.28}$$

$$+ \frac{\dot{q}_i(0)}{\omega_{di}} e^{-\zeta_i \omega_{ni} t} \sin(\omega_{di} t) \quad \forall\, i = 1,2,..,6$$

$$q_i(t) = \frac{1}{\omega_{di}} \int_0^t N_i(t-\tau) e^{-\zeta_i \omega_{ni}(t-\tau)} \sin[\omega_{di}(t-\tau)] dt \quad \forall\, i = 1,2,..,6 \tag{3.29}$$

Putting equation (3.29) in equation (3.18) yielded equation (3.30), which gave the final solution to the EOM described in equation (3.16) for the HISLO vibration problem. The term $\vec{z}_i(t)$ is a 6 x 1 vector specifying the response of each component of truck section described in Figure 3.1.

$$\vec{z}_i(t) = \sum_{j=1}^{6} \vec{u}_j(t) \frac{1}{\omega_{di}} \int_0^t N_i(t-\tau) e^{-\zeta_i \omega_{ni}(t-\tau)} \sin[\omega_{di}(t-\tau)] dt \quad \forall\, i \tag{3.30}$$

$$= 1,2,..,6$$

The resulting forces on the truck body in equation (3.31) were then derived using the Newton's law, where the acceleration for the section $\ddot{\vec{z}}_2(t)$ was computed by taking the second derivative of the generalized displacement expression given by equation (3.30).

$$F_{TB} = m_b a_{TB} = m_b \ddot{\vec{z}}_2(t) \tag{3.31}$$

3.4. SUMMARY

This section described the detailed development of the mathematical model for capturing the dynamic impact force on truck surface during multi-pass shovel loading process. The model captured the cushioning effect of the existing material from previous shovel pass(es) on the subsequent shovel passes. Multi-body Lagrangian mechanics was used to develop the governing equations of the complete system from which the mathematical model of the resulting forces was developed primarily for the truck body surface.

The model is used to understand the generation and propagation of impact force for any high impact shovel loading operation. With such deeper understanding, solutions will be developed to eliminate, or at least reduce, the force magnitudes to keep them within appropriate levels. This model will serve as a stepping stone towards the development to technologies to enhance the health and safety of truck operators.

4. VIRTUAL PROTOTYPE SIMULATION DESIGN FOR HISLO

This section involves detailed description for the development of virtual prototype simulation for HISLO for surface mining operations. The 3D prototype model was designed for simulating the dumping process involving CAT 793D truck and P&H 4100XPC cable shovel. FEA-DEM coupled methodology was used to solve the system dynamics pertaining to gravity dumping of rock/soil material onto the truck bed surface.

4.1. FINITE ELEMENT ANALYSIS – DISCRETE ELEMENT METHOD

Discrete element method (DEM) [102] is a numerical technique for modelling processes involving large number of discrete particles interacting together and with other surfaces. It has been widely used for investigating the behavior of particulate material in mining, civil, chemistry, chemical, food, metallurgical, and ceramic industry [103].

DEM involves designing an explicit dynamic simulation with interacting discrete particles. Each particle is modelled as a single node element with a rigid spherical shape representing an individual grain. These elements are rigid bodies with specific radii. These elements have displacement, as well as rotational degrees of freedom. Upon consideration of friction forces, the particle rotation influences the contact dynamics. DEM particles involve large relative motions with each particle involved in multiple contacts with its neighbors. The particles interact using finite stiffness values, depending upon the operation dynamics.

Figure 4.1 shows the two types of contact interactions among DEM particles. Part (a) shows the actual physical behavior of the interacting granular particles while the part (b) shows the DEM approximation. The distance (center-to-center) between the contacting

spheres remains the same for both the cases. As the two deformed contacting spheres push towards each other, some degree of penetration can be observed based on the contact dynamics. For DEM approximation, the variable 'δ' corresponds to the maximum particle penetration or the approach distance given by equation (4.1).

$$\delta = r_1 + r_2 - d \tag{4.1}$$

Where,

r_1, r_2 = Radii of two interacting spheres

d = Centre-to-centre distance between the spheres

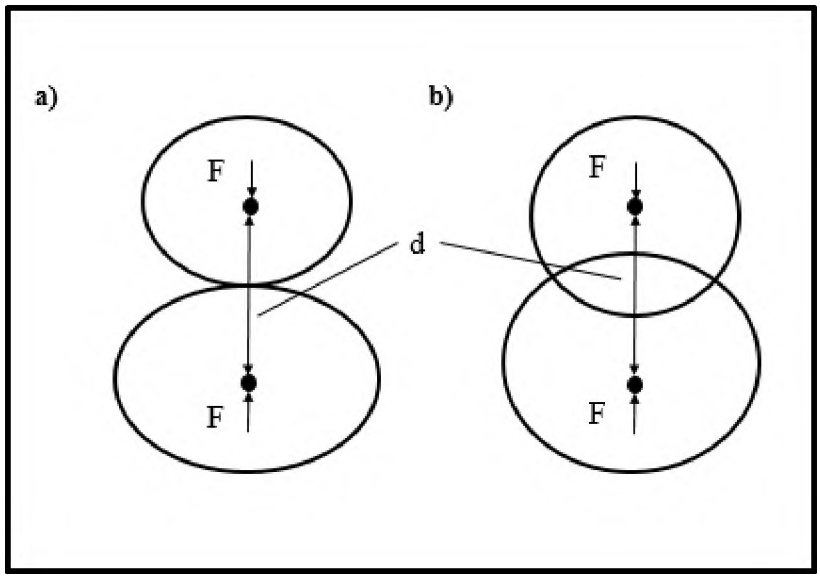

Figure 4.1. DEM Particle Contact Interaction (a) No Penetration (b) Some Penetration

DEM alone is not designed for modelling the deformation of a continuum. However, when combined with finite element analysis (FEA), the interaction of discrete particles with deformable bodies and rigid surfaces can be examined and analyzed. The

contact definitions are extended to include the interaction of DEM particles with finite element based analytical surfaces. In DEM, particle-particle interaction is treated as a dynamic process reaching equilibrium whenever the internal forces balance. Contact forces and displacements of a stressed assembly of particles are found by tracing the movements of individual particles. Movements result from the propagation through the particle system of disturbances. This is a dynamic process in which the propagation speed depends on the physical properties of the discrete system. The dynamic behavior is defined numerically by a time-step algorithm with an assumption that velocities and accelerations are constant within each time step. The solution scheme is identical to the explicit finite-difference method for continuum analysis. DEM is based on the idea that the time step chosen may be so small that, during a single time step, disturbances cannot propagate further from any particle than its immediate neighbors [7]. At all times, the forces acting on any particle are determined exclusively by its interactions with contact particles.

The DEM calculations alternate between the application of Newton's second law to the particles and a force-displacement law at the contacts. Newton's second law is used to determine the motion of each particle from the contact and body forces acting on it, while the force-displacement law is used to update the contact forces arising from the relative motion at each particle contact [104]. FEA technique is used to approximate the solution to the higher order differential equations of the system. The iterative process is repeated for each element in the FE mesh for solution approximation of the system. Force and stress development in a structure is approximated by using the computed displacement, velocity, and acceleration vectors of each element [105].

4.2. VIRTUAL PROTOTYPE GEOMETRY CONSTRUCTION

The first step in designing a virtual prototype simulation is the construction of detailed CAD geometry. Haul truck and shovel dipper are the two components required for virtually simulating a high impact shovel loading operation (HISLO). Once the individual CAD geometries are created, the prototype is assembled while maintaining a proper dumping height.

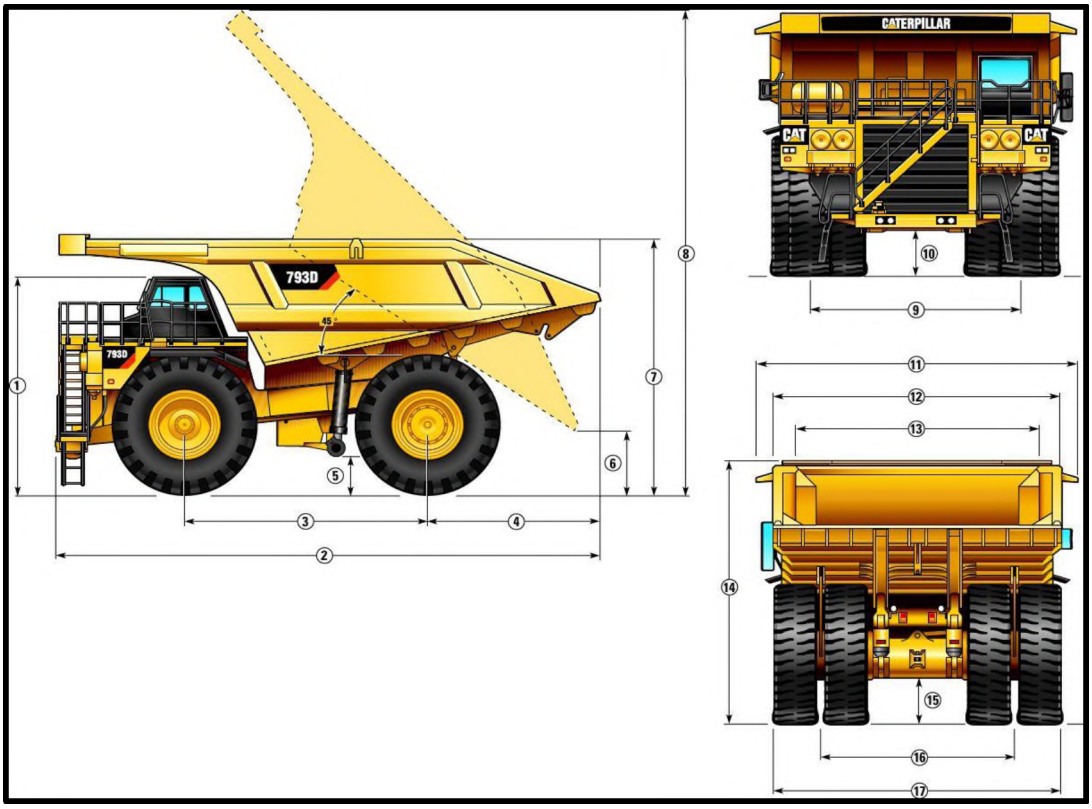

Figure 4.2. Dimensional Sketch of CAT 793D Haul Truck

The CAD geometry for the model was created within SOLIDWORKS using proper dimensions for the actual CAT 793D truck and P&H 4100 XPC shovel dipper. Figure 4.2 shows the schematic with all the marked dimensions for CAT 793D haul truck. Table 4.1

provides all the dimensional parameters referenced in Figure 4.2. The detailed dimensions were used to develop an accurate geometry for CAT 793D haul truck. Figure 4.3 shows the complete CAD geometry for the CAT 793D haul truck designed within SOLIDWORKS. The whole virtual prototype model for the HISLO process was then assembled by maintaining the accurate position of each component relative to the adjoining component(s).

Table 4.1. Dimensions for CAT 793D Truck [7]

Feature	**Dimensions (mm)**
Height to Top of ROPS – Empty, 1	5584
Overall length, 2	12862
Wheelbase, 3	5905
Rear axle to tail, 4	3772
Ground clearance – Empty, 5	1005
Dump Clearance, 6	1364
Loading height – Empty, 7	5871
Overall Height – Body Raised, 8	13113
Centerline front tire width, 9	5610
Engine guard clearance – empty, 10	1294
Overall canopy width, 11	7680
Outside body width, 12	6940
Inside body width, 13	6500
Front canopy height, 14	6494
Rear Axle Clearance, 15	1128
Centerline Rear dual tire width, 16	4963

Figure 4.4 shows the final assembled prototype model representing the HISLO process. The shovel dipper was kept at a proper dumping height relative to the truck bed surface. The minimum distance between the shovel dipper door and the truck body edge, provides the necessary clearance to prevent jolting and to ensure safe, effective, and efficient shovel dumping process.

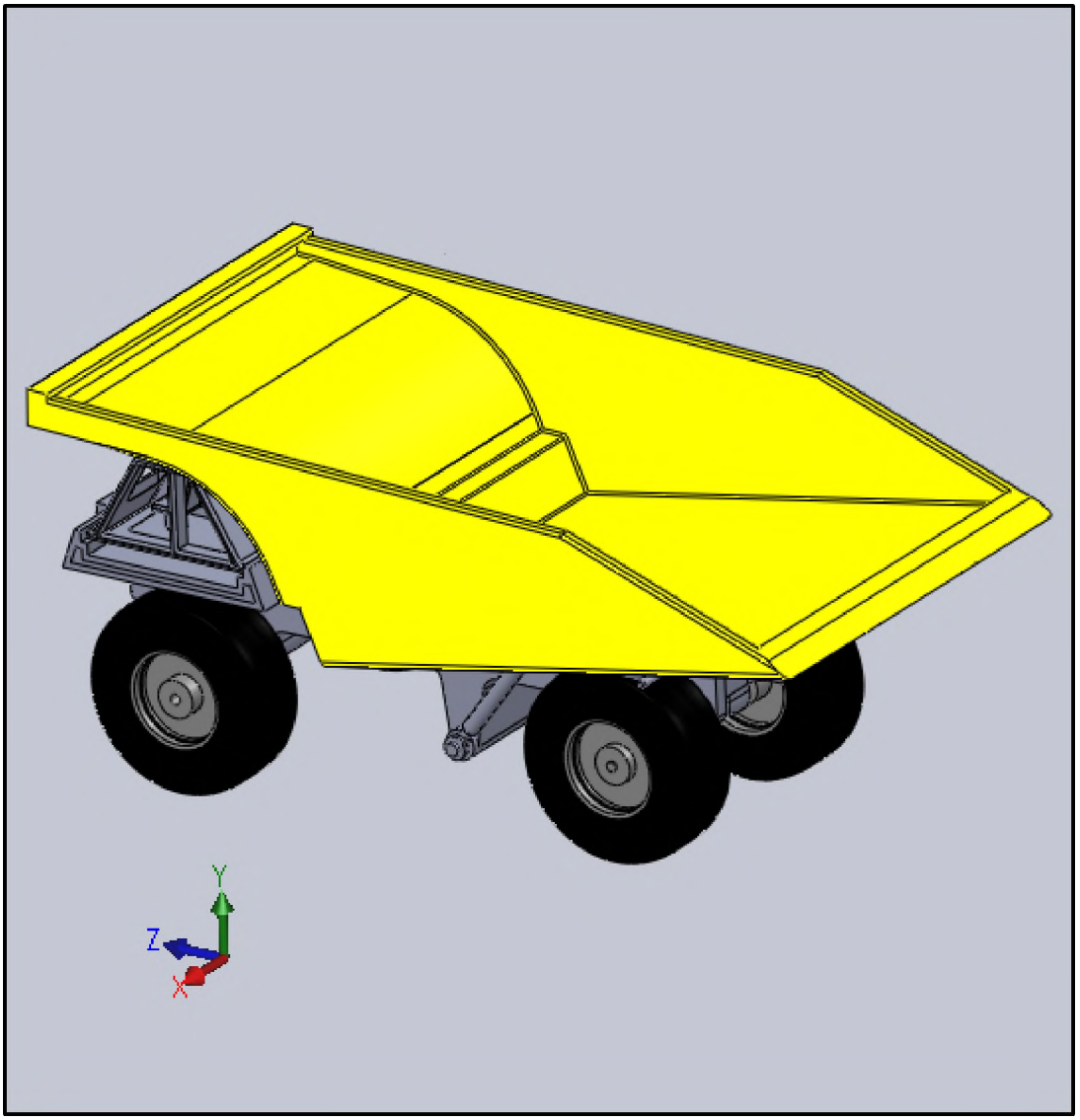

Figure 4.3. CAD 3D Geometry for CAT 793D Haul Truck

4.3. HIGH IMPACT SHOVEL LOADING OPERATION SIMULATION SETUP

The virtual simulation of the HISLO process was carried out using the FEA-DEM methodology, which requires proper meshing of the CAD geometries. Finer meshes are required for complex geometries, which in turn exponentially increases the computational times. Therefore, a prototype model consisting of the truck bed and a simplified shovel dipper were used for virtually simulating the shovel dumping operation. Figure 4.5 shows the simplified prototype model, which was imported into ABAQUS for designing the HISLO process. Figure 4.6 displays the interaction of the shovel dipper with the truck bed surface and the edges. Impact force is generated as the dipper door rotates and the rock/soil material drops under gravity at the truck bed surface. Proper dumping height ensures the minimum clearance between the dipper door and the truck body edges. Failure to maintain the minimum distance would result in dipper door impacting the truck edges thus causing excessive jolting and jarring in addition to the structural damage to both the shovel dipper and body of the haul truck.

The virtual prototype simulation was designed as a two-step process. The DEM technique is the most efficient and accurate methodology for analyzing any process involving a large amount of interacting small granular particles that are in contact with each other, and with other surfaces. A HISLO process involves loose rock/soil material dumped under gravity from the shovel dipper onto the truck bed surface. Therefore, it requires a coupled DEM-FEM [102] technique for an accurate modeling of the process. The DEM technique is used to analyze the system behavior by computing and analyzing the motion of individual particles. The shovel dipper payload was simulated using the DEM technique. This ensures that the true HISLO process is captured because it allows the creation of individual particles with specific properties, which interact with each other, and

with neighboring structural surfaces. ABAQUS was employed as the FEM prototyping platform.

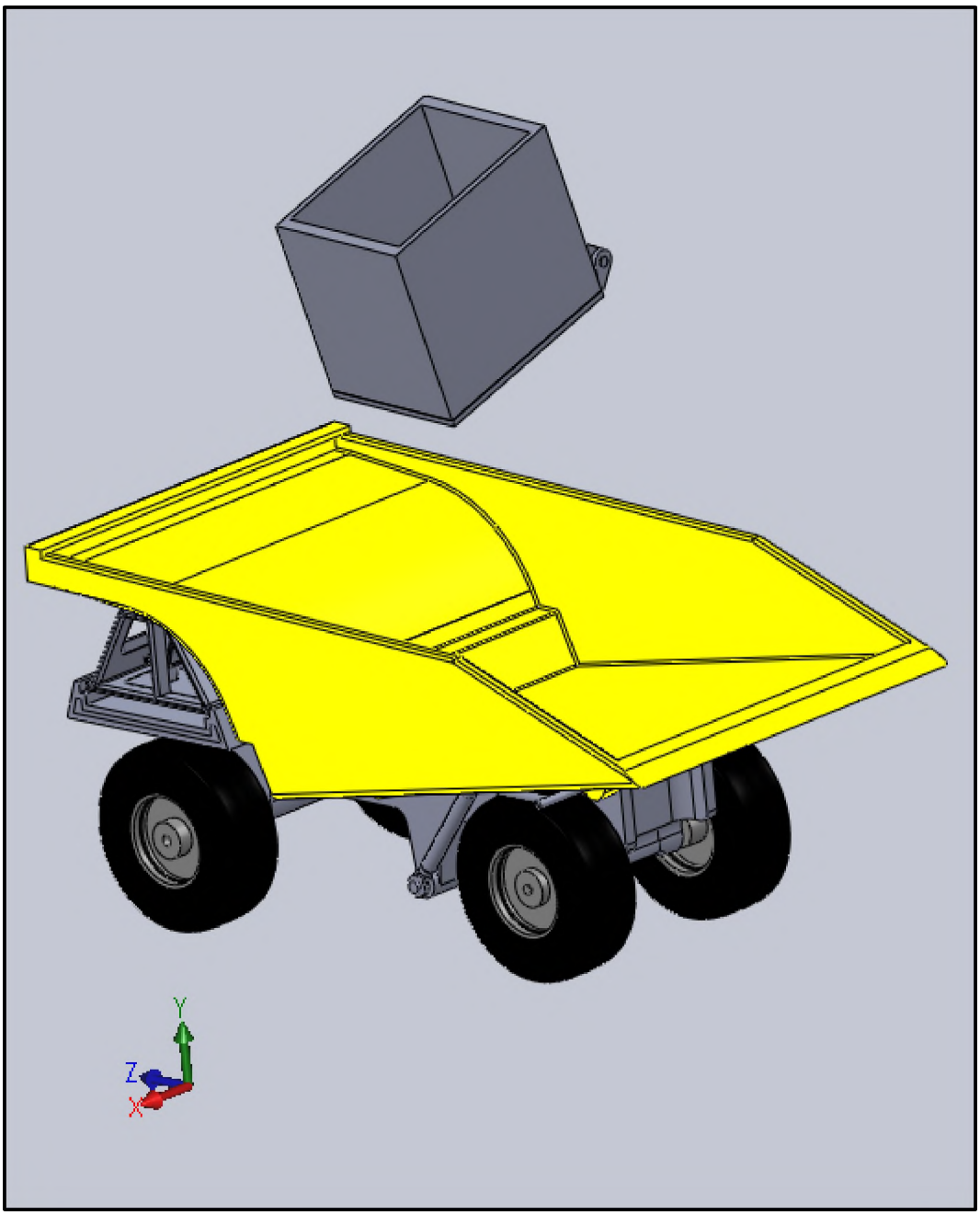

Figure 4.4. 3D Virtual Prototype Assembly representing the Shovel Dumping Operations

The DEM extension was used for particle flow dynamic simulation. Impact force, generated from the interaction between the dumped materials and the truck bed surface was recorded, processed, and analyzed using the coupled FEA-DEM methodology within the ABAQUS software environment.

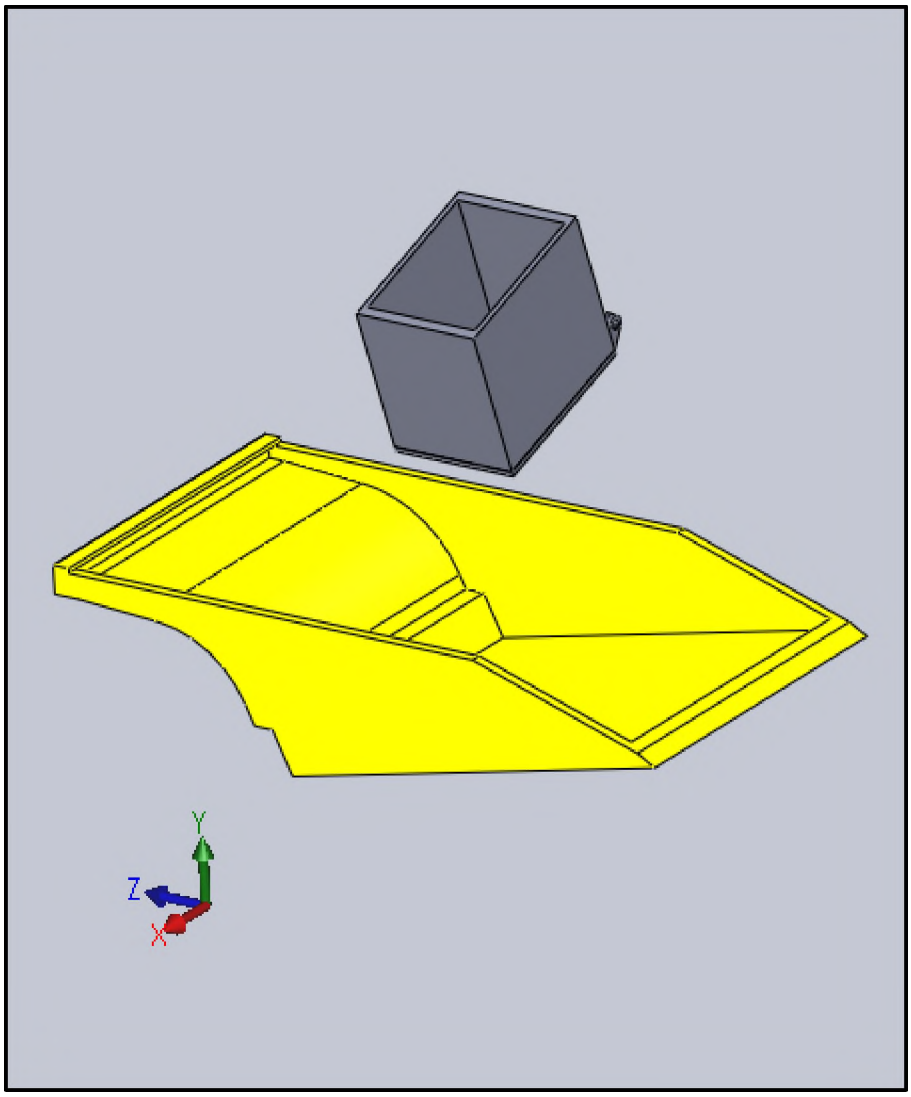

Figure 4.5. Simplified 3D Virtual Prototype Model for HISLO Simulation

Each particle within the rock/soil material, representing an individual grain, in the shovel dipper was modelled as a single-node PD3D element. Particulate rock/soil material with randomly distributed grains was created at an approximate initial position within the shovel dipper domain. The DEM elements, representing the individual particles, use existing ABAQUS functionality to reference element-related features, such as initial conditions, distributed loads, and visualization.

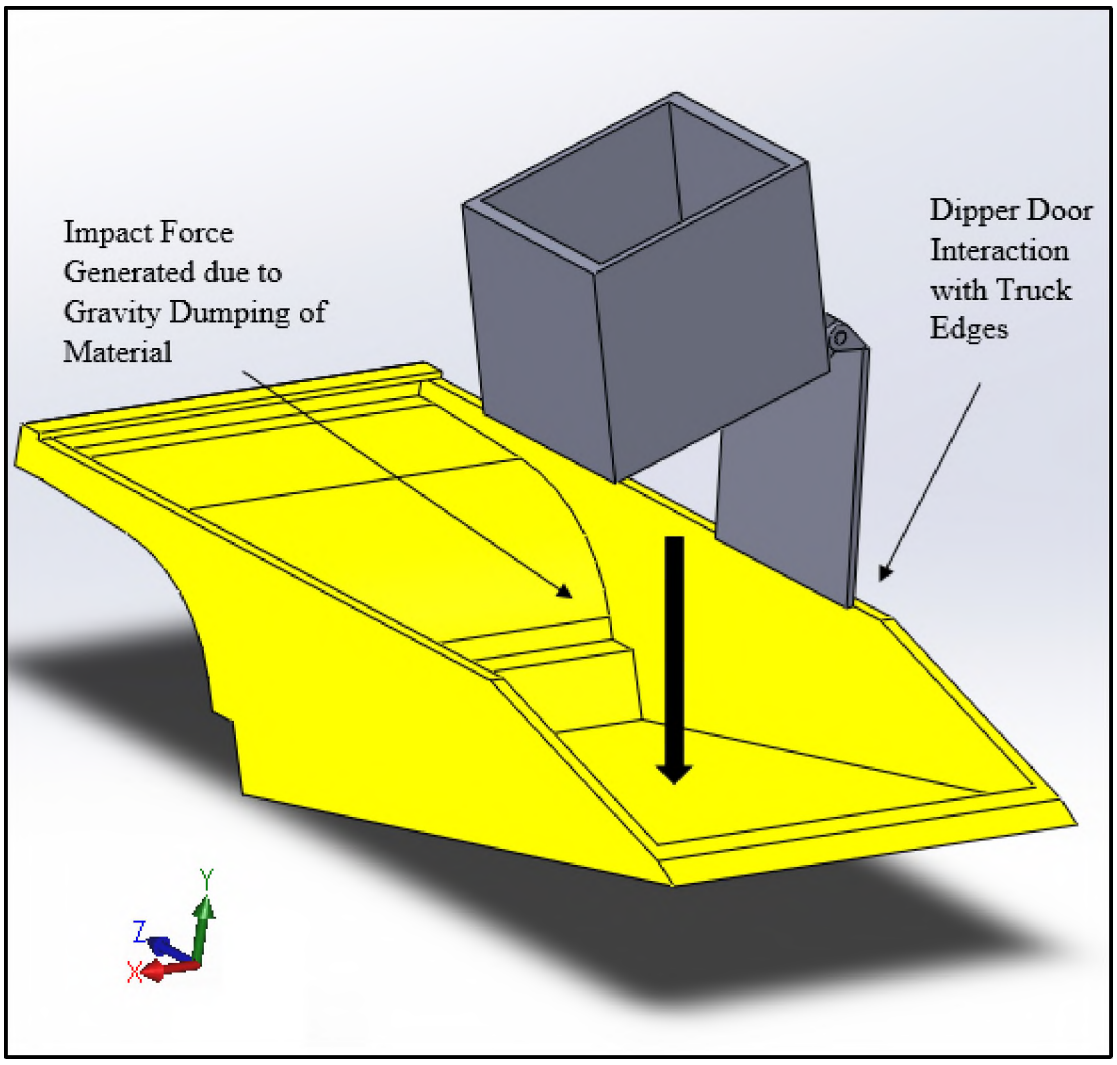

Figure 4.6. Haul Truck and Shovel Dipper Force Interaction

The PD3D elements are Lagrangian elements, and thus these particle nodes can be involved in other features, such as connectors or constraints. The center location of the physical grain within the material was used to reference the approximate coordinates of the node of a particle element while ensuring element-node creation inside the predefined particle tracking box. Overlaps, if any, among the DEM particles upon creation were removed through element re-arrangement. The whole assembly was kept stationary while allowing all the DEM particles to settle under gravity. As the particles losses their kinetic energy and the system is brought into an equilibrium, the particles settle inside the shovel dipper representing a single shovel pass. Material properties were assigned to each component of the virtual prototype, including the rock/soil material.

The material was generated inside the dipper to ensure 100 tons of combined weight for rock/soil material. Impact force and stress development at the truck body surface were recorded for each shovel pass. An accurate representation of the shovel dumping operation requires proper continuous flow dynamics as the rock/soil material drops and settles onto the truck bed surface. Establishing the proper contacts between DEM particles is of prime importance to ensure the accurate continuous flow dynamics for the gravity dumping of material. From the objectives of the study, the development of impact forces on the truck bed surface was very important within the overall dynamic simulation framework. Therefore, the meshing in ABAQUS for the truck body was optimized to ensure proper capturing of the impact forces at its surface. Proper slicing/bisection of the curved surfaces was done in order to eliminate any element distortion. Fine tetrahedral type elements were used to represent the meshed truck body. Figure 4.7 shows the meshed prototype model for

the shovel dumping operation. Meshes for shovel dipper and door were simplified in order to reduce computational time and resources.

Table 4.2. Material Properties for DEM in ABAQUS

Property	**Value**
Normal Stiffness	0.5×10^8 N/m
Coefficient of Friction	0.35
Mass Proportional Damping	5%
Porosity	0.32
Density	2500 kg/m^3
Radius	0.149 m

The simulation started with the generation of material particles, with properties specified in Table 4.2, in the form of spherical balls inside the dipper for each shovel pass. The material density and radius of the individual particles were fixed at 2500 kg/m^3 and 0.149 m, respectively, with random element creation ensuring a total weight of 100 tons. Contact inclusions were used to model the contacts among individual DEM particles, which required that the particles be explicitly included in a general contact as element-based surfaces. The DEM technique models particles as rigid, and thus, contact stiffness was used to account for the physical stiffness characteristics of the DEM particles. Hertz contact model [106] was used to establish the contacts among individual discrete element particles and the shovel dipper walls, truck bed surface, and individual discrete element particles. The contact force, based on the Hertz contact model, is given by equation (4.2). This force depends on the mean effective radius of interacting assembly, approach distance, and the mean effective elastic stiffness. The normal contact stiffness, given by equation

(4.5), is defined as the spring stiffness that acts in contact normal direction as the particles interact with each other, and with the neighboring structural surfaces of the truck bed and the shovel dipper.

$$F = \frac{4}{3} E^* \sqrt{R} \sqrt{\delta^3} \tag{4.2}$$

$$R = \frac{R_1 R_2}{R_1 + R_2} \tag{4.3}$$

$$\frac{1}{E^*} = \frac{1 - {v_1}^2}{E_1} + \frac{1 - {v_2}^2}{E_2} \tag{4.4}$$

$$K_n = 2E^* \sqrt{R} \sqrt{\delta^3} \tag{4.5}$$

Where,

E_1, E_2 = Young's modulus of the two contacting particles

v_1, v_2 = Poisson's ratio of the two contacting particles

R_1, R_2 = Radii of the two contacting particles

δ = Particle contact approach distance

Stability and accuracy of the DEM analysis requires an appropriate time increment size selection, which depends on several different factors. These factors include the specified contact properties, grain size of DEM particles, and the relative motion of the particles. The controlling factors for a stable time increment are problem dependent and vary during the analysis, which makes the appropriate direct time increment selection for a DEM analysis difficult. In ABAQUS, with the definition of the Hertz pressure overclosure, ABAQUS/Explicit automatically controls the time increment size to achieve a stable and accurate solution to the problem system. Out of all the criteria stability dictates the time increment, when particles are confined and subjected to compression. However, with fast-moving and impacting particles, the duration of collision criterion may control the time increment. For collisions with low to moderate particle speed, the scaling factor applied to each of the above criterion is based on numerical experimentation. Contact stiffness increases rapidly for the impact collisions involving high-speed particles. Thus, the scaling factors related to the Rayleigh wave and collision duration require significant reduction.

Once the particles were generated with the specified properties within the given restricted domain, the contacts were established, and the gravity load was activated to allow the free settlement of particles in order to reach equilibrium. Mass proportional alpha damping of 5% was applied to reduce the solution noise generated by numerous opening and closing of contact conditions. The first step of simulation ended as soon as the DEM material particles completely settled inside the P&H 4100 XPC shovel dipper.

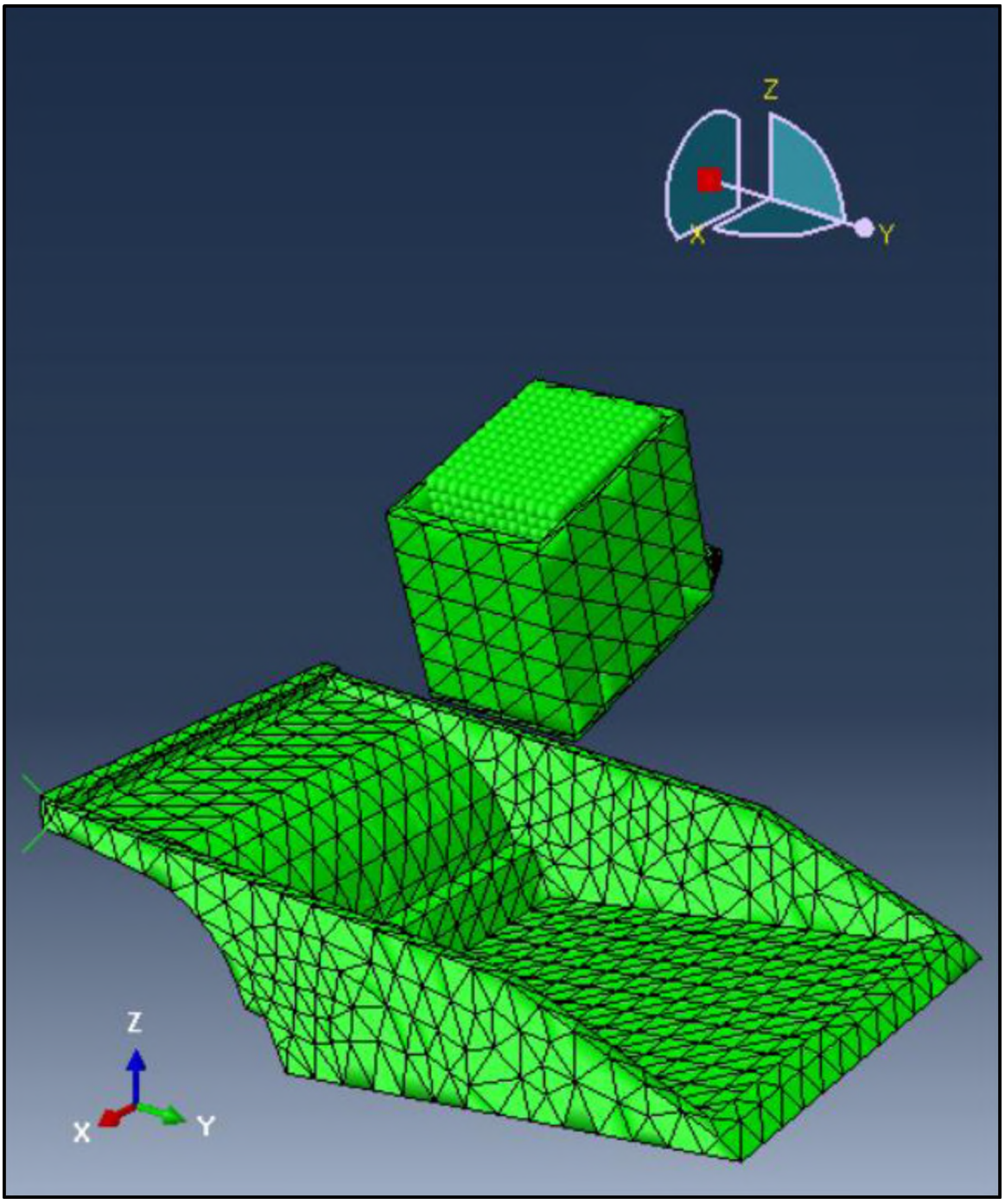

Figure 4.7. Meshed Prototype Model with DEM Particles in ABAQUS

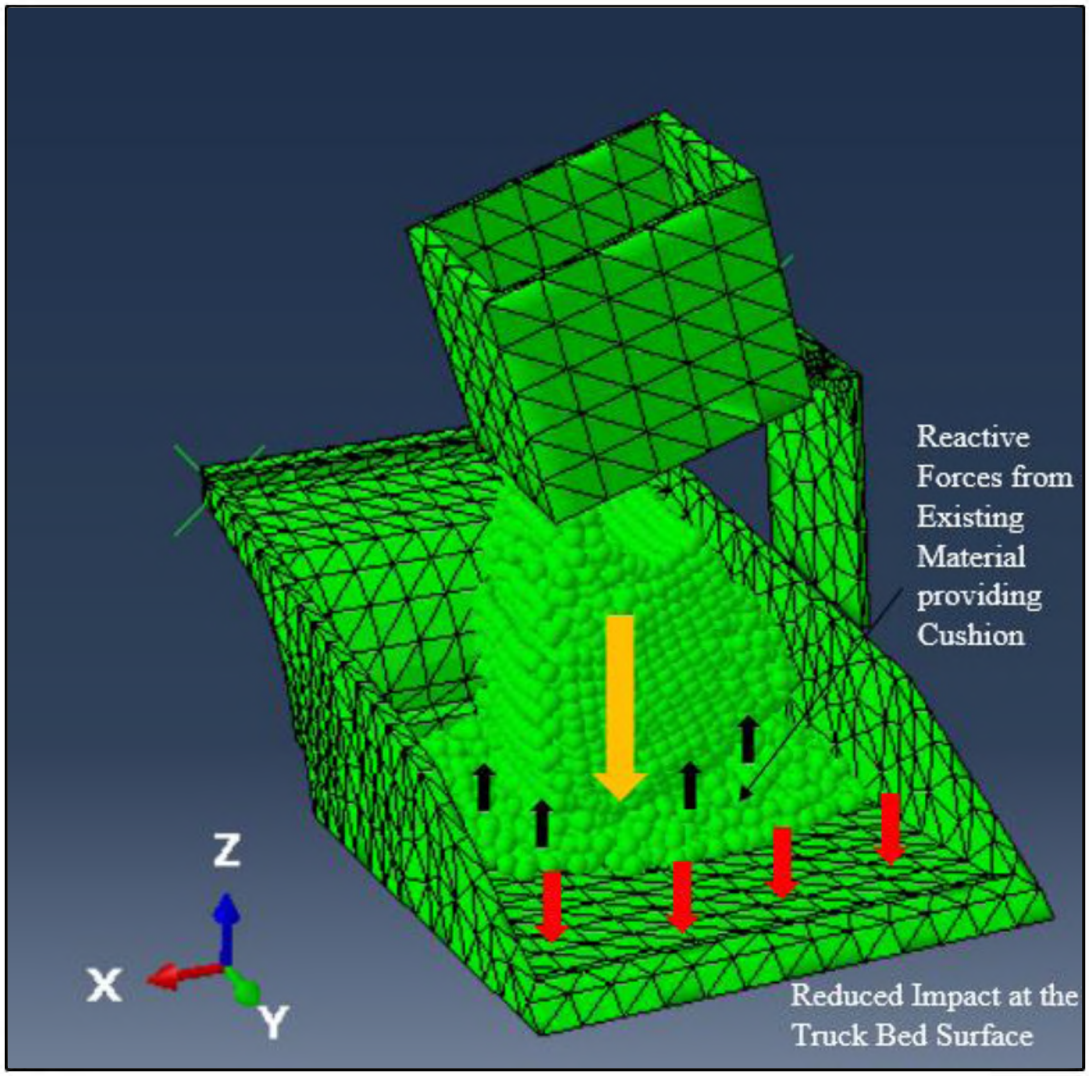

Figure 4.8. Schematic for Dynamic Forces during Second Shovel Pass

The second step of the simulation dealt with the dumping process where the rotation was activated on the shovel dipper door resulting in the opening of shovel dipper and the falling of rock/soil particles onto the truck bed surface. During that dumping step of simulation, DEM dealt with the kinematics of soil/rock particles as they move under gravity along with the contact dynamics of the particles. In DEM, particle-particle interaction is considered a dynamic process that reaches equilibrium whenever the internal forces balance. So the movement of all individual particles is traced and the contact forces

and displacements of a stressed assembly is computed at every time step. DEM is based on the idea that the time step chosen may be so small that, during a single time step, disturbances cannot propagate further from any particle than its immediate neighbors. The DEM calculations alternate between the application of Newton's second law to the particles and a force-displacement law at the contacts. Newton's second law is used to determine each particle motion from the contact and body forces acting on it, while the force-displacement law is used to update the contact forces arising from the relative motion at each particle contact.

FEA is used when those rock/soil particles, falling under gravity, contacts the walls and surfaces of the shovel dipper initially, during the first step of the simulation, and then the haul truck during the second step. FEA approximates the solution to the higher order differential equations of the system. The iterative process was repeated for each element in the FE mesh for solution approximation of the system. The computed displacement, velocity and acceleration vectors of each element generated the internal structural forces and stresses at the truck bed surface. The generation and progression of the impact force at the truck bed surface was recorded until all the particles had settled and the whole system was brought to rest. That marked the end of simulation process for the first shovel pass. The whole process was repeated for the second shovel pass where the dipper swung back to the bench, dug another round of material, swung back to the truck, and then dumped the load on to the truck bed surface. Figure 4.8 shows the schematic for the interactive forces during the second shovel pass. Since the immediate past process was the second pass, the material from the first shovel pass formed a cushioned body that absorbed the shock from the second shovel pass material. As a result of that cushion provided by the material from

the first shovel pass, the impact recorded at the truck bed surface is reduced during the second shovel pass.

4.4. SUMMARY

This section described the detailed construction and development of the virtual prototype model for simulating the HISLO process. The main objective was to capture the generation and progression of the dynamic impact force on the truck bed surface during multi-pass shovel dumping process.

The virtual prototype was designed for simulating the dumping process involving CAT 793D haul truck and P&H 4100XPC cable shovel. The CAD geometry for the model was created within SOLIDWORKS using the proper dimensions for the actual CAT 793D truck and P&H 4100 XPC dipper. The whole assembly for the model was put together by maintaining the accurate position of each component relative to the adjoining component(s). Since the HILSO dumping process involves loose rock/soil material dumped under gravity from the shovel dipper onto the truck bed surface, the DEM technique was used in conjunction with the FEM technique for an accurate representation of the process. ABAQUS was employed as the prototyping platform using the coupled FEA-DEM methodology.

Multi-pass shovel dumping process was simulated and the impact force at the truck bed surface was recorded for each pass. The cushioning effect was observed during any subsequent pass as the material from the previous pass(es) reduced the impact at the truck bed surface.

5. EXPERIMENTAL DESIGN & DETAILED EXPERIMENTATION

This section presents the detailed description for the experimentation conducted for simulating the shovel dumping process and modelling the dynamic impact force at the truck bed surface. The efficiency, effectiveness and accuracy of the new mathematical model were tested initially. The virtual simulator was then used to conduct detailed experimentation to investigate the impact force dynamics under varying operating conditions and material properties. The results were then used for verification and validation of the mathematical model, and for the development of an intelligence-based framework for real-time implementation of impact force monitoring using AI and machine learning latter.

5.1. EXPERIMENTAL DESIGN FOR MATHEMATICAL MODEL TESTING

Numerical testing was conducted following the development of the generalized mathematical model, presented in Section 3. The developed EOMs for the complete vibration system were solved to obtain the displacement vectors. Then using the complete solution for the system, '$\vec{z}_2(t)$' were differentiated twice to transform the displacement expression for the truck body into the acceleration vectors. The final impact force was obtained after multiplying the acceleration field with the mass of the truck body section. The model was then used to capture and visualize the force generation and progression for a multi-shovel pass HISLO operation.

MAPLE was used as the programming platform for conducting the mathematical model testing. The system EOMs were developed and solved using the advanced computing libraries available in MAPLE and with a user-defined programing section. Input

variables, required for solving the complex differential equations (DEs), were obtained from a real-world high impact shovel loading operation.

Experiments were designed for investigating the multi-pass shovel dumping operation. Impact forces, resulting from the gravity dumping of rock/soil material, were recorded and visualized. The cushioning effect due to previously dumped material was also captured and analyzed during every subsequent shovel pass.

5.2. EXPERIMENTAL DESIGN FOR VIRTUAL HISLO SIMULATION

The virtual prototype model, designed in Section 4, was used to conduct detailed experimentation for understanding the dynamic impact force using proper continuous flow dynamics. Multi-pass shovel dumping process was virtually simulated using the FEA-DEM coupled methodology. A high impact shovel dumping process involves dumping of loose rock/soil material under gravity onto the truck bed surface. An accurate capturing of the flow dynamics under gravity is important to model the dynamic impact forces with the utmost precision. DEM allows the modelling of loose rock/soil material as individual particles/grains, which interact with each other and with the neighboring structural surfaces.

ABAQUS was employed as the FEM prototyping platform and its DEM extension was used for particle flow dynamic simulation. Two shovel pass dumping process was designed with each pass being a two-step process. The first step dealt with the generation of DEM particles within the shovel dipper domain and the activation of the contact interactions. The system was then brought to rest with particles completely settled inside the shovel dipper. The second step dealt with the gravity dumping of material into the truck bed surface. Impact force was captured until the material was completely settled onto the

truck bed surface. After the completion of the first shovel pass, the shovel dipper dug another round of material and then the same process was repeated when simulating the second shovel pass. However, this time the material contacted the previously dumped material, so that the system can observe and capture the cushioning effect.

Detailed HISLO experiments were designed and conducted for three primary purposes. Firstly, the research seeks to investigate the generation and progression of dynamic impact force at the truck bed surface using the proper continuous flow dynamics with FEA-DEM methodology. Secondly, the research seeks to verify and validate the mathematical model for capturing the impact force for a multi-pass shovel dumping operation. Thirdly, the research seeks to gather data for designing and training a deep learning model for impact force monitoring and, to evaluate it against the four most widely used machine learning algorithms. The detailed understanding of the impact force generation and progression was used to design the solution strategies for reducing the forces and controlling the WBV at the operator seat during HISLO.

5.3. DATA ACQUISITION FOR DEEP LEARNING AND AI MODELS

Deep learning and AI algorithms require sufficient data, pertaining to the operation, for any sort of model development. Therefore, experiments were conducted using the virtual prototype simulator in ABAQUS to acquire data that provided insight into impact force generation during a HISLO process. The insight was then used by the deep learning model to learn the underlying pattern for the impact force prediction. Impact force in a shovel dumping operation essentially depends on the amount of load the shovel dipper is dumping, the type of material being dumped, and the height from which the shovel is

dumping the load, given that the environmental and ground conditions remain the same [9].

A total of 1120 experiments were conducted to examine the resulting impact force on the truck bed surface during a HISLO process. Considering the dependencies of the impact force, as described above, the following conditions were varied which served as the input parameters during the experimentation: density of material, porosity of the material, dipper fill (percentage of the dipper space filled), and the dumping distance. In order to ensure general applicability, a wide range of rock/soil materials were tested, with density ranging from 1500 to 2700 kg/m^3 and porosity ranging from 0.2 to 0.5. Considering a variety of shovel operators and digging conditions, the dipper fill was varied from 88% to 102% for each of those materials. Variation of dumping distance plays a key role in impact force generation; therefore, the dumping distance was varied between 7.3 m and 4.3 m for each of those material type and dipper fill variation. Impact force generated on the truck bed surface was recorded as a single output for every experiment. Data acquired through the detailed experimentation was then used as the training and testing data for the models.

5.4. EXPERIMENTATION FOR MATHEMATICAL MODEL TESTING

Numerical techniques were employed to solve the six second coupled DEs representing the HILSO vibration process. The inclusion of damping not only made the model more representative of a real-world phenomenon but also resulted in the coupled DEs, which increased the model complexity. The first step in solving such a system was to find the solution to the Eigen value problem for the undamped system. The solution resulted in natural frequencies and Eigen vectors of the system, which were later used to

compute the actual damped frequencies and generalized displacements of the 6 DOF forced vibration system. Equation (5.1) gives the EOM for the undamped system.

$$\vec{M}\,\ddot{\vec{z}}(t) + \vec{K}\,\vec{z}(t) = 0 \tag{5.1}$$

Equation (5.3) was obtained by substituting the general solution, equation (5.2) to the free vibration problem in equation (5.1). For simplification of the computation, $\lambda = \omega_{ni}^2$ was substituted in equation (5.3), which resulted in equation (5.4).

$$\vec{z}_i(t) = Z_i e^{j\omega_{ni}t} \tag{5.2}$$

$$\left[\vec{K} - \omega_{ni}^2\,\vec{M}\right] Z_i e^{j\omega_{ni}t} = \vec{0} \tag{5.3}$$

$$\left[\vec{K} - \lambda\,\vec{M}\right] Z_i e^{j\omega_{ni}t} = \vec{0} \tag{5.4}$$

Equation (5.4) can have a non-trivial solution if and only if the determinants of the coefficients are set to zero. Equation (5.5) was obtained by setting the determinant of the 6 x 6 matrix, i.e., $\left[\vec{K} - \lambda\,\vec{M}\right]$, to zero.

$$\begin{vmatrix} K_1-\lambda m_1 & -K_1 & 0 & 0 & 0 & 0 \\ -K_1 & K_1+K_2-\lambda m_2 & -K_2 & 0 & 0 & AK_2 \\ 0 & -K_2 & e^*-\lambda m_3 & -K_{3f} & -K_{3r} & f^* \\ 0 & 0 & -K_{3f} & K_{3f}+K_4-\lambda m_4 & 0 & -BK_{3f} \\ 0 & 0 & -K_{3r} & 0 & K_{3r}+K_5-\lambda m_5 & DK_{3r} \\ 0 & AK_2 & f^* & -BK_{3f} & DK_{3r} & g^*-\lambda I \end{vmatrix} = \begin{Bmatrix} 0 \\ 0 \\ 0 \\ 0 \\ 0 \\ 0 \end{Bmatrix} \quad (5.5)$$

The Gaussian elimination method was used to compute the determinant of equation (5.5) in MAPLE, which resulted in the characteristic equation of order 6 in terms of 'λ', given by equation (5.6).

$$Y_1\lambda^6 + Y_2\lambda^5 + Y_3\lambda^4 + Y_4\lambda^3 + Y_5\lambda^2 + Y_6\lambda + Y_7 = 0 \quad (5.6)$$

The terms Y_1, Y_2, Y_3, Y_4, Y_5, Y_6, and Y_7 are the coefficients of characteristic equation involving 720 terms that were computed using the numerical modelling platform, MAPLE. Equation (5.6) is the general symbolic characteristic equation for the 6-DOF HILSO vibration problem. This equation can be solved using any numerical method, including Newton Raphson method, Taylor Series expansion, and Steffensen's method.

The natural frequencies of the system were obtained by solving equation (5.6) for 'λ', which were then used to compute the corresponding Eigen vectors/normal modes '$\vec{u}_j(t)$' of the system. Those Eigen vectors/normal modes were then used to obtain the normalized modal matrix 'P,' which were further used to develop the solution of the 6-DOF HILSO vibration system given by equation (3.30).

The damped frequencies 'ω_{di}' in equation (3.30) and the damping constant 'ζ_i' were obtained through equations (3.27) and (3.24), respectively. Firstly, 'α' and 'β' were derived using equation (3.17) with inserting proper matrices '$\vec{M}$', '$\vec{C}$' and '$\vec{K}$', for the particular truck under investigation, in order to compute the solution for the corresponding HILSO operation.

From the obtained complete solution of the truck vibration, the modal displacement for truck body, given by '$\vec{z}_2(t)$', and the mass of the particular truck body section under investigation were used to obtain the final mathematical model for the impact force at the truck body. That final mathematical model was then plotted over shovel dumping process to investigate the generation and the recorded magnitudes of the dynamic impact force in a HISLO operation.

Experimentation for a specific scenario was conducted as a sequel to the solution of the final impact force mathematical model. Specifically, the experiment entailed the loading of a CAT 793D dump truck by a P&H 4100 XPC shovel with multiple shovel passes. Tables 5.1 and 5.2 give the specifications in terms of truck component masses along with the spring-damper characteristics given by spring constant and damping coefficients.

Using the specifications and spring-damper characteristics for each component of the truck, the EOMs were derived for the 6-DOF undamped free HISLO vibration system, as given by equation (5.7). Substituting equation (5.2) into equation (5.7), simplifying and setting the determinant to zero yielded the characteristic equation for the HISLO complete system, consisting of a six-degree polynomial in terms of '$\lambda = \omega_{ni}$', as given by equation (5.8).

Table 5.1. Mass Properties for Various Components of CAT 793D Truck

Truck Component	**Mass (kg)**
Total Weight	383,749
Truck Body	54,431
Chassis	116,707
Tire/Axle/Wheel Assembly	8651.83

Newton Raphson method was used to solve the six-order characteristic function in equation (5.8) to obtain the Eigen values for the system, which corresponded to the natural frequencies, as given by Table 5.3. Using the computed Eigen values and equation (5.7), normalized Eigen vectors for the particular 6-DOF HISLO system were computed. The matrix 'P', containing the Eigen vectors/Normal modes, is given by equation (5.9).

$$\begin{bmatrix} 90718.5 & 0 & 0 & 0 & 0 & 0 \\ 0 & 54431 & 0 & 0 & 0 & 0 \\ 0 & 0 & 116707 & 0 & 0 & 0 \\ 0 & 0 & 0 & 8651.83 & 0 & 0 \\ 0 & 0 & 0 & 0 & 8651.83 & 0 \\ 0 & 0 & 0 & 0 & 0 & 1608913.4 \end{bmatrix} \begin{Bmatrix} \ddot{z}_1 \\ \ddot{z}_2 \\ \ddot{z}_3 \\ \ddot{z}_4 \\ \ddot{z}_5 \\ \ddot{\theta} \end{Bmatrix} + \tag{5.7}$$

$$\begin{bmatrix} 3.22\times10^{7} & -3.22\times10^{7} & 0 & 0 & 0 & 0 \\ -3.22\times10^{7} & 3.25\times10^{7} & -273700 & 0 & 0 & 303807 \\ 0 & -273700 & 3.094\times10^{6} & -1.224\times10^{6} & -1.596\times10^{6} & -1.4021\times10^{6} \\ 0 & 0 & -1.224\times10^{6} & 1.274\times10^{6} & 0 & -3.6139\times10^{6} \\ 0 & 0 & -1.596\times10^{6} & 0 & 1.646\times10^{6} & 4.7122\times10^{6} \\ 0 & 303807 & -1.40214\times10^{6} & -3.6139\times10^{6} & 4.712\times10^{6} & 2.492\times10^{7} \end{bmatrix}$$

$$\begin{Bmatrix} z_1 \\ z_2 \\ z_3 \\ z_4 \\ z_5 \\ \theta \end{Bmatrix} = \begin{Bmatrix} 0 \\ 0 \\ 0 \\ 0 \\ 0 \\ 0 \end{Bmatrix}$$

Table 5.2. Spring-Damper Characteristics of CAT 793D Truck

Truck Component	**Spring Constant (N/m)**	**Damping Coefficient (Ns/m)**
Truck Body	2.15 x 10^6	2.737 x 10^5
Suspension System (Rear)	1.927 x 10^7	1.596 x 10^6
Suspension System (Front)	1.327 x 10^7	1.224 x 10^6
Tires (Rear/Front)	8.945 x 10^4	5 x 10^4

$$\lambda^6 + 201.16\lambda^5 - 379077.45\lambda^4 + 238766721.3\lambda^3 - 7708001467.2\lambda^2 + 11132095744.45\lambda - 3855887685.5 = 0 \quad (5.8)$$

$$P = \begin{bmatrix} -0.0008129 & -0.503531 & 0.002710 & 0.416950 & -0.482471 & 0.124902 \\ 0.002891 & 0.862174 & -0.005777 & 0.392354 & -0.481981 & 0.124690 \\ -0.078191 & -0.005169 & 0.068037 & -0.460027 & -0.379250 & 0.326616 \\ 0.054040 & -0.048916 & -0.994382 & -0.351829 & -0.153428 & 0.879366 \\ 0.995356 & -0.026290 & 0.079054 & -0.579076 & -0.601453 & -0.230550 \\ 0.014941 & 0.001219 & 0.016893 & 0.038369 & 0.076154 & 0.189040 \end{bmatrix} \quad (5.9)$$

Table 5.3. Eigen Values for the Undamped HISLO Vibration System

DOF	**Eigen value**
1	2511.29157488308
2	1494.87449062042
3	1725.99573257569
4	32.5134030331735
5	0.558992766633338
6	0.938347424931986

The inclusion of damping increased the complexity of the system and made the EOM of the coupled system, as stated in Section 3. The Rayleigh method was used to de-couple the complex EOM of the 6-DOF vibration system for this particular case using equation (3.17). The parametric values of the Rayleigh proportional damping coefficients (α and β) were computed, as given by equation (5.10). Substituting the coefficient values in equation (3.17), the viscous damping equation was derived, as given by equation (5.11).

Based on equation (5.11), it was concluded that the damping of this system was stiffness proportional with damping forces occurring parallel to the elastic forces. The system may, thus, be called internally damped.

$$\left.\begin{matrix} \alpha = 0 \\ \beta = 0.644 \end{matrix}\right\} \tag{5.10}$$

$$\vec{C} = 0.644\,\vec{K} \tag{5.11}$$

Equation (5.3) was used to de-couple the complex EOMs. Then it was multiplied with $\vec{P}^T$ (the transpose of the model matrix $\vec{P}$) given by equation (3.20). The final de-coupled EOMs for the 6-DOF HILSO vibration system were then derived as given by equation (5.12).

$$\begin{bmatrix} 9670.15 & 0 & 0 & 0 & 0 & 0 \\ 0` & 63494.26 & 0 & 0 & 0 & 0 \\ 0 & 0 & 9610.85 & 0 & 0 & 0 \\ 0 & 0 & 0 & 55189.28 & 0 & 0 \\ 0 & 0 & 0 & 0 & 63212.12 & 0 \\ 0 & 0 & 0 & 0 & 0 & 79357.88 \end{bmatrix} \begin{Bmatrix} \ddot{q}_1 \\ \ddot{q}_2 \\ \ddot{q}_3 \\ \ddot{q}_4 \\ \ddot{q}_5 \\ \ddot{q}_6 \end{Bmatrix} + \tag{5.12}$$

$$\begin{bmatrix} 2055908.99 & 148300.20 & -12579.17 & -19612.28 & -25959.32 & -7757.46 \\ 148300.20 & 60267794.07 & -321263.80 & -866779.43 & 18226.56 & -9033.81 \\ -12579.17 & -321263.80 & 1573157.94 & 14803.02 & 4316.22 & -37261.36 \\ -19612.28 & -866779.44 & 14803.02 & 261747.07 & 15237.11 & -6664.07 \\ -25959.32 & 18226.56 & 4316.22 & 15237.11 & 19374.97 & 142.21 \\ -7757.46 & -9033.81 & -37261.36 & -6664.07 & 142.22 & 41377.53 \end{bmatrix}$$

$$\begin{Bmatrix} \dot{q}_1 \\ \dot{q}_2 \\ \dot{q}_3 \\ \dot{q}_4 \\ \dot{q}_5 \\ \dot{q}_6 \end{Bmatrix} +$$

$$\begin{bmatrix} 24284553.45 & 0 & 0 & 0 & 0 & 0 \\ 0 & 94915949.41 & 0 & 0 & 0 & 0 \\ 0 & 0 & 16588283.01 & 0 & 0 & 0 \\ 0 & 0 & 0 & 1794391.30 & 0 & 0 \\ 0 & 0 & 0 & 0 & 35335.12 & 0 \\ 0 & 0 & 0 & 0 & 0 & 74465.26 \end{bmatrix}$$

$$\begin{Bmatrix} q_1 \\ q_2 \\ q_3 \\ q_4 \\ q_5 \\ q_6 \end{Bmatrix} = \begin{Bmatrix} 0.0008129F_1(t) \\ 0.5035312F_1(t) \\ 0.0027104F_1(t) \\ 0.4169504F_1(t) \\ 0.4824707F_1(t) \\ 0.1249023F_1(t) \end{Bmatrix}$$

As part of model validation, the final de-coupled EOMs, given by equation (5.12), and the standard general model derived in equation (3.23) were compared. The coefficients of generalized coordinates 'q_i' were found to be in accordance with the square of the natural frequencies 'ω_{ni}^2' of the system, as presented in Table 5.4. The damping constant

values for the system derived by utilizing equation (3.24) and equation (5.12) for the vibration system are also given in Table 5.4.

To solve for the actual damped HISLO vibration problem, the complete decoupled EOMs, given by equation (5.12), were solved using Laplace transformation. The resulting equations were then solved and simplified using the system's initial condition, given by equation (5.13). Inverse Laplace transformation was then done, using the transfer function, given by equation (5.14), along with the convolution integral, to obtain the 6 modal participation coefficients for HISLO vibration system.

Table 5.4. Natural Frequencies and Damping Constants for the Vibration System

Natural Frequency, ω_{ni} (rad/sec)	**Damping Constant**
ω_{n1}= 50.113	ζ_1= 2.12
ω_{n2}= 38.663	ζ_2= 12.28
ω_{n3}= 41.545	ζ_3= 1.97
ω_{n4}= 5.702	ζ_4= 0.42
ω_{n5}= 0.748	ζ_5= 0.21
ω_{n6}= 0.969	ζ_6= 0.27

$$q_i(0) = \dot{q}_i(0) = \ddot{q}_i(0) = 0 \tag{5.13}$$

$$TF = \frac{1}{s^2 + 2\zeta_i\omega_{ni} + {\omega_{ni}}^2} \tag{5.14}$$

The resulting six modal participation coefficients, along with the normal mode matrix in equation (5.40), were then used to obtain the final displacement vector '$\vec{z}(t)$' for the complete vibration system.

Finally, the impact force profile for the truck body was computed by using the 2nd order derivative of the displacement expression and the mass of the truck body for multi-pass shovel dumping operation.

5.5. MODEL CONVERGENCE, VERIFICATION, AND VALIDATION

Newton Raphson method was used for solving the characteristic equation of the 6-DOF HISLO system. It is the most powerful technique for solving any nonlinear equation or system of nonlinear equations of the form '$f(x) = 0$' [107]. The error tolerance of the magnitude 10^{-4} was set during the iterative approximation solution. Newton Raphson method approximated the roots through an iterative process involving the function and its derivate. For any given non-linear function that is differentiable with non-zero derivatives and with an initial approximation to the solution close enough to the neighborhood of one of the expected roots, Newton Raphson method guarantees the quadratic convergence with

a stable solution [108]. Quadratic convergence means that the number of the correct decimals in the solution approximation approximately doubles in each iteration. With the characteristic equation of the HISLO vibration system satisfying the underlying conditions, solution stability and the quadratic convergence to the exact roots was achieved during the numerical approximation. Solving the characteristic equation for 'λ' using the Newton Raphson method during the experimentation, provided the natural frequencies of the system which were then used to compute the corresponding Eigen vectors/normal modes '$\vec{u}_j(t)$' of the system.

Verification of the HISLO simulation model was done through a three-step process. Stability and solution convergence in FEA largely depends on the mesh quality or the correctness of constraint definition. So the first step in this verification of the virtual prototype model was done through ABAQUS, once the meshing was completed along with the specification of material properties, load definitions, boundary condition, and contact establishment. Datacheck function provided by ABAQUS/CAE allows for the inspection of every property or constraint definition based on the requested analysis output. It also allows for the identification of any mesh elements that could cause any convergence error/issue during FEA-DEM analysis. The model successfully passed the datacheck and mesh quality verification thus ensuring stability and solution convergence during simulation.

Then, for the second step in model verification, the complete HILSO operation was simulated and the animation was visualized. The inspection of the animation was done to ensure that the simulation model is actually representing the HISLO operation. The animation showed that the particles are generated inside the shovel bucket, the dipper

rotates as soon as the equilibrium is reached, then the whole material starts flowing down under gravity and drops onto the truck bed surface as a continuous material. That ensured the verification of the model that it is representative of the real-world shovel dumping operation and a proper truck loading system.

As part of the final step in the model verification process, the model results for HISLO process were reviewed. First, and foremost, plots for the reaction force generated by the truck bed surface were inspected. A total load of 100 tons for the rock/soil material is dumped during the process, and as the material starts falling down under gravity and contacts the truck bed surface, it would generate a reaction force to balance the external load from the material. As more material settles onto the truck bed surface the reaction force would increase in order to support the cumulative load. Since, a HISLO process is simulated, the rock/soil material with a total load of 100 tons is generated, therefore, once the material has completely dropped and settled onto the truck bed surface, it would support the entire load which would be equal to the total gravitational load imposed by the 100 tons of material. Based on this theory, the reaction force plot for the simulation experiment was inspected and it showed that the reaction force would increase and then eventually it would reach a point where its magnitude would be equal to the total gravitational load of the material, following that the curve would flatten out since all the material has completely fallen off and shovel pass has completed.

In this third and final model verification step, an important verification item is the profile for dynamic impact force recorded at the truck bed surface. Examination of the impact force profile, allowed the qualitative verification of the impact force generation and progression in addition to the validation for the simulation model to ensure that it

represented an actual real-world HISLO process. The impact force profile needed to be a continuous plot captured over the entire shovel pass. As the material contacted the truck bed surface, the force increased, then as the majority of the material dropped, the peak force was recorded. Then as the remaining material dropped and settled on the truck bed surface, the impact force began to reduce, eventually, with the material completely settling down, the profile flattened out as a constant force acted on the truck bed surface. Examination of the impact force profile proved the validity of the simulation model and its ability to capture an accurate impact force profile for shovel dumping operation. This complete three-step model verification procedure showed that the prototype model represented an actual real-world HISLO process.

Model validation is an important step which was used to test whether the model was capable of an accurate computation and capturing of the impact force or not. It allowed the examination of the accuracy of the system, designed in this study, for capturing the impact force at the truck bed surface. For this purpose, the impact force results from a study conducted by Iverson et al. [29] were used. A single particle drop test was conducted with the developed 3D simulation model in ABAQUS, under the same conditions and properties defined by Iverson et al. [29] study. First, a single DEM particle of PD3D type with a radius of 0.0127 m and a density of 3000 kg/m^3 was created. During the experimentation, the defined particle was allowed to drop under gravity from three different heights of 10, 15, and 20 m. Impact force was recorded for each of those experiments and the results were compared with the Iverson et al. [29] study, which are summarized in Table 5.5. The comparison of the results showed that the values of the drop test were significantly close for each of these experiments. In particular, the percentage error for each of these

experiments was less than 7%, which shows a strong agreement between the impact force results. This indicates that the developed simulation model has the capability of capturing the accurate impact force values.

Therefore, detailed verification and validation of the 3D prototype model showed that it not only represented the real-world HILSO phenomenon but also had the ability to accurately compute and capture the impact force at the truck bed surface and now was ready to be utilized for the detailed experimentation.

Table 5.5. Model Validation Results

Drop Height	**Virtual Simulation Impact Force Results**	**Iverson et al. [29] Impact Force Results**	**Percentage Difference**
m	MN	MN	%
10	43.1	45.7	5.69
15	53.9	57.8	6.75
20	62.4	66.9	6.73

5.6. IMPACT FORCE EXPERIMENTATION

A coupled FEA-DEM methodology was utilized for simulating the HISLO process using the 3D virtual prototype model. FEA-DEM coupled process with complex geometries is a computationally intensive process in ABAQUS. Thus, a simplified prototype model was used consisting of P&H 4100XPC cable shovel dipper and the CAT

793D dump truck to complete the experimentation process using available computation resources.

A multi-pass shovel dumping operation was investigated in this study. Simulation of each shovel pass was designed as an essential two-step process. The first step ensured the modelling and settling of all the particles in the shovel dipper without any significant overlap. Particles were modelled as spherical balls with a fixed radius of 0.149 m for each ball. After the creation of particles, contacts were established between individual particles, as well as with the dipper sides and door. The particles started losing their kinetic energy as they began to settle inside the dipper. The second step is initiated once the dissipation of the particles' initial energy was complete. The actual dumping process was simulated in the second step. It involved the rotation of the dipper door so that the material could be dropped into the truck body under gravity. With the activation of gravity and rotation of dipper door, the particles are dumped, and ABAQUS/Explicit would begin to solve the equation of motion for each particle using DEM. The displacement and contact forces are computed for every time increment. Impact forces and stresses are developed as the particles interacted with the truck bed surface. The force and stress distributions are recorded at the truck bed surface. The computation for particle displacement, contact forces, and stresses continued until the particles completely settled on the truck bed surface after losing all the kinetic energy.

The CAD geometry of the truck-dipper model was imported into the ABAQUS for virtual prototyping. Detailed meshing was done especially for the truck body since the focus of the work was to record the dynamic impact force at its bed surface. Four different sets of Hertzian contact was established as between DEM particles – DEM particles, DEM

particles – shovel dipper surfaces, DEM particles – dipper door surface, and finally DEM particles – truck bed surfaces. Two shovel passes were simulated for a HILSO process. The simulation began with the generation of material particles, with appropriate properties defined in Section 4, as spherical balls inside the dipper for each shovel pass. The material was generated in the dipper to ensure 100 tons of combined weight for rock/soil material. The impact force and stress development at the truck body surface were recorded for each shovel pass. During the second shovel pass, the material from the first shovel pass already existed on the truck bed surface. The previously dumped material acted as a cushion during the second shovel pass and, thus, reduced the impact force and stress at the truck bed surface – a phenomenon commonly known as cushioning effect.

Experiments were conducted to capture the dynamic impact force during a multi-pass shovel dumping operation. With proper contact definitions, and gravity activation, DEM ensured continuous flow of material from shovel dipper onto the truck bed surface. Dumping height was kept to an optimum height of 4.3 m by maintaining a minimum safe distance between the shovel dipper door and the truck body edge, to ensure necessary clearance to prevent jolting along with safe, effective, and efficient shovel dumping process. Figure 5.1 shows the kinematics of dumping step of simulation for the first shovel pass with part (a) displaying the rotation of the dipper door and rock/soil material in form of DEM particles beginning to fall from shovel dipper under gravity. Figure 5.1 (b) shows the rock/soil material flowing under gravity from the shovel dipper. It can be seen that the whole material is not falling down together as a single entity. In fact, there is a small portion of material closer to the truck bed surface with major portion of the material following under gravity.

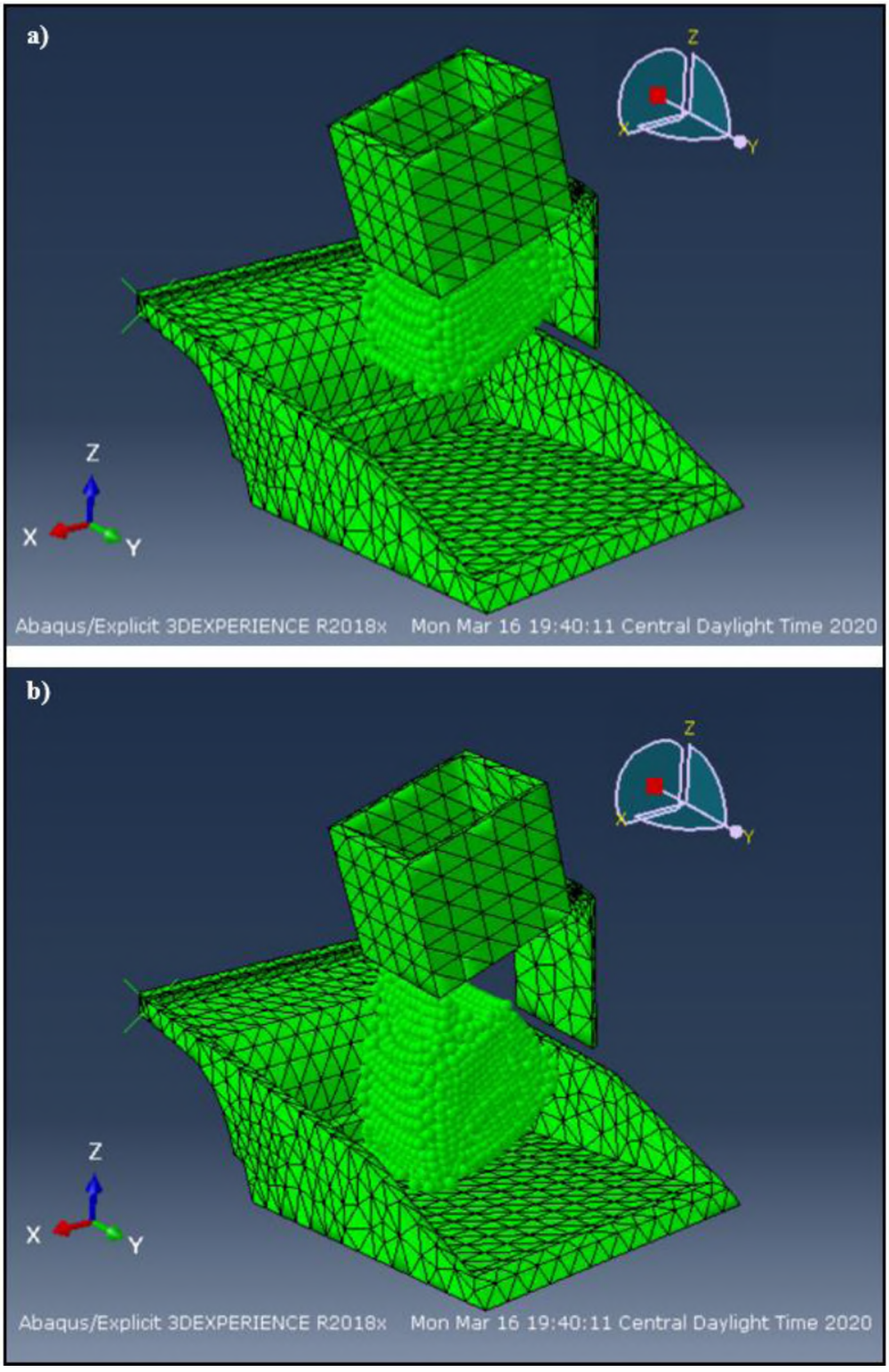

Figure 5.1. Kinematics of First Shovel Pass (a) Material Flowing Out of Dipper (b) Continuous Material Flow under Gravity

This proper continuous material flow dynamics ensured accurate recording of impact force magnitudes during its development and complete progression for both the shovel passes while also capturing the cushioning effect during the second shovel pass.

5.7. SUMMARY

This section described the details for the experiment design and in-depth procedural information for the detailed experimentation using both mathematical model and virtual prototype, presented in Sections 3 and 4, respectively.

Numerical testing was done for the mathematical model through rigorous experimentation. A thorough analysis was conducted for the case of CAT 793D dump truck getting loaded by a large cable shovel, i.e., P&H 4100 XPC.

A multi-pass high impact shovel loading operation experiments were conducted to model the dynamic impact force at the truck bed surface and observe the cushioning effect during subsequent passes.

The 3D virtual prototype model designed in Section 4, was used to conduct detailed high impact shovel loading experiments using FEA-DEM methodology. The purpose of the experiments was firstly, to investigate the generation and progression of dynamic impact force at the truck bed surface during shovel dumping operation with proper continuous flow dynamics using FEA-DEM coupled methodology. Secondly, the research verified and validated the mathematical model. Thirdly, the research gathered data for developing AI and machine learning models for real-time monitoring of impact force during any multi-pass HISLO process.

The deeper understanding, can then be used to design and develop solutions for reducing the dynamic impact forces at the truck bed surface, which would in-turn reduce

or possibly eliminate the vibration levels at the operator seat. The developed intelligence-based model, using the experimental result data, will serve as a major step towards improving the HISLO process by enhancing the health and safety of truck operators.

6. DEEP LEARNING, ARTIFICIAL INTELLIGENCE, AND MACHINE LEARNING IMPLEMENTATION

The detailed procedures for data transformation and development of intelligence-based real-time impact force monitoring framework have been described in this section. A deep learning algorithm has been used to train the model for HISLO process. The optimized model was then evaluated against the four most widely used machine learning algorithms. Proper statistical indicators have been selected for model performance evaluation, analysis and inferences.

6.1. DATA PREPERATION AND TRANSFORMATION

The whole process of intelligence-based framework development using deep learning, AI, and machine learning involves four phases: data acquisition, data transformation, model development and training, and model validation.

Data acquisition is the first stage that deals with acquiring the dataset required for model development. Detailed experimentation was conducted using the virtual prototype model, developed in Section 4. The shovel dumping process was simulated for varying operating condition and material properties in order to get a comprehensive set of data for dynamic impact force during a complete shovel dumping process. Impact forces were recorded for those simulated experiments and were used for the model development.

The completion of data acquisition marks the beginning of the data processing and transformation phase. Data has to be carefully prepared for model development. The AI algorithms require data in specific formats, and thus, the process may require proper transformation. The data set will be cleaned with the deletion of unnecessary and redundant data. Statistical analysis is carried out using the clean data to gain useful insights. Data

scaling is an essential task during the data transformation and preprocessing stage. Data scaling ensures improved quality with dimension reduction and an equal treatment of each value of the variable irrespective of its magnitude [109]. An appropriate data scaling technique, such as linear transformation, min-max normalization, or decimal scaling is used for this purpose. Feature transformation is then carried out to transform certain numerical explanatory variables to categorical variables. This process improves the information extraction, and the selection of important features from the data and the algorithm performance and computational cost. The latter is achieved by training a weak classifier/regressor. In this process, a weak regressor would be trained for selecting the most important features that effect the dynamic impact force generation and progression during a shovel dumping operation. Most of intelligence-based algorithms do not accept the categorical variables so every such explanatory variable has to be transformed using one-hot-encoding [110].

Figure 6.1 describes the complete process of deep learning, AI, and machine learning model development and evaluation. The first step in machine learning model development is partitioning the final dataset that was acquired at the end of the data transformation and preparation stage. The dataset is partitioned into two subsets i.e. training and testing, using 70-30 or 80-20 division, with choosing an appropriate partition ratio based on the criteria of maximizing the model performance [111]. The validation subset is also taken out from the original training set, which is later used for hyper-parameter tuning of the model. The selection of the AI and machine learning model performance evaluation metric is extremely important as learning and prediction

capabilities of such frameworks are assessed based on those metrics during model evaluation and validation phase using the hold-out dataset.

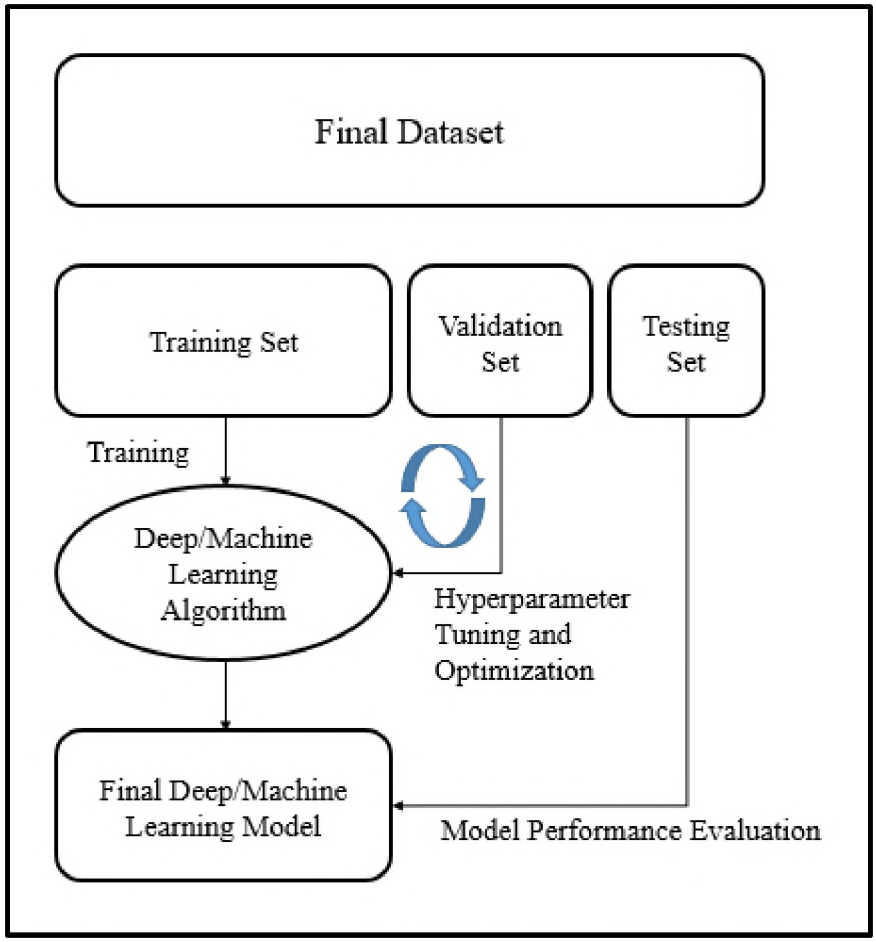

Figure 6.1. Deep Learning, AI, and Machine Learning Model Development and Evaluation Process

The data for this study was acquired through detailed experimentation where impact force at the truck bed surface was captured during high impact shovel loading operations. Since it was an experimental dataset captured in a controlled environment, data cleaning was not required in this process. The captured dataset was divided into training and testing set, using the 80% and 20% partition, respectively. Table 6.1 shows the statistical analysis

for both training and testing datasets. Both the datasets had 4 inputs: material density, porosity, bucket fill factor, and shovel dumping height. The datasets had a single response variable, which was the resulting impact force at the truck bed surface during a shovel dumping operation. The training dataset was used to develop the models, and the testing dataset was used to validate and evaluate the models.

Table 6.1. Statistical Data Analysis of Training and Test data sets

	Minimum	**Maximum**	**Mean**	**Standard Deviation (SD)**	**Coefficient of Variation (%)**
Training Data					
Material Density (kg/m^3)	1500	2700	2104.9	421.01	20.00
Material Porosity	0.2	0.5	0.35	0.1115	31.87
Shovel Bucket Fill (%)	88	102	95.10	4.525	4.76
Shovel Dumping Height (m)	4.3	7.3	5.74	1.06	18.54
Impact Force (kN)	275	849	584.5	140.88	24.10
Test Data					
Material Density (kg/m^3)	1500	2700	2080.1	436.46	20.98
Material Porosity	0.2	0.5	0.35	0.1128	32.24
Shovel Bucket Fill (%)	88	102	94.60	4.79	5.06
Shovel Dumping Height (m)	4.3	7.3	5.84	1.00	17.18
Impact Force (kN)	288	842	577.8	148.30	25.67

Python was used as the programming language/platform for data analysis, processing and transformation, model development, and performance evaluation of the model. Deep learning model was built using Keras framework in Python. Since all the input and output values were widely distributed, scaling was done by employing linear mapping, as given by equation (6.1). Scaled data was then used during model development. Data was

de-normalized once the model was trained, to obtain the actual values for the response variable.

$$Z_n[0,1] = \frac{Z - Z_{min}}{Z_{max} - Z_{min}} \tag{6.1}$$

Where,

Z_n = Scaled/Normalized value for variable 'z'

Z_{max} = Highest value of variable 'z'

Z_{min} = Minimum value of variable 'z'

Z = Real value of variable 'z'

6.2. DEEP LEARNING – INTRODUCTION

Deep learning (DL) is a state-of-the-art artificial intelligence technique based on artificial neural network [112]. DL is a powerful approach that allows complex leaning and knowledge extraction and that can be applied to both supervised and unsupervised learning [113]. DL has shown exceptional performance in the areas of computer vision and object recognition through images [114–116], medical image analysis [117–121], text and speech recognition (natural language processing) [122–125], and voice recognition [126]. State-of-the-art performance has also been reported for regression tasks in the areas of human head and body pose recognition [127–129] and landmark detection for face and fashion [127, 130, 131].

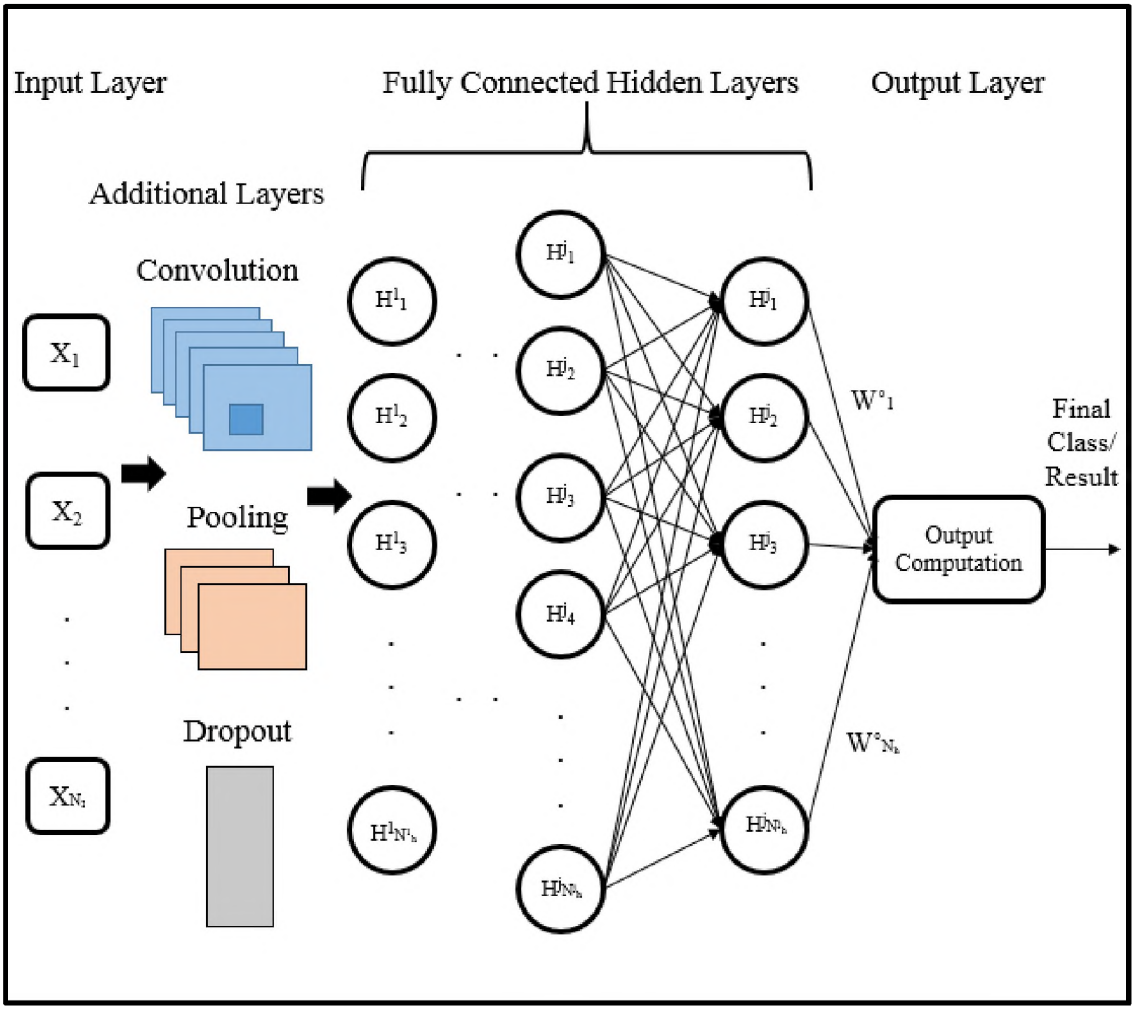

Figure 6.2. General Architecture of DL Model

All of the aforementioned work identified the general architecture of a deep learning model which consisted of one or more additional layers, i.e., convolution layer(s), pooling layer(s), dropout layer(s), normalization layer(s), and fully connected hidden layer(s) in between the input and output layer (Figure 6.2). The final optimized architecture, with regards to arrangement, connection, and the quantity of each of these layers, was obtained through extensive experimentation. Majority of these aforementioned applications, for both classification and regression tasks, involved convolutional neural

network (CNN), which contained a convolution and pooling layer, in addition to the input, output, and multiple fully connected hidden layers [132]. For a non-imagery and non-structured dataset, a DL model does not contain convolution and pooling layer(s). However, the model contains more than one hidden layers depending on the complexity of the problem.

6.3. MACHINE LEARNING ALGORITHMS

Four of the most widely used state-of-the-art machine learning algorithms, namely, artificial neural network (ANN), random forest, support vector machine (SVM), and k-nearest neighbors (kNN) were used in this study.

6.3.1. Artificial Neural Network (ANN). Artificial neural network is a robust computational technique developed with inspiration drawn from the human brain functioning [133]. Structurally, ANN consists of essentially three types of layers namely input layer, output layer, and hidden layer. Figure 6.3 shows the basic architecture of a shallow single hidden layer ANN with a single response variable. For a single shallow network, there can only be one input, output, and hidden layer. Network processing is carried out by small powerful units known as neurons or nodes. These neurons are interconnected among the immediate neighboring layers. The connection weights between these neurons dictate the degree of influence each neuron from the previous layer has on the output of its next connecting neurons in the subsequent layer [134]. The number of neurons for input or output layer depends upon the number of input and output variables, respectively. The number of neurons for one, or more than one, hidden layer is a hyper-parameter, which requires optimization during model development.

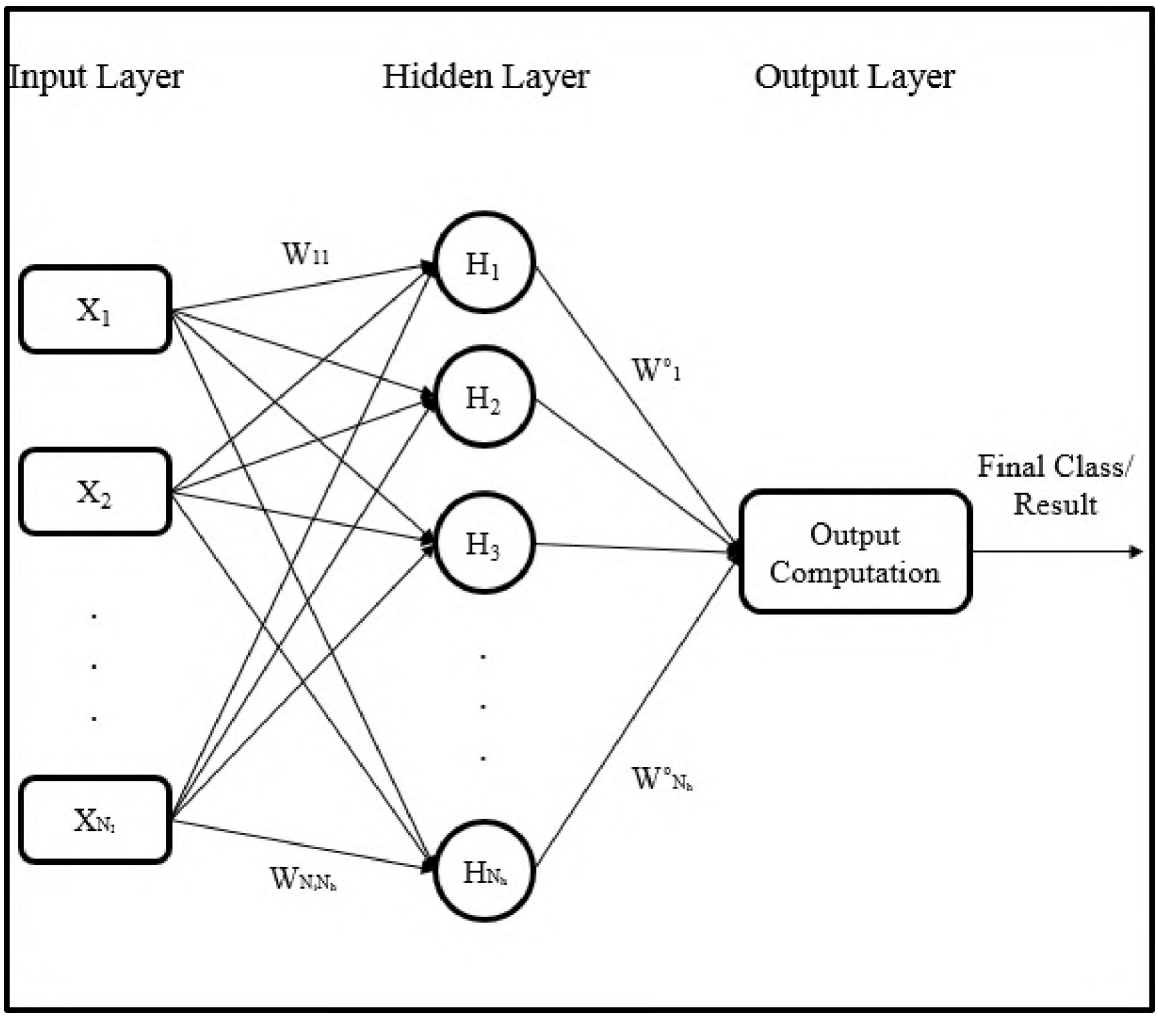

Figure 6.3. Basic Architecture of Single Hidden Layer Feed Forward ANN

6.3.2. Tree-Based Algorithms. Tree-based algorithms, particularly random forest (RF), are some of the most widely used models in the field of machine learning due to their exceptional accuracy in predictive modelling, stability, and knowledge interpretation [135–137]. RF applies the ensemble learning methodology, where meta-learners, also known as decision trees, are developed and trained. The final outcome is reached by combining the predictive abilities of those individual learners. Figure 6.4 shows the working principle of an RF algorithm. The concept of decision trees for both

classification and regression tasks was introduced by Breiman [138] as Classification and Regression Tree (CART). It consists of a binary tree with root node representing an input variable and daughter nodes at the split containing the output variable. The input space is partitioned to create the binary learners. A greedy algorithm, i.e., recursive partitioning, is used for the variable selection at each node split to ensure that the cost function is minimized [139]. The data points used for constructing each tree are selected randomly from the input space, thus removing the biasness in the model. The reduced degree of correlation between the individual learners is of vital importance in determining the accuracy of random forest as it ensures the generality of the overall model.

6.3.3. Support Vector Machine (SVM). SVM, developed by Vapnik and Vapnik [140], is an advanced pattern recognition soft computing learning technique primarily used for classification and regression. SVM minimizes the generalization error by computing a decision boundary/plane that would maximize the margin between the closest samples and the decision plane. Figure 6.5 shows a simplified demonstration of the SVM working principle for the 2D data domain.

Consider an input data set of $X = (\overrightarrow{x_i}, y_i)_{i=1}^{N} \in R^d$ with the input space having 'd' dimensions (number of input variables of each sample). Equation (6.2) gives the conventional target function of SVM algorithm. '$\varphi(x)$' is the non-linear transformation of the input space $\overrightarrow{x_i}$. Equation (6.3) defines the cost function for SVM. The first term in the cost function gives the regularization term defining the margin. The second term stands for the margin violation or the error. The parameter 'C' is the tradeoff between the regularized term and margin violation (error). Equation (6.4) gives the conditions to which the equation

(6.3) is subjected to. Quadratic programming is used to compute the two parameters, ‘w’ and ‘b’, required for SVM by minimizing the cost function given by equation (6.3).

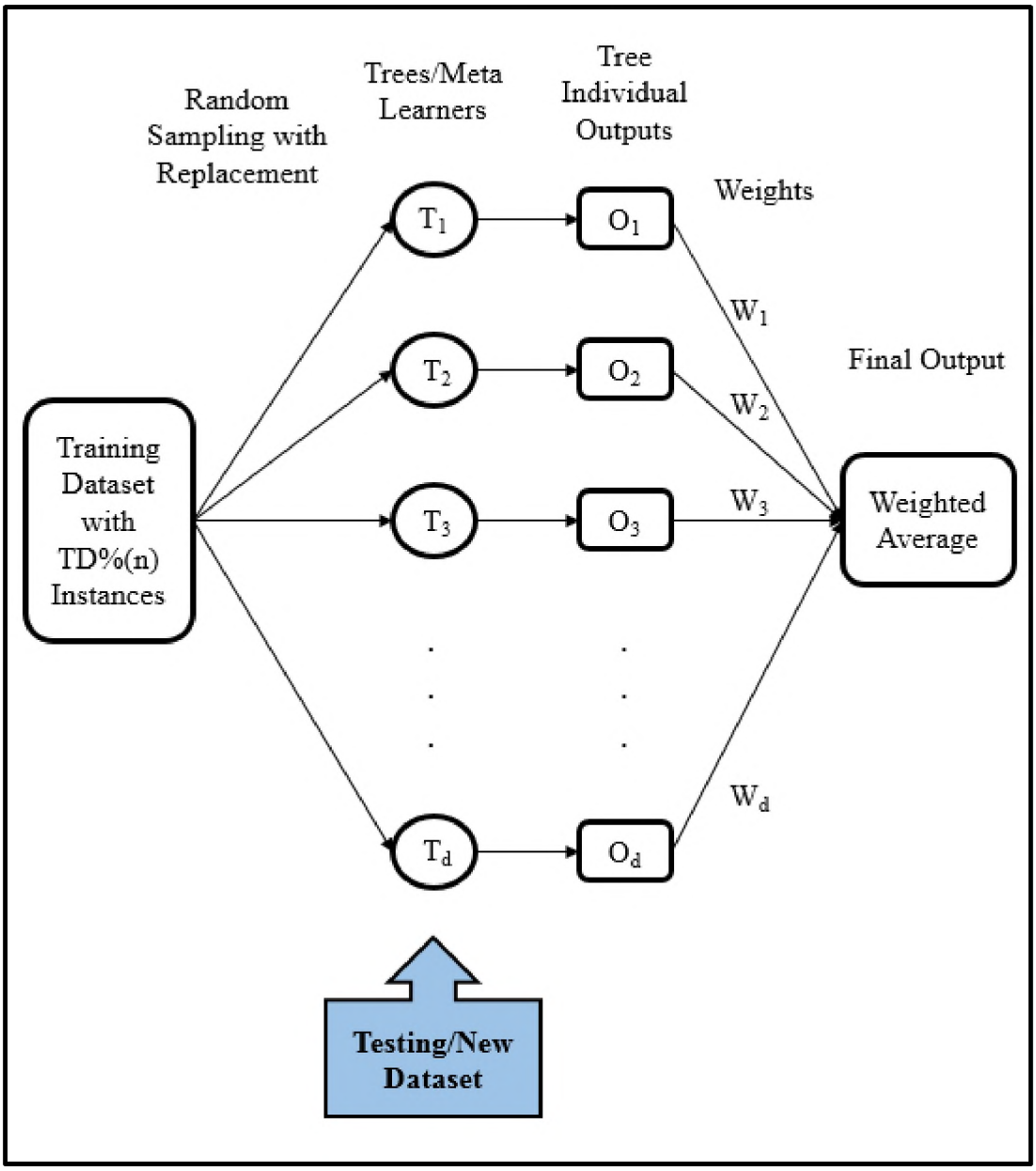

Figure 6.4. Working Principle of RF Algorithm

$$F(x) = y = wZ + b = w\varphi(x) + b \tag{6.2}$$

$$O = \frac{1}{2}w^T w + C\frac{1}{N}\sum_{i=1}^{N}(\zeta_i + \zeta_i^*) \tag{6.3}$$

$$\begin{cases} y_i - w\varphi(\overrightarrow{x_i}) + b \leq \varepsilon + \zeta_i \\ w\varphi(\overrightarrow{x_i}) + b - y_i \leq \varepsilon + \zeta_i^* \ \forall\, i = 1, \ldots, d \\ \zeta_i, \zeta_i^* \geq 0 \end{cases} \tag{6.4}$$

ζ_i = Upper bound for margin violation

ζ_i^* = Lower bound for margin violation

ε = Error tolerance acceptable during model development

For better and fast computation, equation (6.5) is used as the target function. '$K(x, \overrightarrow{x_i})$' is the kernel function given by the dot product of the non-linearly transformed input space in equation (6.6). By using the kernel function, a non-linear learning machine is generated by using dot product and the original input space, which makes it faster, compared to the traditional vector transformation. Linear, polynomial, and Gaussian (radial basis) functions, as given by equations (6.7), (6.8), and (6.9), respectively, are the most commonly used kernel functions in SVM.

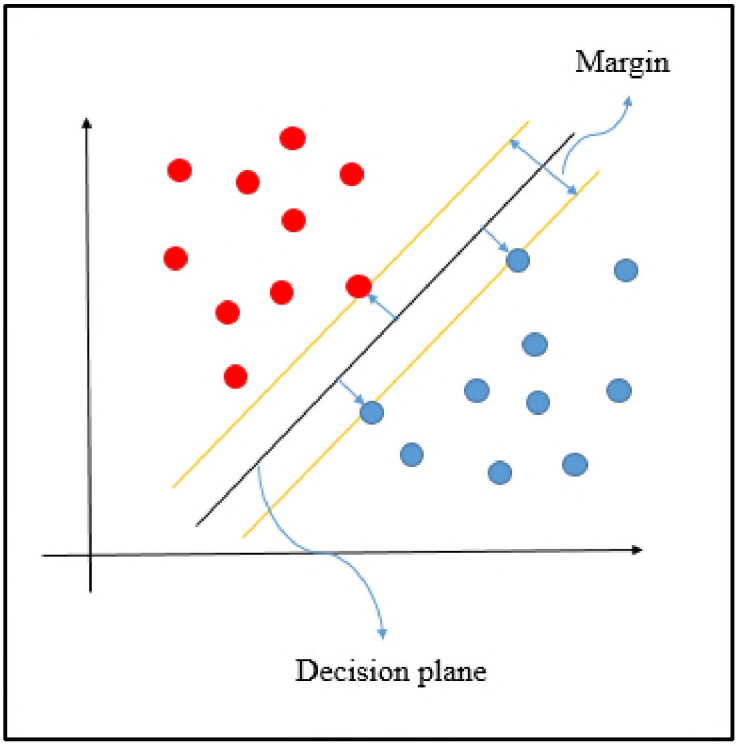

Figure 6.5. Illustration of SVM Algorithm for 2D Data Domain

$$F(x, \beta_i, \beta_i^*) = \sum_{i=1}^{N} (\beta_i - \beta_i^*) K(x, \overrightarrow{x_i}) + b \tag{6.5}$$

$$K(x, \overrightarrow{x_i}) = \varphi(x).\varphi(\overrightarrow{x_i}) \tag{6.6}$$

$$K(x, \overrightarrow{x_i}) = x^T x_i \tag{6.7}$$

$$K(x, \overrightarrow{x_i}) = (\alpha + \gamma x^T x_i)^Q \tag{6.8}$$

$$K(x, \overrightarrow{x_i}) = exp(-\gamma \|x - x_i\|^2) \tag{6.9}$$

Where,

Q = Order of the polynomial transformation

α, γ = Kernel parameters

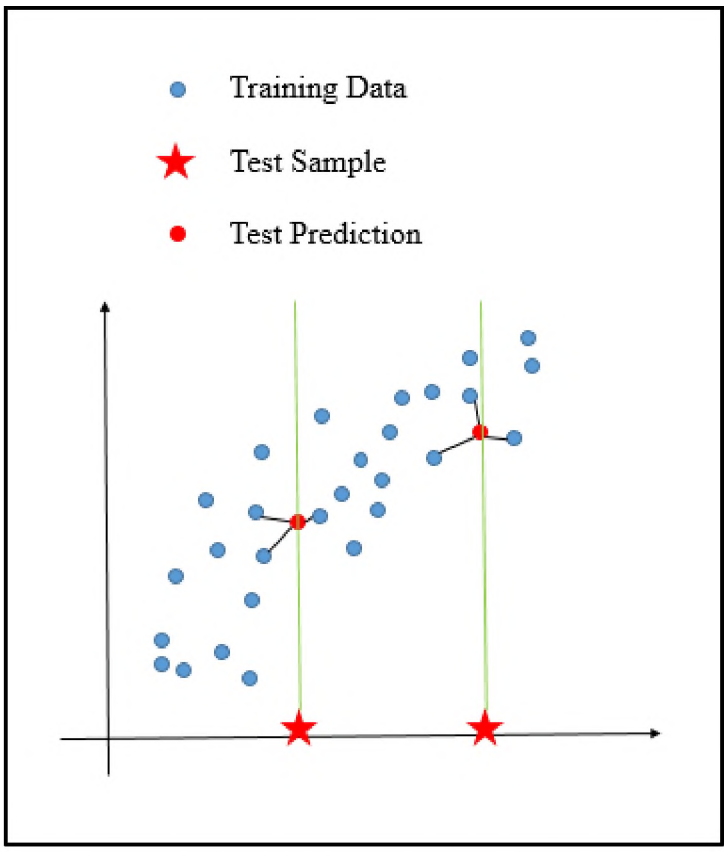

Figure 6.6. Working Principle of kNN Algorithm

6.3.4. k-Nearest Neighbors (kNN). kNN is one of the simplest and, yet, one of the most effective non-parametric algorithms in predictive modelling and machine learning [141–149]. kNN algorithm is based on the assumption that, in any local neighborhood

pattern, the expected output value of the response variable is the same as the target function value of the neighbors [150]. Therefore, once the patterns are recognized, for any new data point, the output value (or label) is computed as the average of the output value of its 'k' nearest neighbors [151]. Figure 6.6 illustrates the working principle of kNN algorithm. Euclidean and Manhattan distances, given by equations (6.10) and (6.11), respectively, are the two main metrics used to compute the distance between the new and all the training instances within the input space for a continuous variable [152]. Equation (6.12) [150] shows the computation of the mean value for any n^{th} data instance using its k-nearest neighbors.

$$\sqrt{\sum_{i=1}^{m}(x_i - z_i)^2} \qquad (Euclidean\ Distance) \tag{6.10}$$

$$\sum_{i=1}^{m}|x_i - z_i| \qquad (Manhattan\ Distance) \tag{6.11}$$

$$y_n = \frac{1}{k}\sum_{j=1}^{k} y_i \qquad \forall\, j \in D_k(x_n) \tag{6.12}$$

Where,

x is the input vector for the new instance

z is the input vector for the training instance

m is the total number of input variables

y_n is the output of the nth data point

$D_k(x_n)$ is the set of 'k' neighboring instances for the nth data point

6.4. DL IMPLEMENTATION FOR IMPACT FORCE MONITORING

Deep learning (DL), a state-of-the-art artificial intelligence technique, was used to develop an intelligence-based framework for real-time impact force monitoring during the HISLO process. Table 6.2 contains the detailed illustration of the learning algorithm. It is a supervised learning algorithm, and thus, it requires clean and appropriately processed data for model development. Once the clean and fully transformed training dataset is loaded into the system, the algorithms starts with random initialization of the connection weights. The first phase of the algorithm deals with the feed-forward processing of each data instance, which would involve computing the activated output using equation (6.13) for the immediate hidden layer connecting the input layer, and equation (6.14) for any subsequent hidden layer(s).

$$HO_j^1 = f_h^1\left[\sum_{i=1}^{N_I} w_{ji}^1 \cdot X_i + B_{j0}\right] \tag{6.13}$$

Where,

w_{ji}^1 = Connection weight for jth neuron of 1st hidden layer connecting the ith input node

f_h^1 = Transfer (activation) function of the 1st hidden layer

X_i = Input data vector

B_{j0} = Hidden layer neuron bias

$$HO_j^m = f_h^m \left[\sum_{i=1}^{N_h^{m-1}} w_{ji}^m \cdot HO_i^{m-1} + B_{jo}^m \right] \tag{6.14}$$

Where,

w_{ji}^m = Connection weight for jth neuron of mth hidden layer connecting the ith input node

f_h^m = Transfer (activation) function of the mth hidden layer

N_{HL} = Total number of hidden layers

N_h^{m-1} = Total number of neurons in (m – 1)th hidden layer

B_{jo}^m = Neuron bias term for mth hidden layer

Equation (6.15) is then used to compute the final output, a vector exhibiting the value of the response variable based on the given set of the input explanatory variables representing the HISLO process, for every node in the output layer. Upon the process completion of all data instances, the performance metric and the mean error are computed and compared with pre-defined allowable error tolerances. Since the process started with random initialization of the connection weights, it would be extremely unlikely that the error would drop below the allowable tolerance at the end of first feed-forward iteration. Therefore, the algorithm attempts to learn the pattern from the experimental training dataset and use that knowledge to optimize the weights. The basic idea would be to compute the error contribution of each neuron and then adjusting/optimizing the connection weights and bias, such that the error in the output layer can be brought within the required tolerance.

Table 6.2. DL Algorithm for Real-Time Impact Force Monitoring System

Loading final transformed dataset as an input
Random initialization of connection weights
Repeat until error drops below tolerance or maximum number of allowed iterations reached
Repeat for each data instance
Repeat for each neuron of hidden layer, ∀ m = 1.. N_{HL}
If m = 1, use equation 1 to compute the output
For m = 2…N_{HL} , use equation 2 to compute the output
Repeat for each output node
Compute the impact force value based on input data instance using equation 6.15
Compute the overall performance metric
Stop if error drops below tolerance or max number of allowed iterations reached
Repeat for each output node
Computing the gradient of cost function w.r.t. connection weight using equation 6.16
Repeat for each neuron of N_{HL} hidden layer
Updating weight using equation 6.17
Updating hidden layer bias term using equation 6.18
Repeat for each hidden layer going backwards (N_{HL}-1…1)
Repeat for each neuron
Computing the gradient of cost function w.r.t. connection weight using equations 8
Updating weight using equation 6.20
Updating Bias term using equation 6.21

The gradient of the cost function with respect to each weight and bias term, is computed for understanding the degree of change caused by each weight and bias term to the cost function. The process of learning and correction moves backwards. First, equation

(6.16) computes the gradient of cost function with respect to the connection weights between the last hidden layer and the output layer. Based on the computed error, the algorithm updates the connection weights using equation (6.17). This process is followed by updating the bias term for the output layer using the equation (6.18). The same process is used to compute the gradient in equation (6.19), update the connection weights using equation (6.20) and the bias terms using equation (6.21). This process continues until all the first hidden layer neurons are updated. Then the updated architecture is used to carry out the second iteration of the feed-forward processing. Since the network has now learned from the data, the error would certainly be reduced at the end of the second iteration. The whole process is repeated until the connection weights are fully optimized, which marks the end of the learning process. The final model is then evaluated for its generalization capability during the model evaluation phase.

$$\tilde{y}_k = f_o\left[\sum_{j=1}^{N_h^{N_{HL}}} w_{kj} \cdot f_h^{N_{HL}}\left(\sum_{i=1}^{N_h^{N_{HL-1}}} w_{ji}^{N_{HL}} \cdot HO_i^{N_{HL}-1} + B_{jo}^{N_{HL}}\right) + B_{k0}\right] \tag{6.15}$$

Where,

f_o = Output layer transfer (activation) function

w_{kj} = Connection weight for kth output node connecting the jth hidden neuron

B_{k0} = Output layer neuron bias

$$\frac{\partial C}{\partial w_{kj}^{o}} = \frac{\partial C}{\partial \tilde{y}_k} \times \frac{\partial \tilde{y}_k}{\partial z_k} \times \frac{\partial z_k}{\partial w_{kj}^{o}} \tag{6.16}$$

Where,

C = Cost Function

z_k = Weighted score of kth output node

w_{kj}^{o} = Connection weight for kth output node connecting the jth hidden layer neuron

$$w_{kj}^{o}{}^{+} = w_{kj}^{o} + \left(\eta \times \frac{\partial C}{\partial w_{kj}^{o}}\right) \tag{6.17}$$

Where,

η = Learning rate

$$B_k^{o+} = B_k^{o} + \left(\eta \times \frac{\partial C}{\partial \tilde{y}_k} \times \frac{\partial \tilde{y}_k}{\partial z_k}\right) \tag{6.18}$$

$$\frac{\partial C}{\partial w_{ji}^{m}} = \sum_{i=1}^{N^{m+1}} \left[\frac{\partial C}{\partial HO_{ji}^{m+1}} \times \frac{\partial HO_{ji}^{m+1}}{\partial z_{ji}^{m+1}} \times w_{ji}^{m+1}\right] \times \frac{\partial HO_j^{m}}{\partial z_j^{m}} \times HO_i^{m-1} \tag{6.19}$$

Where,

N^{m+1} = Total number of neurons in (m + 1)the layer. If m = N_{HL}; then $N^{m+1} = N_o$

N_o = Total number of output nodes

$$w_{ji}^{m+} = w_{ji}^{m} + \left(\eta \times \frac{\partial C}{\partial w_{ji}^{m}}\right) \tag{6.20}$$

$$B_{j}^{m+} = B_{j}^{m} + \left\{\eta \times \sum_{i=1}^{N^{m+1}} \left[\frac{\partial C}{\partial HO_{ji}^{m+1}} \times \frac{\partial HO_{ji}^{m+1}}{\partial z_{ji}^{m+1}} \times w_{ji}^{m+1}\right] \times \frac{\partial HO_{j}^{m}}{\partial z_{j}^{m}}\right\} \tag{6.21}$$

The illustrated algorithm was used to develop the DL model for real-time impact force monitoring during the shovel dumping process. The experimental data was divided into two sections, i.e., training and testing. Both datasets had 4 inputs: material density, material porosity, bucket fill, and shovel dumping height. The datasets had a single response variable, which was the resulting impact force at the truck bed surface during a shovel dumping operation.

The model was developed using the training dataset, and validation was done using testing dataset. Performance evaluation of the model was done using three main performance indicators, namely, R-squared, MAE (mean absolute error), and RMSE (root mean square error). R-squared measures the goodness of fit in relative terms. Whereas both RMSE and MAE measure the average prediction error for a model in absolute terms, RMSE gives an indication of the variance of frequency distribution of the error terms, while MAE provides an insight into the absolute variance of error terms. Computational time and execution speed were not considered as performance metrics because the dataset lacked the basic quality of being a large dataset, both in terms of dimensionality and volume.

Later, the Wilcoxon signed-rank test, which is a robust null hypothesis non-parametric statistical test, was conducted. The purpose of this test was to investigate the reliability of the performance of the DL model. During the statistical testing, p-value was used to quantify the evidence against the null hypothesis. The p-value computed through the test was then compared to the globally accepted minimum threshold value of 0.05 (5%) to draw a final conclusion regarding the acceptance or rejection of the null hypothesis.

The DL model consists of multiple fully connected hidden layers in addition to the basic input and output layers. Different DL architectures were tested in this work, including different number of fully-connected hidden layers, different number of neurons in each of those hidden layers, dropout layers at different locations, and varying the degree of dropout in the model.

Table 6.3 provides the architectural details of the DL variants tested using the same training dataset in this study. Firstly, the DL model used a network with input layer, hidden layer with 25 neurons, hidden layer with 15 neurons, and the output layer. Secondly, the DL model used a network with input layer, hidden layer with 35 neurons, hidden layer with 20 neurons, and the output layer. Thirdly, the DL model used a network with input layer, hidden layer with 35 neurons, hidden layer with 20 neurons, hidden layer with 12 neurons, and the output layer. Fourthly, the model used a network with input layer, hidden layer with 35 neurons, dropout layer with a 15% drop, hidden layer with 20 neurons, hidden layer with 12 neurons, and the output layer. Fifthly, the model used a network with input layer, hidden layer with 35 neurons, dropout layer with a 25% drop, hidden layer with 20 neurons, hidden layer with 12 neurons, and the output layer; and sixthly, network with input layer, hidden layer with 35 neurons, dropout layer with a 15% drop, hidden layer

with 20 neurons, dropout layer with a 15% drop, hidden layer with 12 neurons, and the output layer.

Table 6.3. DL Architecture Variants. Note – I: Input layer; H_N: Hidden Layer with '$_N$' Neurons; D_P: Dropout Layer with 'P'% Drop Rate; and O: Output layer.

Variant	Architecture
1	$I - H_{25} - H_{15} - O$
2	$I - H_{35} - H_{20} - O$
3	$I - H_{35} - H_{20} - H_{12} - O$
4	$I - H_{35} - D_{15} - H_{20} - H_{12} - O$
5	$I - H_{35} - D_{25} - H_{20} - H_{12} - O$
6	$I - H_{35} - D_{15} - H_{20} - D_{15} - H_{12} - O$

The training for each of those architecture variants was done with the same base conditions. Rectified Linear Units (ReLU) was used as the activation function for every fully connected hidden layer, and identity function was applied at the output layer for every model training. Adam [153] was used as the learning optimization algorithm with the mean square loss as the cost error function for the gradient-based optimization. Overfitting was avoided by using holdout methodology, where 20% of the training data was set as the validation dataset during model training. In some of the architectures tested, an additional dropout layer was added in an attempt to further suppress overfitting [154]. A total of 200 epochs – training cycle running through the entire training dataset – were set for the model development phase. Early stopping was set up at four epochs in order to ensure the stoppage of training process provided a decrease in validation error loss was observed within four

consecutive epochs. Model training was done in batches with an individual batch size of 20 instances.

6.5. MACHINE LEARNING MODEL IMPLEMENTATION

Four of the most widely used state-of-the-art machine learning algorithms, namely, artificial neural network (ANN), random forest (RF), support vector machine (SVM), and k-Nearest neighbors (kNN) were used to test and evaluate the developed DL model. All the four models were developed using the same training dataset, and validated using the same testing dataset, as that of the DL model. Moreover, the performance of the models was evaluated using the same three main performance indicators, namely, R-squared, MAE, and RMSE.

A shallow feed-forward neural network with a single hidden layer was built using the training dataset with 4 inputs and single response variable. Limited-memory BFGS (L-BFGS) was used as the optimization algorithm and square loss as the cost function during weight updating and error back propagation. Rectified Linear Units (ReLU) and identity functions were used as the activation functions for hidden and output layer, respectively. Model overfitting was avoided by using 5-fold cross validation and L2 regularization with an alpha value of '0.001' during the training process.

Optimization, based on trial and error, was carried out in an attempt to find the optimum number of hidden neurons in order to build the best performing single hidden layer neural network architecture [100, 135, 155]. Figure 6.7 displays the performance of neural network with varying number of hidden neurons. From Figure 6.7, the performance of the network stabilized as the number of hidden neurons reached a total of 23. Increasing

the neurons beyond 23 in the hidden layer did not increase the performance of the neural network. Rather, it increased the computational cost.

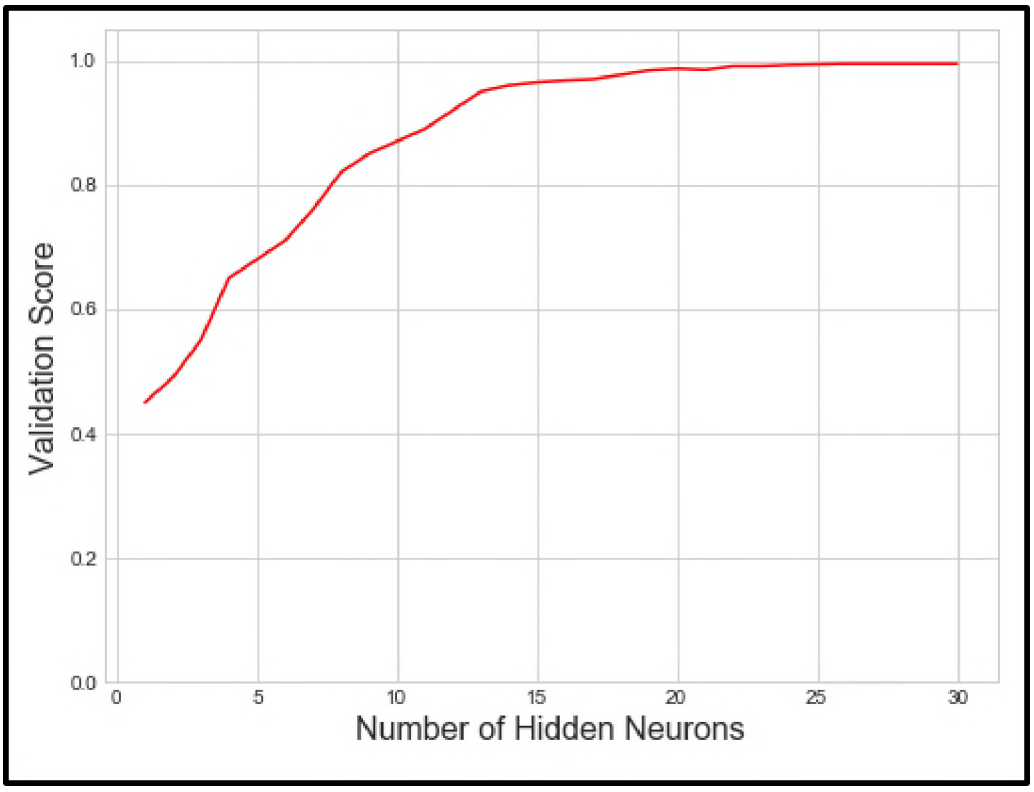

Figure 6.7. Performance Evaluation of Neural Network with Varying Number of Hidden Neurons

The final neural network model was then developed using the optimum number of hidden neurons (23). The training process stopped as soon as convergence, which was defined with an error tolerance of 0.0001, was reached. Figure 6.8 shows the final single hidden layer neural network. The thickness of lines connecting the subsequent neurons/nodes indicate the relative magnitude of the connection weights: the thicker the line, the larger the weight between the node and the neuron. Once the model was developed,

it was put through validation by using the test dataset in an attempt to evaluate its ability to predict the impact force resulting from a shovel dumping process.

RF, an ensemble learner, was trained by building the individual learners using sub-samples drawn from the original training dataset. The number of trees/learner grown in a forest and the number of explanatory features selected for every node split are two of the most important hyper-parameters for an RF model and, thus, require optimization. Increasing the number of trees increases performance. However, beyond the optimum number, computational cost increases without any performance gain [135, 156]. Feature selection for each node split was carried out randomly from the given set of input features. This was critical in ensuring state-of-art performance of the model.

A rigorous grid search was carried out in an attempt to optimize the hyper-parameters. A 5-fold cross validation was implemented during the grid search to avoid any model overfitting. Figure 6.9 shows the grid search results for the RF model. It can be seen that 13 and 4 were obtained as the optimum values for the number of trees in the model and the number of features to be selected for each node split, respectively, as the overall model performance stabilized around that mark. Figure 6.10 shows the relative importance of the features in terms of model development. Material density and the dumping distance were the two most important features in modelling and predicting impact force resulting during the HISLO process, whereas material porosity was the least important of all the features. Optimum values for the hyper-parameters were then used to train the final RF model followed by model testing using the unused dataset.

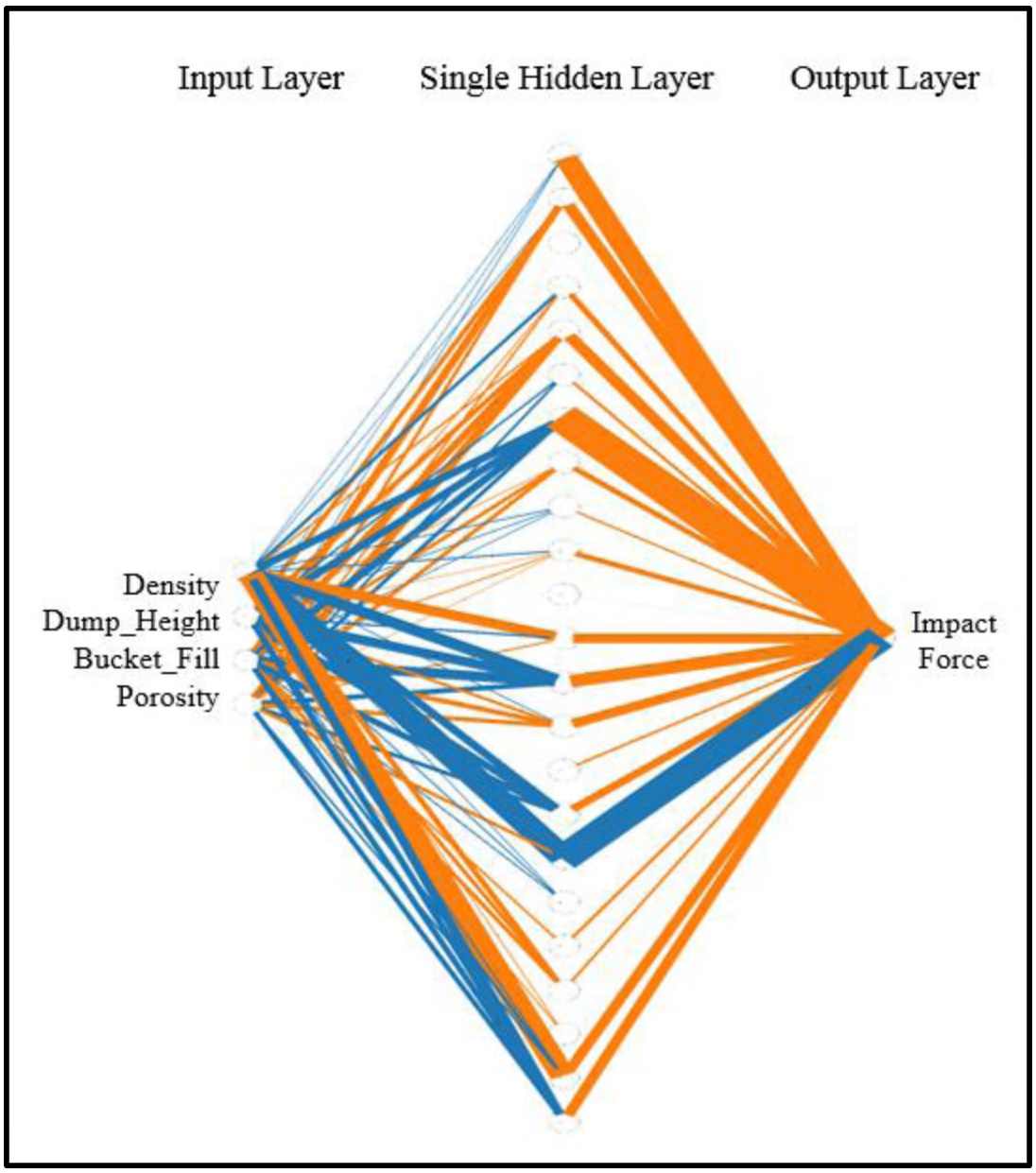

Figure 6.8. Final Single Hidden Layer Neural Network (Note: Thickness of lines shows relative magnitude of the connection weights)

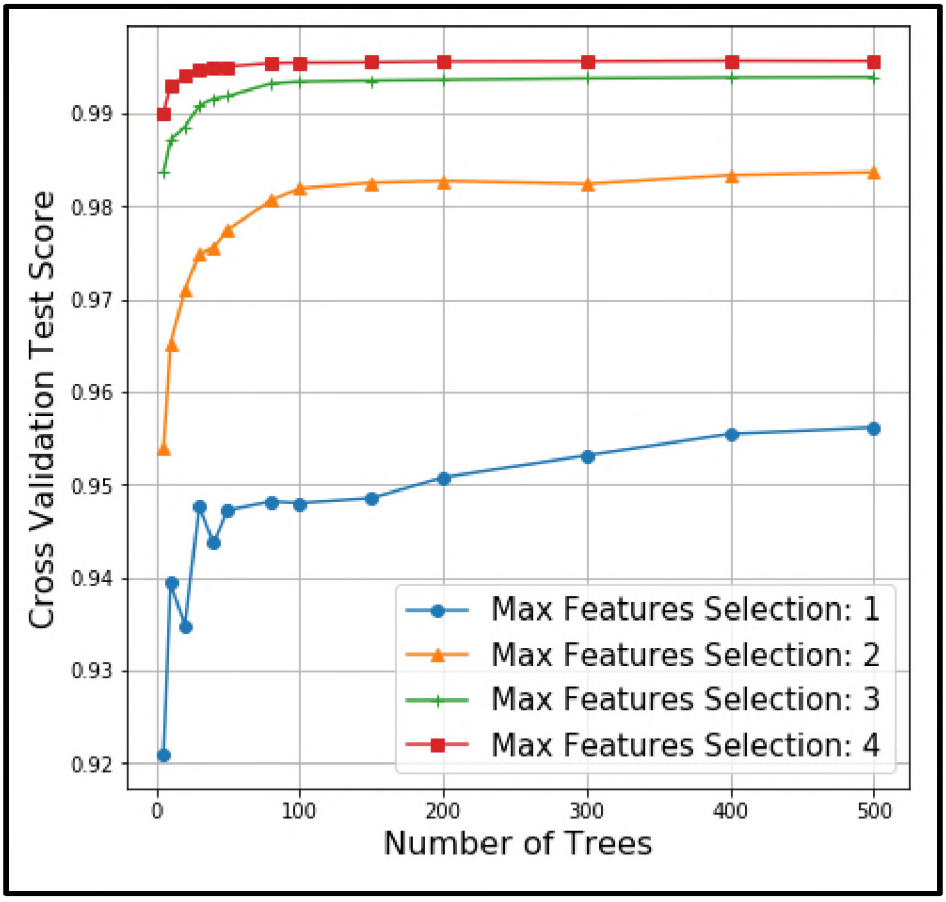

Figure 6.9. Grid Search Results for Random Forest Model

For k-nearest neighbors (kNN) model, two of the most important hyper-parameters include the number of neighbors to be accounted for in a local neighborhood to approximate the response variable and the weights given to each neighbor during function value approximation. A wide grid of neighborhood was tested with neighbors ranging between 1 and 50 for two weight parameters. These parameters were described as 'uniform' indicating that each neighbor would get the same weight in value approximation and 'distance' metric implying that each neighbor would be assigned a relative weightage based on its distance from the instance, meaning, closer neighbors to a query instance would have a greater influence, as compared to a farther neighbor.

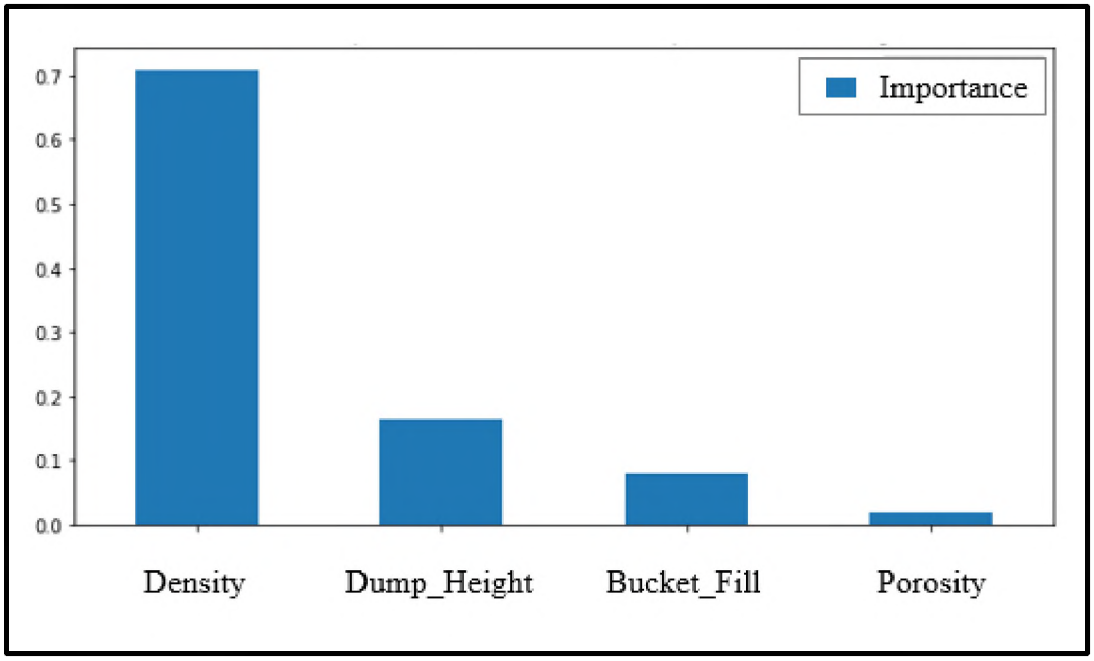

Figure 6.10. Relative Feature Importance Quantification for RF Model Development

Figure 6.11 shows the grid search results for the kNN model. It is evident that '4' data points in the neighborhood and the 'distance' metric for the weight given to each of those 4 neighbors, displayed the best performance result with least error on the validation dataset. Those optimum values for both hyper-parameters were then employed to train the final kNN model.

The same training data set was used for the development of the SVM model. Since the Gaussian kernel (radial basis function) has proven to be simpler, faster, robust, and more efficient than other kernel functions [157–159], it was used for developing the SVM model with a tolerance of 0.001. For RB kernel, gamma was the main parameter that required tuning. Apart from gamma, for every SVM, the cost parameter 'C' also requires optimization. Therefore, a grid search was made between the values of 0.01 to 5 for 'γ' and 1 to 500 for the parameter 'C.' Figure 6.12 shows the results for the grid search. It can be

seen that the value of 0.1 for the RB function parameter 'γ' and the value of 500 for cost error penalty parameter 'C' optimized the performance of RB-SVM model. Similar to the other machine learning models, a 5-fold cross validation was carried out during the hyper-parameter optimization in order to avoid any overfitting.

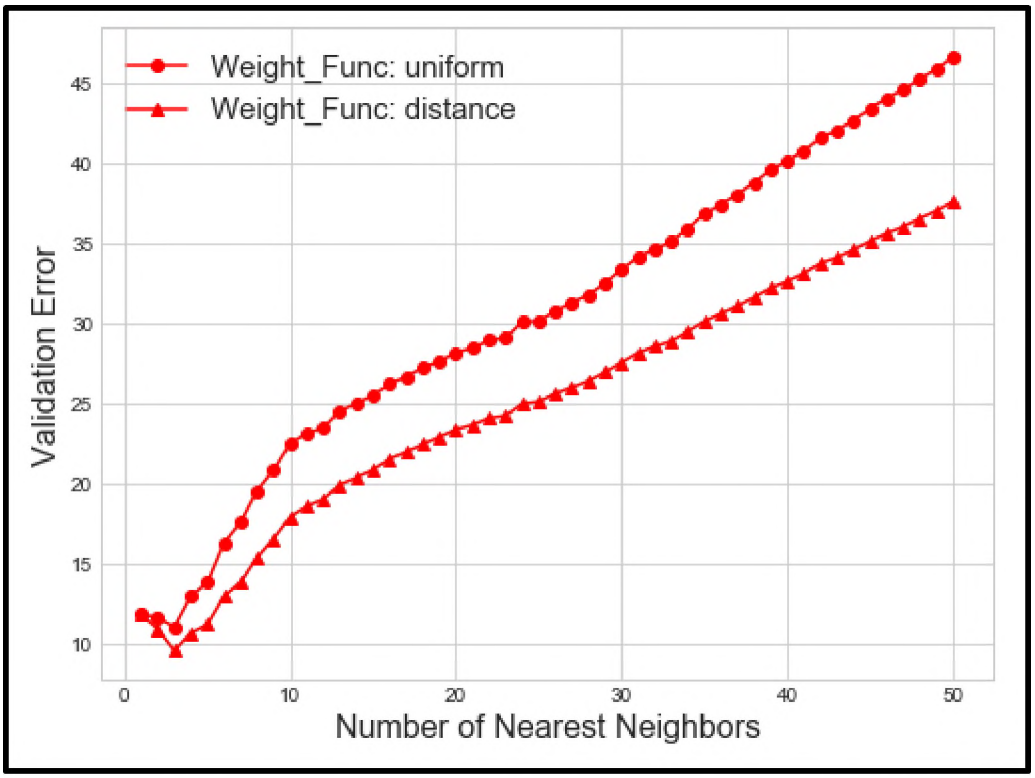

Figure 6.11. Grid Search Results for k-Nearest Neighbors (kNN) Model

Once the final ANN, RF, SVM, and kNN models were developed using the optimized parameters and the training was completed, all the models were put through rigorous test during the testing/validation phase. Furthermore, Wilcoxon signed-rank test was conducted for all the developed and validated models in order to investigate the

reliability of the performance results along with evaluating the novel DL model against these four machine leaning models.

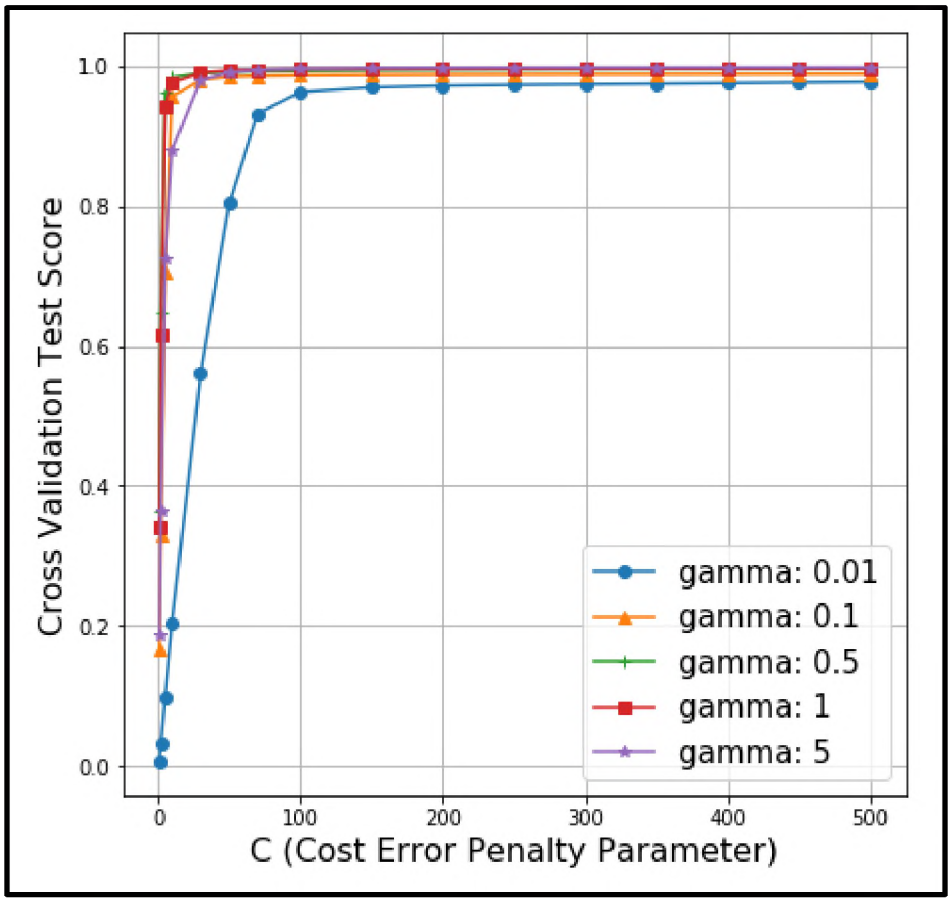

Figure 6.12. Grid Search Results for Support Vector Machine (SVM) Model

6.6. SUMMARY

This section described the detailed procedures for developing and implementing DL and AI based framework for real-time impact force monitoring during HISLO process.

Experimental data was used to develop the DL, AI, and machine learning models. A novel DL architecture was introduced for impact force monitoring during a HILSO operation. The DL model was tested and evaluated against four of the most widely used

state-of-the-art machine learning algorithms, namely, ANN, RL, SVM, and kNN. The experimental data was divided into two segments, i.e., training and testing with 80-20 proportion. Training dataset was used for model development and the testing dataset, was used to carry out the model evaluation. Three of the most widely used performance indicators, R-squared, MAE, and RMSE were used to evaluate the model performance.

The developed state-of-the-art DL-based model can be implemented for a real-time impact force monitoring during HISLO operation for every shovel pass. This allowed for an improved operation optimization resulting in reduced forces at the truck bed surface, and reduced vibration levels at the operator's seat. The technology will greatly improve the health and safety of truck operators.

7. ANALYSIS AND DISCUSSIONS OF RESULTS

This section presents the results of all the experiments conducted through mathematical model and virtual prototype model along with detailed discussions. The results and detailed discussions focus on experimentation of the DL, AI, and machine learning models in this study. The purpose of mathematical and virtual simulation experiments was to capture an accurate generation and progression of dynamic impact force at the truck bed surface during the HISLO process. The purpose of the AI modelling was to develop a framework for real-time impact force monitoring during the HISLO process.

7.1. RESULTS AND DISCUSSION FOR MATHEMATICAL MODEL

Detailed experimentation was conducted for testing the impact force capturing methodology and the constructed model. The experiments were conducted for the case of the P&H 4100XPC shovel loading the CAT 793D truck in a HISLO process. The EOMs for the complete vibration system were developed and solved to obtain the displacement vector. From the complete solution for the system, the displacement expression for the truck body '$\vec{z}_2(t)$' was differentiated twice and multiplied with the mass of the truck body section to obtain the final impact force model for the multi-pass HISLO process.

Figures 7.1 and 7.2 show the resulting dynamic impact force development and progression from the shovel dumping of the material under gravity during the first and second shovel pass, respectively. As the material came in contact with the truck surface, impact force began to develop. The force on the surface increased as more materials were dumped into the truck bed. The impact force reached a maximum magnitude when the bulk

of the material had dropped and hit the truck surface. This happened somewhere in the middle of the process when impulse acted on the truck surface. Once the bulk of the material had dropped, the forces on the truck body began to decrease and stabilize. At the end of the shovel pass, the force acting on the truck surface was just the static gravitational load (dead weight) due to all the material resting on that truck body.

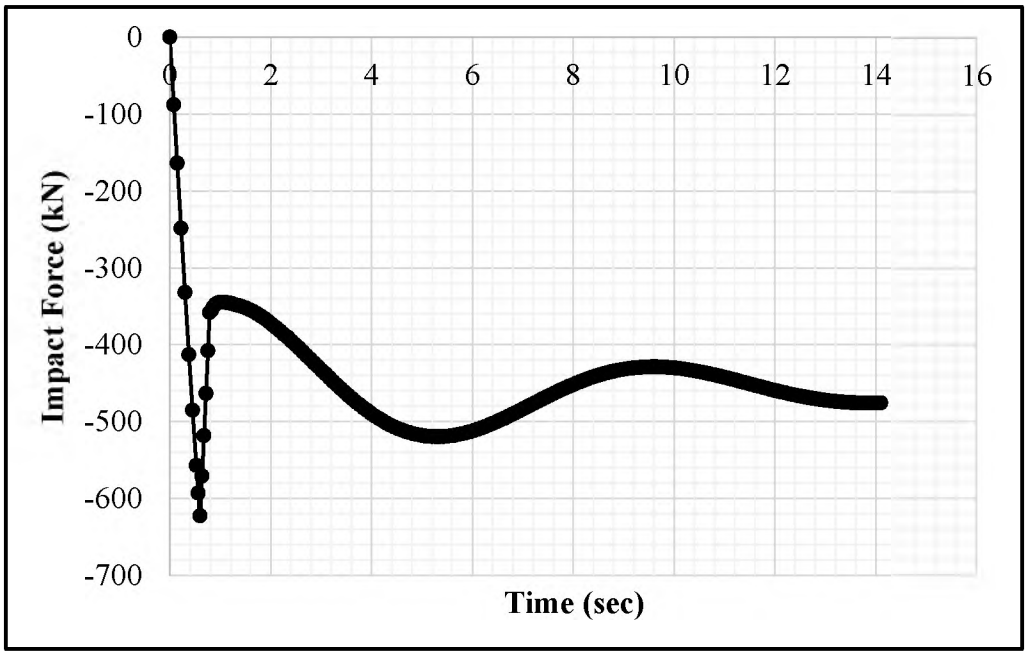

Figure 7.1. Impact Force during First Shovel Pass under HISLO process

The magnitude of the impact force is shown as a negative value to indicate the direction of the force acting on the truck surface as downward under gravity (negative z-direction). It is evident, by comparing Figures 7.1 and 7.2 that the development and the progression of the impact force followed the same trajectory for both shovel passes. The maximum absolute magnitude of the force for the second shovel pass was significantly reduced, as compared to that of the first shovel pass. Since there was no material on the

truck bed during the first shovel pass, the material came in direct contact with the surface and, thus, resulted in a higher degree of force, with magnitude of 623 kN, and a stronger impact. During the second shovel pass, however, the material from the first shovel pass was already on the truck body surface. Therefore, the rock/soil material from the second shovel pass did not come in direct contact with the truck body surface. The effect of the lack of direct contact was a reduced impact with a magnitude of 478 kN.

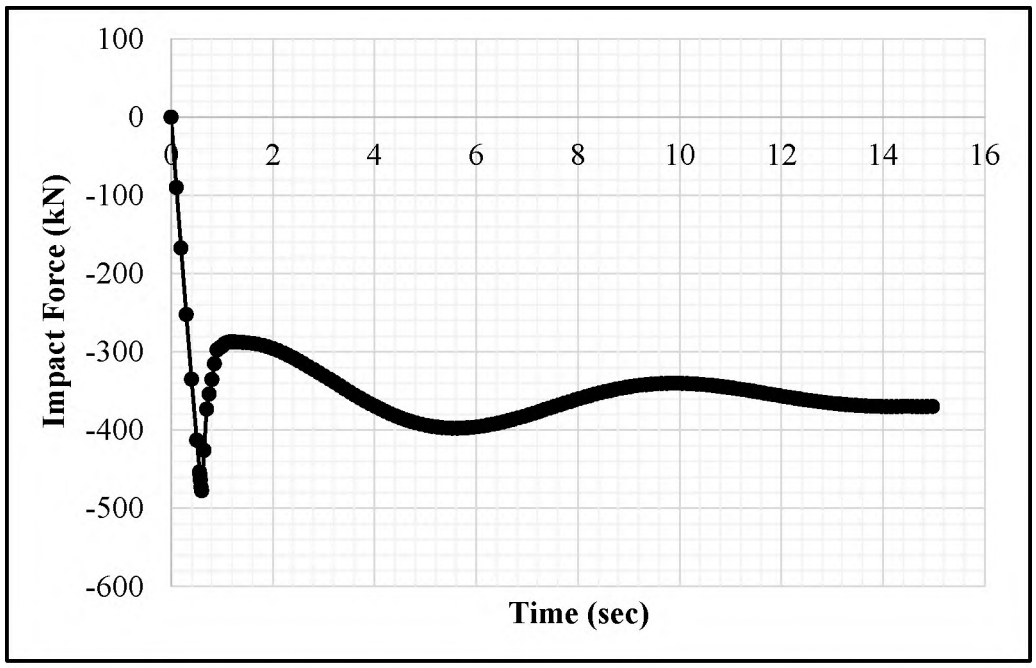

Figure 7.2. Impact Force during Second Shovel Pass under HISLO process

Table 7.1 clearly shows the effect of cushioning phenomenon being modelled and captured by the current impact force model. It can be seen that the maximum magnitude of the resulting force for the second shovel pass was reduced by 23.27% as a result of this cushioning effect.

Table 7.1. Cushioning Effect Observed during the Second Shovel Pass

Impact Force Maximum Magnitude during First Shovel Pass	**Impact Force Maximum Magnitude during Second Shovel Pass**	**% Difference**
kN	kN	
623	478	23.27

The work has contributed significantly by developing a mathematical model for capturing the resulting impact force during a HILSO operation for a multi-shovel pass dumping process. Truck body parameters, which play an important role in the development of these forces, have also been included using the modelling technique. Also, the cushioning effect, which is observed during any subsequent shovel pass after the first shovel pass in any HISLO process, has also been modelled and captured. This effect was not included in previously developed mathematical model of impact force.

7.2. RESULTS AND DISCUSSION FOR THE VIRTUAL SIMULATION

Detailed experiments were conducted using virtual prototype for CAT 793D truck and P&H 4100XPC cable shovel. Impact force at the truck bed surface generated due to material dumping under gravity into the truck body during the HISLO process was captured through those experiments. An improved representation of the HISLO process, with continuous flow dynamics ensured through FEA-DEM coupled methodology, allowed an accurate capturing of impact force. Controlled impact at the truck bed surface reduces the dynamic force which, in turn, reduces the resulting high frequency vibrations [8].

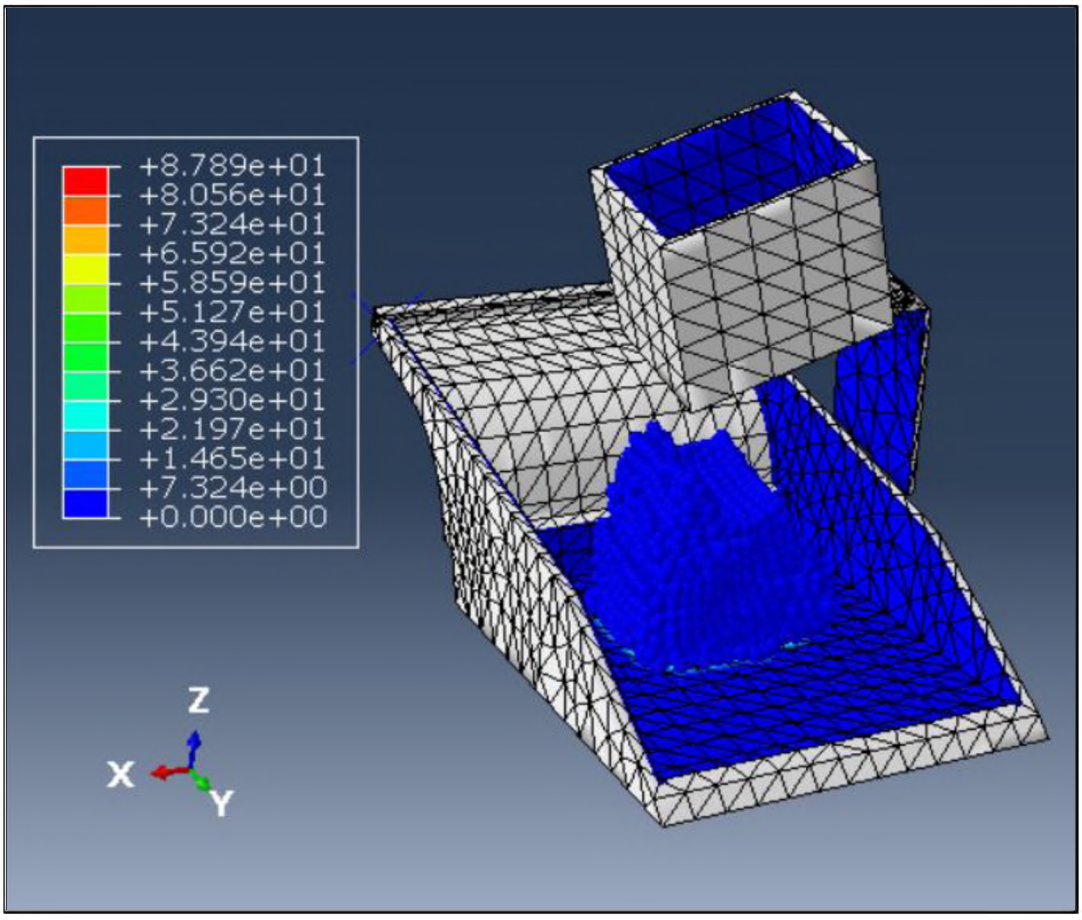

Figure 7.3. Material Contact during First Shovel Pass with Contact Force Distribution

Figures 7.3 and 7.4 display the dynamics for the first shovel pass along with the contact distribution during the experimental simulation process as the material contacts the truck bed surface initially and as the material settles down at the end of shovel pass, respectively. Figure 7.5 exhibits the initialization of dumping step of the HILSO experiment which starts off with the rotation of the dipper door as the material slides off the door surface and makes its way to the truck bed surface. Figure 7.6 provides the transitional phase of the dumping step with the dipper door completely opened and the rock/soil material almost out of the dipper. It can be seen that the door does not make any contact with the truck edges thus maintaining a safe clearance to prevent jolting and

ensuring operational safety and efficiency. Figure 7.7 shows the dynamics and the contact force distribution for the second shovel pass during the experimental simulation as the material contacts the previously dumped material. Figure 7.8 shows the dynamics and the contact force distribution for the same second shovel pass as the material finally settles to complete the second pass.

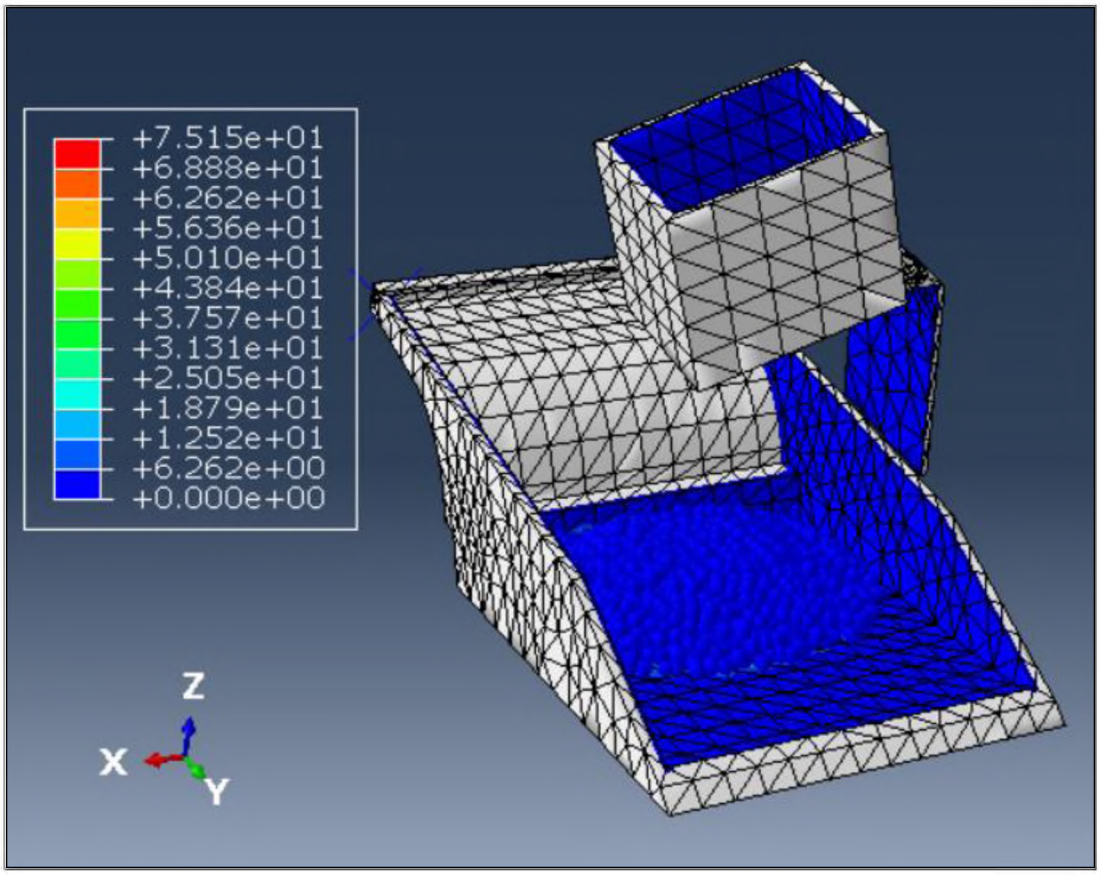

Figure 7.4. Material Settlement during First Shovel Pass with Contact Force Distribution

FEA-DEM coupled methodology examined the high impact shovel loading experiments in ABAQUS. DEM technique was used to simulate the shovel dipper payload. Each particle of the rock/soil material, representing an individual grain, in the shovel dipper

was modelled as a single-node PD3D element. The creation of DEM elements ensured individual material particles development inside the dipper with specific properties and interactive capabilities with each other, and with the neighboring structural surfaces, thus representing an actual dipper payload for any surface mining operation.

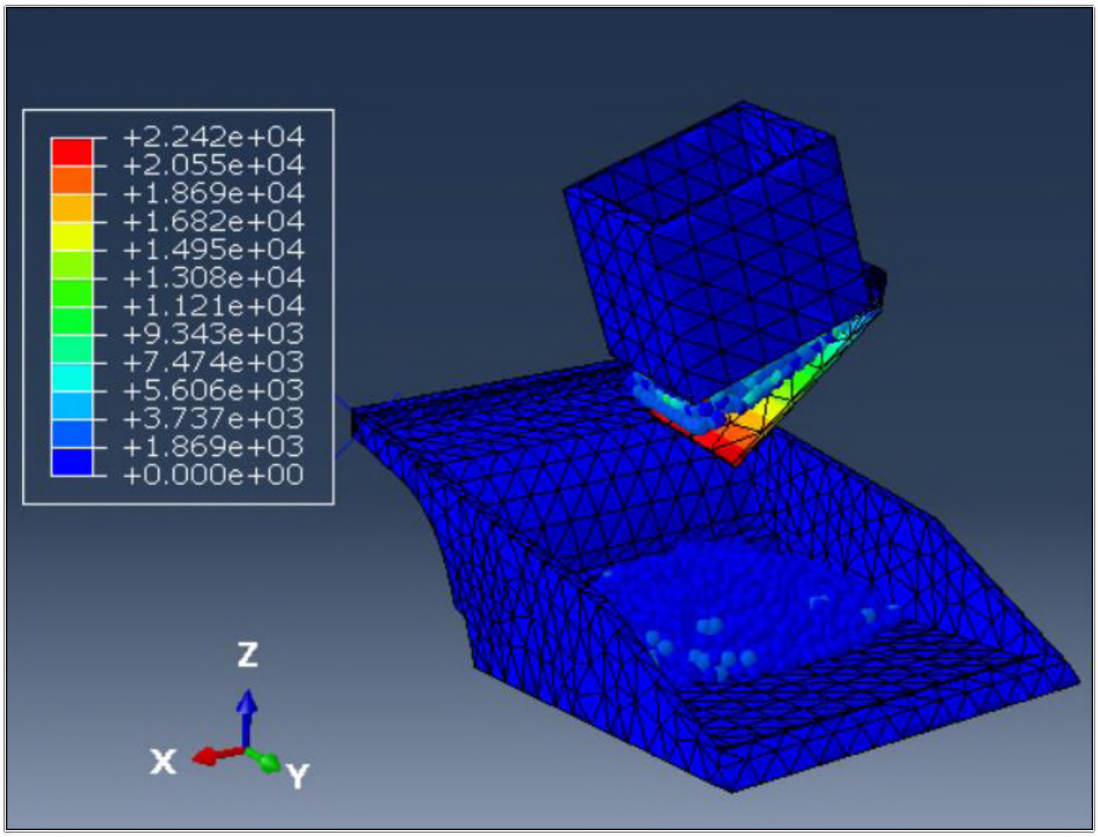

Figure 7.5. Initialization of Dumping Step with the Door Rotation and Material Sliding off the Door

For each experiment, the model took the initial 3 seconds to achieve stability. The rock/soil particles were created as DEM elements, rearrangement of the elements was done to remove any particle overlaps, material properties were assigned, contacts were established, forces were balanced, kinetic energies were dissipated, and material settled inside the shovel dipper. The cumulative weight of the material was kept to 100 tons to

model the high impact shovel loading operation. Once the particles lost their kinetic energy and the system was brought to an equilibrium, the settled particles inside the shovel dipper represented a single shovel pass.

ABAQUS/Explicit automatically specified the time increment based on the contact properties, DEM particle size, and the applied loads, in order to achieve a stable and accurate solution to the problem system. The dumping process started with the dipper door rotation, as soon as the model became stable. The material started flowing from the dipper under gravity and made its way onto the truck body.

During the dumping step of the experiment, the kinematics and the contact dynamics of soil/rock particles were generated within DEM as they moved under gravity. DEM considered the particle-to-particle interactions as dynamic process, and thus, equilibrium was reached as the internal forces balanced out. The basis of DEM is that the choice of time increment, during any single time step, should be such that the disturbances from any individual particle are confined to only its immediate neighbors. During the simulation process, every particle movement was traced, during each time step, with continuous computation and updating of the contact forces and displacements of the stressed assembly.

DEM calculations involved the application of Newton's second law to the individual particle elements and a force-displacement law at the contacts. The motion of the particles was computed using the Newton's second law along with the body forces acting on them. The force-displacement law was applied to compute and update the contact forces arising from the relative motion at each particle contact during every single time step. Establishing proper contact ensured a continuous flow of the material from the shovel

dipper to the truck bed surface, thus representing an accurate shovel dumping operation. FEA was activated as soon as the rock/soil particles, falling under gravity, were in contact with the walls and surfaces of the haul truck during the second step of the simulation.

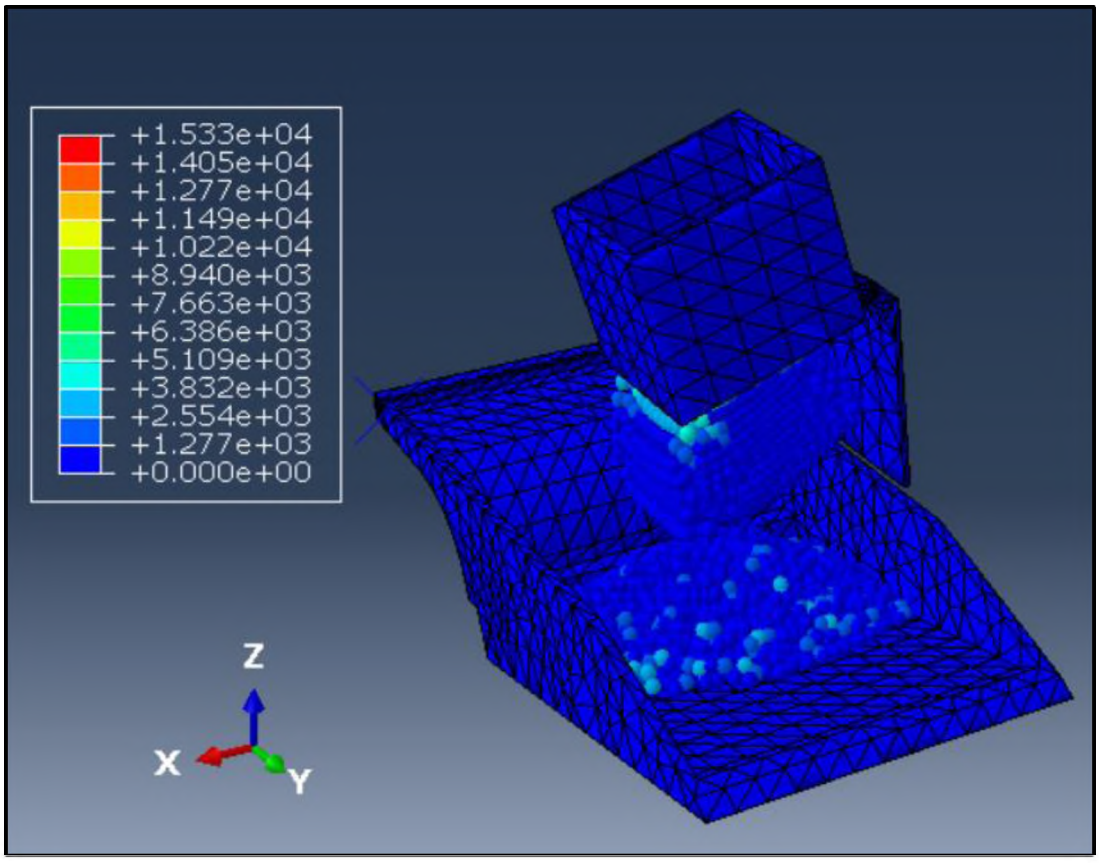

Figure 7.6. Dumping Step with Door Rotation Completed and Material Exited the Dipper

The solution to the higher order differential equations of the system was computed by FEA and the iterative numerical computation process was repeated for every element in the subjected FE mesh. The displacement, velocity and acceleration vectors of each element was computed through FEA, which generated the internal structural forces and stresses at the truck bed surface.

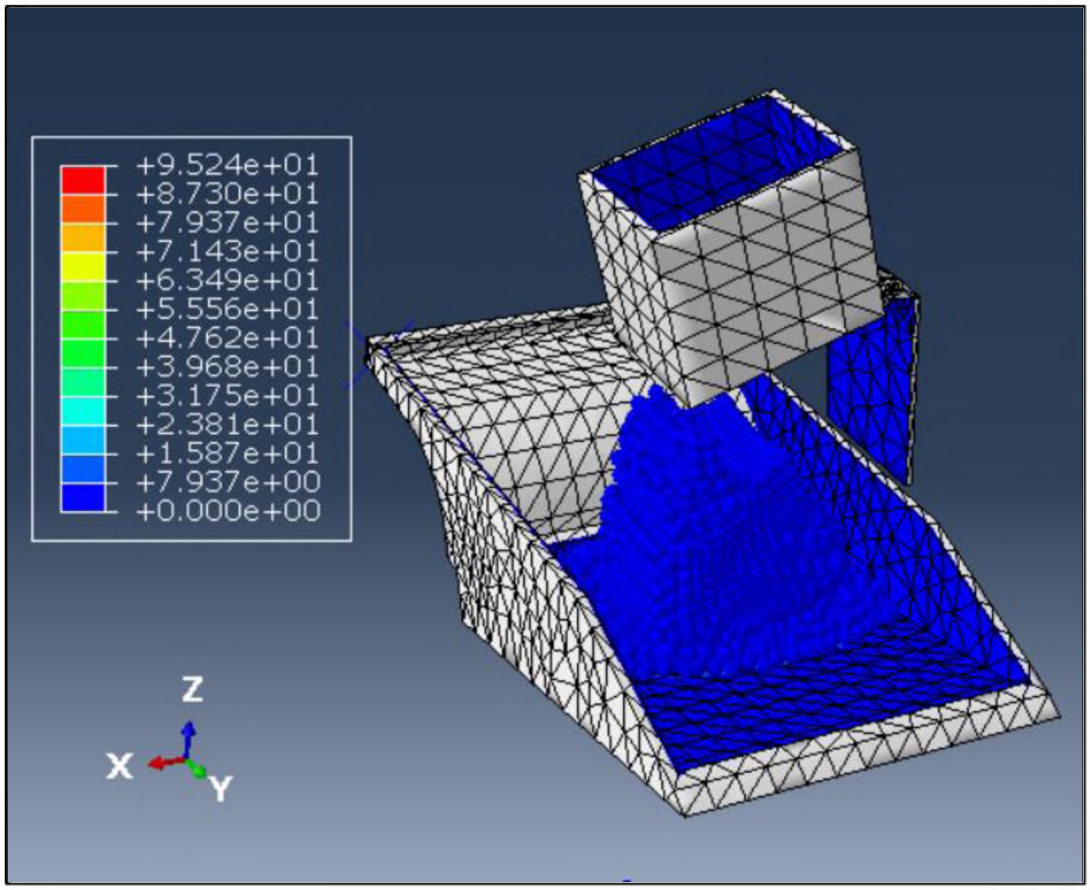

Figure 7.7. Material Initial Contact with Pre-existing Material during Second Shovel Pass with Contact Force Distribution

Figure 7.9 shows the resulting impact force on the truck body during the first two shovel pass for the experiment conducted with CAT 793D haul truck and P&H 4100XPC shovel. The development of the impact force, approximated through FEA, was recorded as soon as the material made contact with the truck bed surface. As majority of the material was dumped, the force increased rapidly and reached a maximum average amplitude of 571 kN at 6.85 s. Since the bulk of the material had already been dumped, the impact force began to reduce as the remaining material dropped and settled on the truck bed surface. The first shovel pass was completed at 8.6 s, and the shovel swung back to gather the next load of 100 tons. The material came to complete rest at 9.65 s, with impact force

stabilization. At this point, the truck bed surface experienced a constant force by the settled material. The shovel swung back to the bench, took another 100 tons load, swung back towards the truck, and dumped the material into the truck as the second shovel pass.

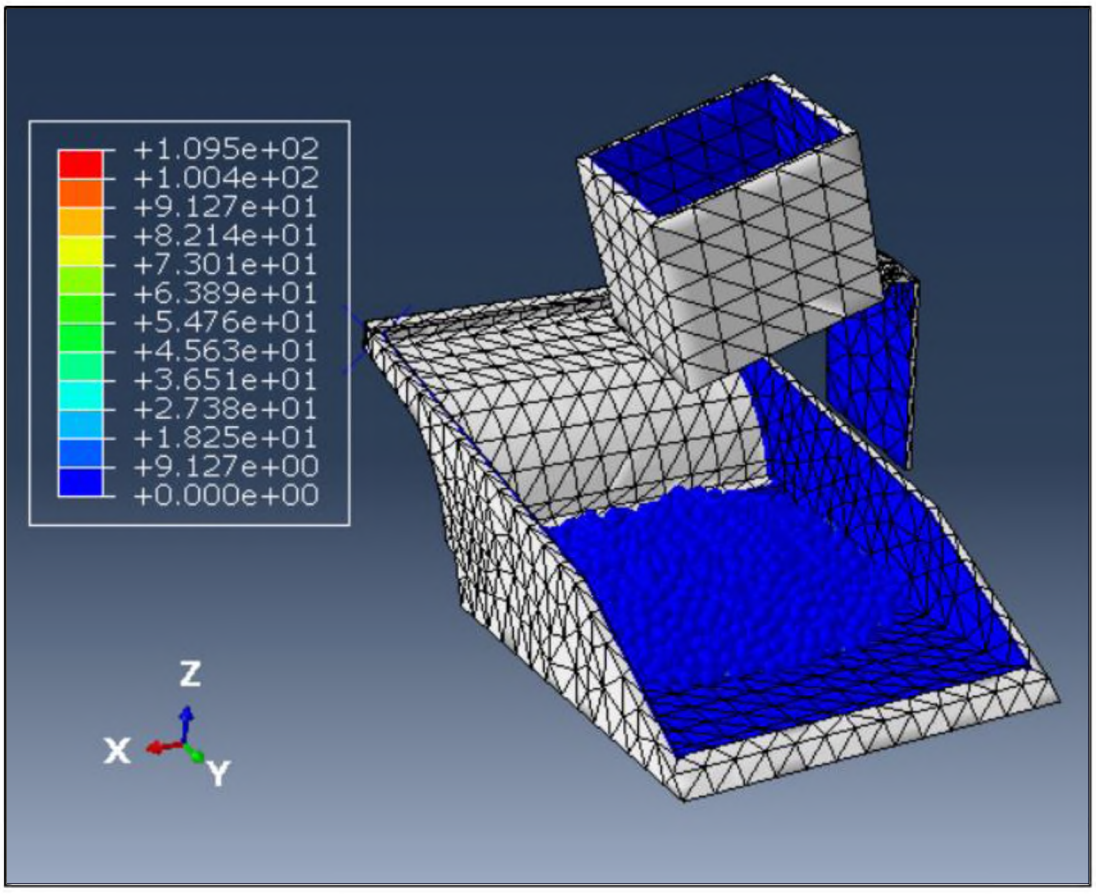

Figure 7.8. Material Settles Down with Pre-existing Material during Second Shovel Pass with Contact Force Distribution

Similar to the first shovel pass, the system took 3 seconds to attain equilibrium as the particles settled inside the shovel dipper. As the system initiated the dumping step, the dipper door rotated and the material from the second shovel pass fell onto the previously dumped material from the first shovel pass. The initial contact of the material happened at 16.2 s with increasing impact force on the truck body. The maximum amplitude of 422 kN

was recorded at 17.8 s when the bulk of the material from the second shovel pass had been dumped on the previously dumped material. The maximum impact force was reduced during the second shovel pass. This reduction was attributed to the material from the first shovel pass acting as a cushion. This cushioned material dampened the impact received by the truck bed during the second shovel pass. The material settled down, and the impact force on the surface reached a constant value of 896 kN at 21 s.

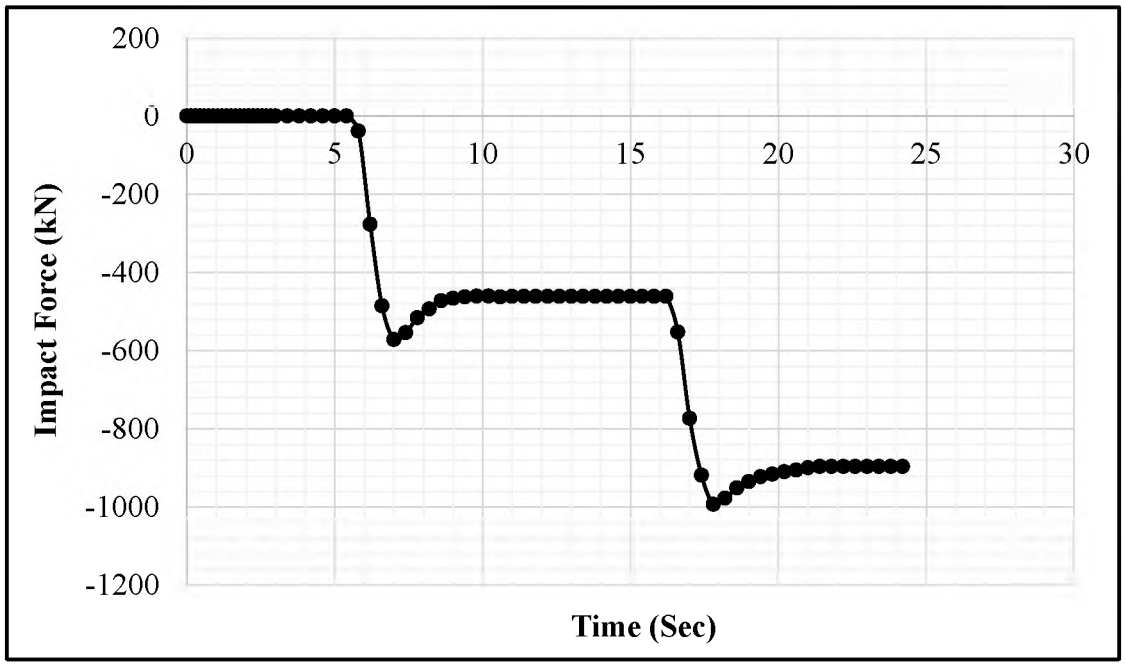

Figure 7.9. Average Incidental Impact Force Experienced by Truck Body

Figure 7.10 shows the cumulative reactive forces by the truck body during high impact shovel loading experiment. The reaction force of the truck bed started increasing after the material, at 5.8 s, made the initial contact. As the material was continuously dumped, the force increased and reached a maximum magnitude of 864 kN at 7.2 s. Once the first shovel pass had completed, and all the material had settled, the reaction force

stabilized at a value of 854 kN, which corresponded to the static gravitational load of the material supported by the truck bed. During the second shovel pass, as the material made contact with the previously dumped material, the truck body began to exert a reaction force to support the load. The reaction force reached a maximum amplitude of 1716 kN as the shovel pass completed. After the material from the second shovel pass had settled, the truck bed supported the total gravitational load of the material, which was 1708 kN from both shovel passes.

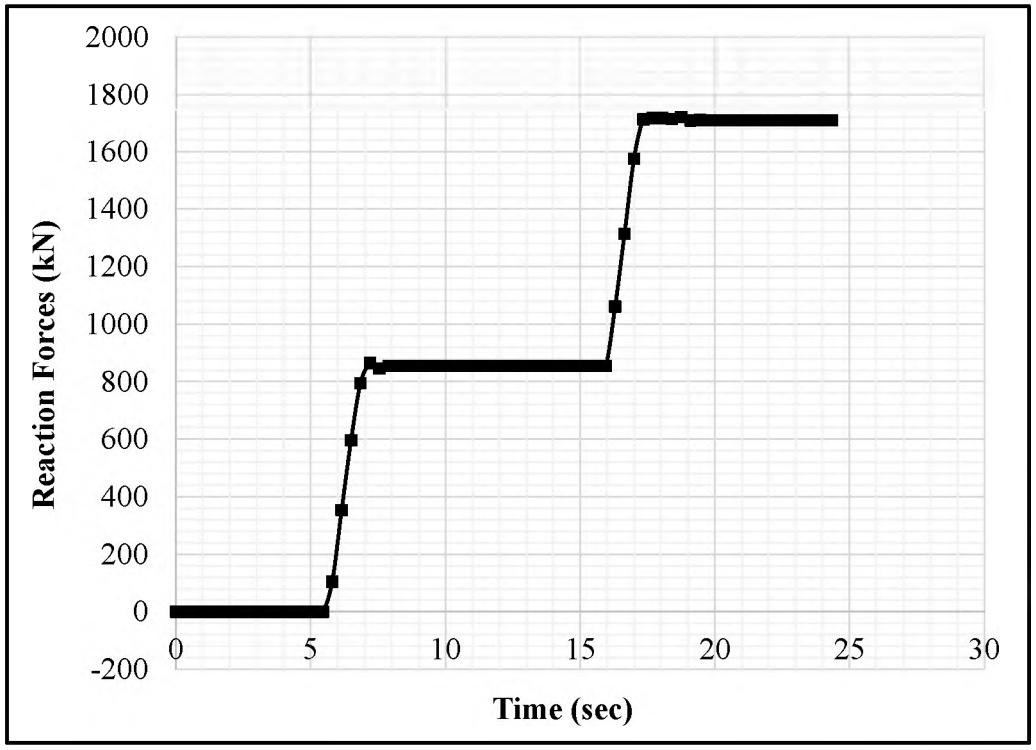

Figure 7.10. Cumulative Reactive Forces by the Truck Body

Table 7.2 displays the percentage reduction in the maximum impact force amplitude at the truck body during the second shovel pass in comparison to the first shovel pass. This shows the cushioning effect captured through the FEA-DEM coupled

methodology during the simulation experiment of HISLO process. The observed cushioning effect was significant as the maximum magnitude of the resulting force for the second shovel pass was reduced by 26.09%. This reduction is caused by the previously dumped material from the first shovel pass.

Table 7.3 provides a comparison of the recorded impact force maximum amplitudes through the simulation experiments with the existing approximated impact force level. Percent reduction is computed in order to quantify the effect of accurate modelling in terms of the recorded force magnitude. In the absence of the continuous flow modelling and capturing of the cushioning effect, the impulse force with an absolute of magnitude of 1000 kN was being used to analyze the multi-pass HISLO process [160]. The impact force captured in this study using the coupled FEA-DEM methodology shows a realistic representation of the actual shovel dumping process. The analysis shows a significant reduction of 42.9% and 57.8%, achieved during the first and second shovel pass, respectively, as 100 tons of rock/soil material is dropped at the truck bed surface.

Table 7.2. Cushioning Effect Captured through 3D Virtual Prototype during the Second Shovel Pass

Maximum Impact Force during First Shovel Pass	**Maximum Impact Force during Second Shovel Pass**	**% Difference**
kN	kN	
571	422	26.09

The results of the experiments showed an accurate capture of dynamic impact force through an improved modeling of shovel loading process by using the coupled FEA-DEM methodology. The recorded impact forces of 571 kN and 422 kN, for the first and second shovel passes showed a percent reduction of 42.9% and 57.8%, respectively, at the truck bed surface. These significantly reduced impact force magnitudes would translate into the vibration levels of 2.28 m/s^2 and 1.57 m/s^2, for the first and second shovel passes, respectively, based on [8], at the operator's seat. This translates to a vibration level reduction of 35.96% and 55.90%, during the first and second shovel passes, respectively, at the operator's seat. Thus, this accurate representation of shovel loading process with proper continuous flow dynamics can result in RMS acceleration value that falls under 'Uncomfortable' category, a significant improvement from the previous 'Extremely Uncomfortable' level, according to the ISO [4, 5, 22, 23] standards.

Table 7.3. Percent Reduction in Impact Force at the Truck Bed Surface during HISLO Process with Accurate Modelling

	Impact Force Used in Previous Studies [24, 160]	**Impact Force Captured during Present Study**	**% Reduction**
	kN	**kN**	
First Shovel Pass	1000	571	42.9%
Second Shovel Pass	1000	422	57.8%

7.3. RESULTS AND DISCUSSION FOR DL, AI, AND ML IMPLEMENTATION

A wide range of experiments were conducted to gather all the data pertaining to HISLO process. A DL model was developed and its performance evaluated against state-of-the-art ML models, including shallow feed-forward ANN, RF, kNN, and SVM. The data gathered from experiments was randomly divided into two parts: 80% of the data, comprising the training set, was used for model development while the remaining 20% was used for model validation.

Different DL architectures were trained and then put through validation using the training and testing datasets, respectively, for predicting the impact force on a truck bed during any HISLO process. Table 7.3 provides the performance results for different DL architectures. The training of all the DL architectures ceased before reaching the maximum number of epochs. It can be seen that as the network architecture got deeper and wider, in terms of number of fully-connected hidden layers and/or the number of hidden neurons, the number of trainable model parameters increased exponentially, thus requiring more computational time. It was interesting to note that with the addition of the dropout layer to a given network architecture, the error loss during model validation increased, though the sole purpose of the dropout layer was to avoid overfitting. Thus, it can be concluded that dropout layer failed to do its job during the model training.

The DL model, which will be referred to as 'DeepImpact,' consisted of three fully connected hidden layers between the basic input and the output layers. The model has 35, 20, and 12 neurons, respectively, starting from the first hidden layer that connected with the input layer. A novel architecture performed best, with the least error loss and highest accuracy, during model validation.

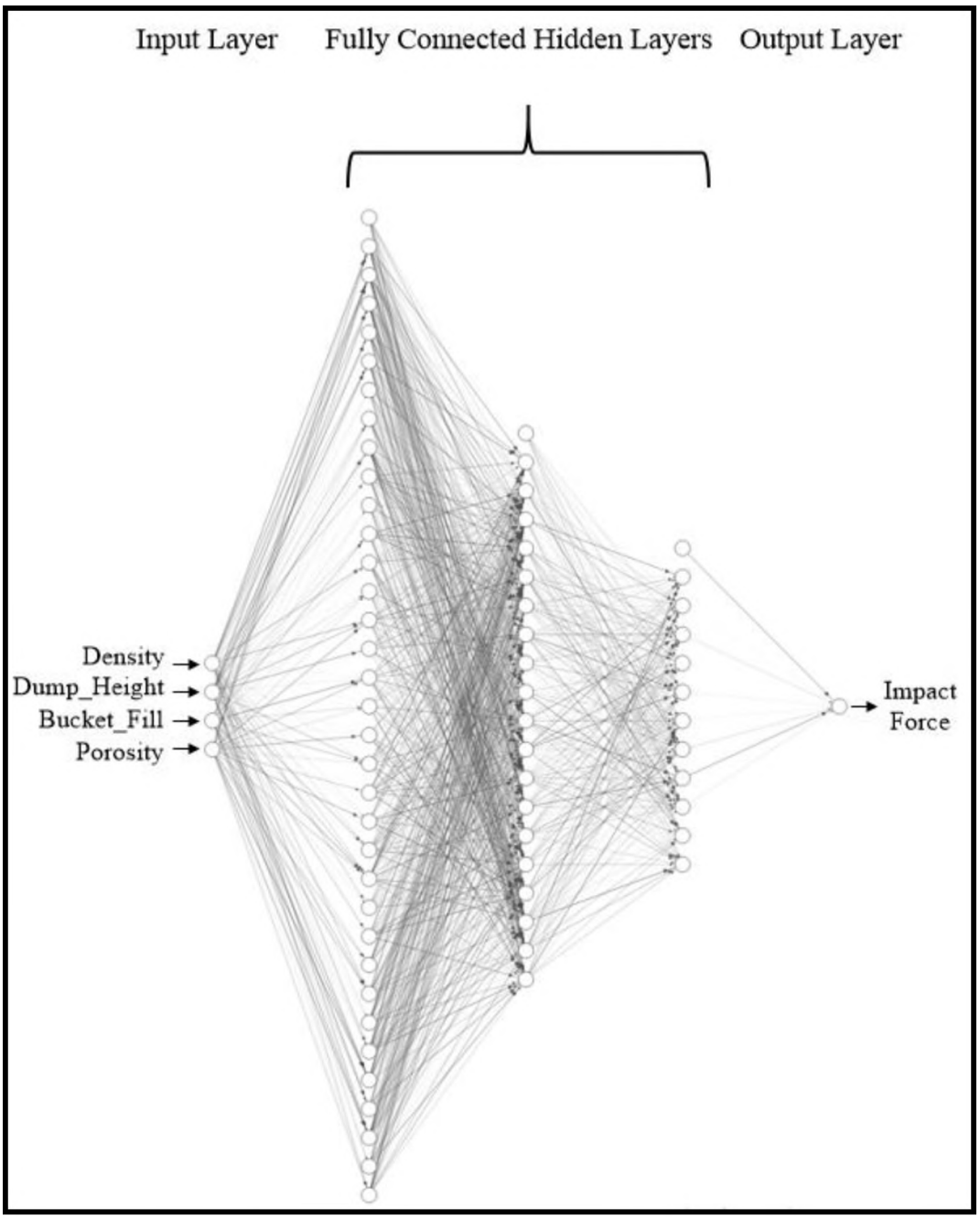

Figure 7.11. Final Deep Learning Model 'DeepImpact'

Figure 7.11 shows the final DL model 'DeepImpact,' with three fully connected hidden layers having 35, 20, and 12 neurons, respectively, between the input and output layer. The thickness and the darkness of the arrows connecting the neurons and the nodes

are proportional to the corresponding magnitude of the connection weight. The stronger the connection, the higher the magnitude of the connection weight and the thicker and darker the line connecting the corresponding neuron(s) and/or nodes.

Table 7.4. Performance Results for Different Deep Learning Architectures

Deep Learning Model Architecture	**Number of Trainable Model Parameters**	**Number of Epochs Utilized**	**Mean Error Loss during Model Validation**	**Mean Accuracy during Model Validation**
IN – HD(25) – HD(15) – OT	606	81	15.70	0.024
IN – HD(35) – HD(20) – OT	1021	74	15.75	0.023
IN – HD(35) – HD(20) – HD(12) – OT	1265	163	6.21	0.078
IN – HD(35) – DO(15%) – HD(20) – HD(12) – OT	1265	43	14.25	0.031
IN – HD(35) – DO(25%) – HD(20) – HD(12) – OT	1265	40	16.12	0.023
IN – HD(35) – DO(15%) – HD(20) – DO(15%) – HD(12) – OT	1265	25	16.00	0.031

Figure 7.12 shows the error loss evaluation for both training and validation phases during the final 'DeepImpact' model development using the optimized architecture. It can be seen that validation error loss for both training and validation phases began with an

extremely high value indicating a random initialization of the network. However, as the training continued, the deep network learned at an extremely rapid pace. Within five epochs, the performance stabilized, with training ending after 163 epochs as the validation error loss did not reduce further within four consecutive epochs.

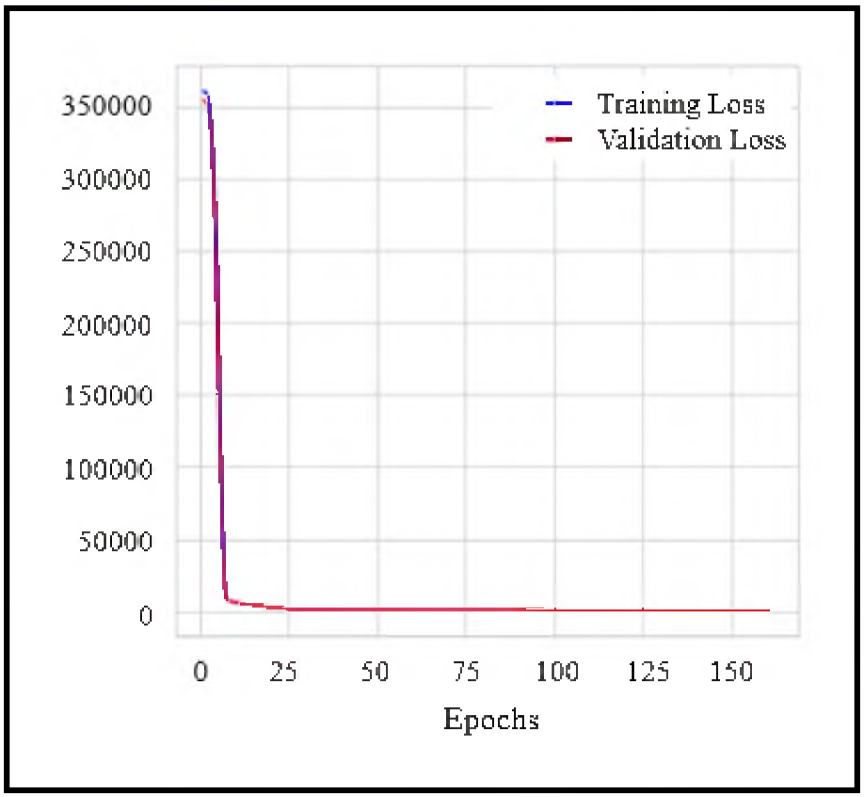

Figure 7.12. Error Loss Evaluation for Training and Validation Phase of 'DeepImpact' Model Development

The same training dataset was then used to develop the four aforementioned widely accepted state-of-the-art ML models, with validation carried out using the same testing dataset. The performance of the final DL architecture 'DeepImpact' was then evaluated against those ML algorithms, based on the most common and widely used statistical performance evaluation metrics, including R^2, the coefficient of determination (COD);

RMSE; and MAE. As a final step of the process, Wilcoxon signed-rank test was conducted to examine the reliability and statistical significance of the DL-based 'DeepImpact' model performance. The test investigated the possibility of the exhibited exceptional model performance being due to a random chance, noise in the data, or sampling error.

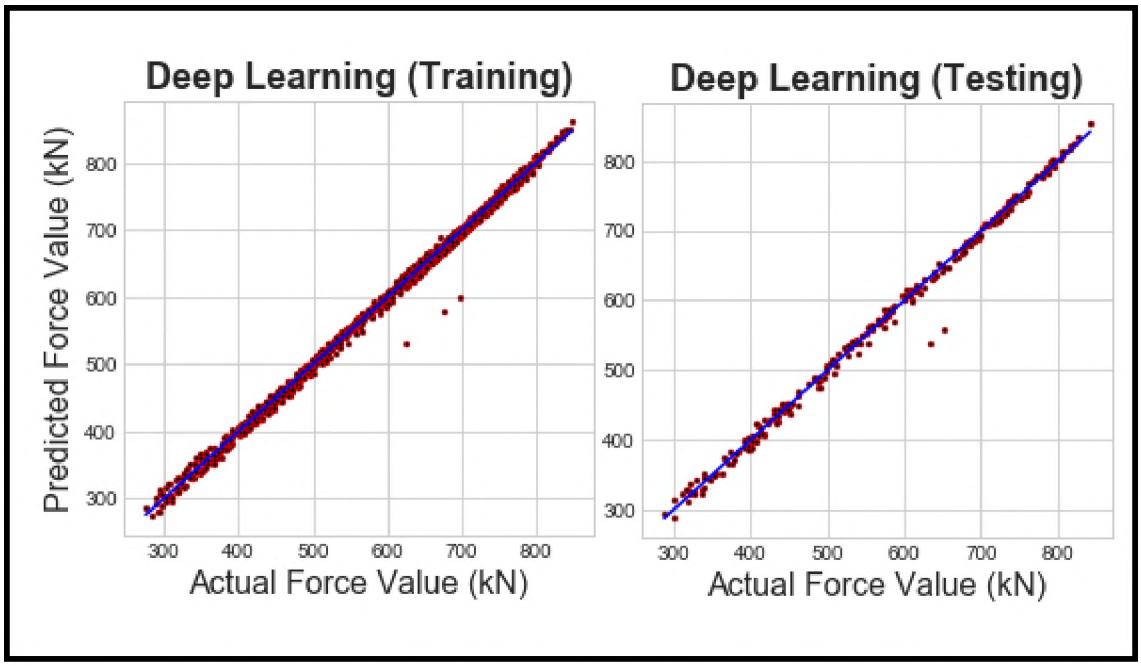

Figure 7.13. Real vs Predicted Plot for Deep Learning 'DeepImpact' Model

Figures 7.13, 7.14, 7.15, 7.16, and 7.17 show the plots for real vs predicted impact force values for the DL, kNN, RF, ANN, and SVM models, respectively, for both training and testing phases. A 1:1 correlation line has been included for every plot showing the goodness-of-fit between the actual impact force values and the predicted force values by the corresponding model during both stages.

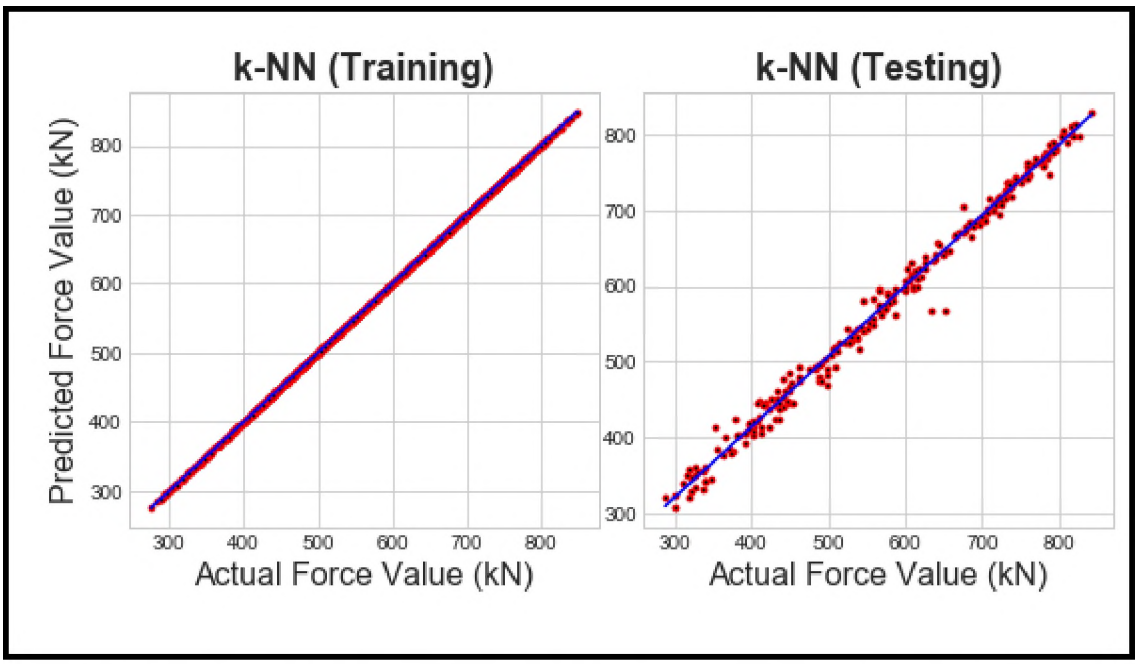

Figure 7.14. Real vs Predicted Plot for k-Nearest Neighbors (kNN) Model

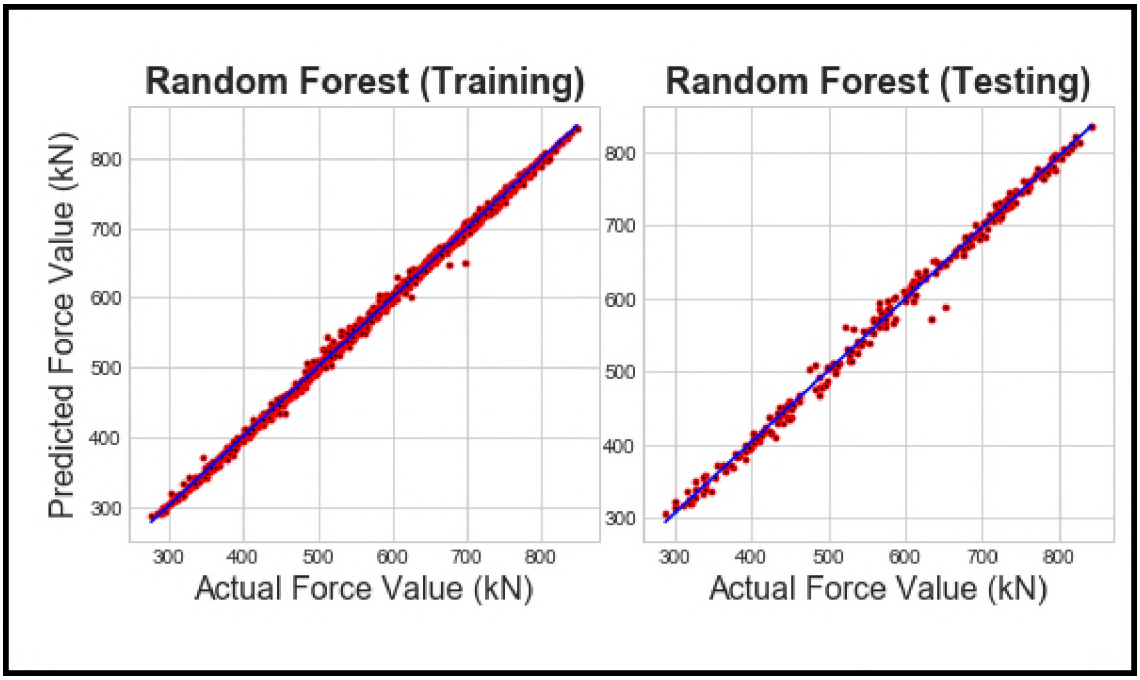

Figure 7.15. Real vs Predicted Plot for Random Forest (RF) Model

Table 7.4 provides the results of the performance evaluation of the ML algorithms and the 'DeepImpact' model. It can be seen that the testing error metrics, i.e., RMSE and MAE, were higher with coefficient of determination, indicating the goodness-of-fit, being lower as compared to that of the corresponding training metrics for every model. That resulted from the fact that the testing was done on a hold-out dataset, which was not used during model development. This provides an insight into the generalization ability of a model, and thus, performing deficiently in comparison to the training dataset. It must also be noted that the performance results during the testing phase were given more importance, when different data-based learning algorithms were evaluated against each other, for any given specific task, due to this demonstration of their ability to generalize for this operation/problem.

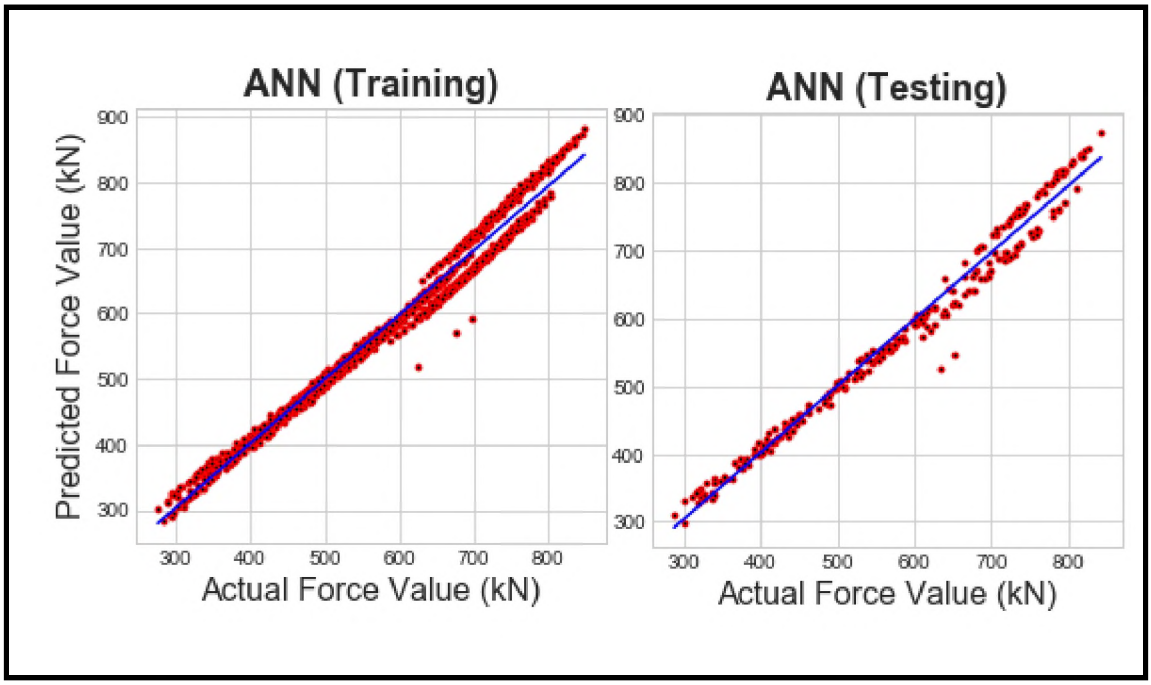

Figure 7.16. Real vs Predicted Plot for Shallow Artificial Neural Network (ANN) Model

Figure 7.17. Real vs Predicted Plot for Support Vector Machine (SVM) Model

The DL model 'DeepImpact' gave an R^2 value of 0.9948 during the testing phase, and RMSE and MAE values of 10.750 kN and 6.33 kN, respectively. Earlier, during the training phase, the model gave an R^2 value of 0.9958 and RMSE and MAE values of 9.106 kN and 6.192 kN, respectively. The k-nearest neighbor model performed best during the training phase with an R^2 value of 1 and a value of 0.0 for both RMSE and MAE. During the testing phase, the KNN model gave an R^2 value of 0.9875 and RMSE and MAE values of 16.58 kN and 12.05 kN, respectively.

A shallow feed-forward artificial neural network gave an R^2 value of 0.9812 during the training phase, and RMSE and MAE values of 19.44 kN and 15.45 kN, respectively. The model gave an R^2 value of 0.9810 and RMSE and MAE values of 20.36 kN and 15.69 kN, respectively, during the testing phase. The RF model performed fairly well during both training and testing phases as it gave R^2, RMSE, and MAE values of 0.9985, 5.537 kN,

and 3.864 kN, respectively, during the training stage and values of 0.9944, 11.05 kN, and 7.962 kN, respectively, during the model testing. The R^2, RMSE, and MAE values, for the SVM model came out to be 0.9892, 14.64 kN, and 9.110 kN, respectively, for the training phase and 0.9890, 15.54 kN, and 9.052 kN, respectively, for the testing phase.

Table 7.5. Performance Evaluation of 'DeepImpact' Model with other ML Models

	Training			**Testing**		
	R^2	**RMSE (kN)**	**MAE (kN)**	**R^2**	**RMSE (kN)**	**MAE (kN)**
RF	0.9985	5.537	3.864	0.9944	11.05	7.962
ANN	0.9812	19.44	15.45	0.9810	20.36	15.69
kNN	1.0	0.0	0.0	0.9875	16.58	12.05
SVM	0.9892	14.64	9.110	0.9890	15.54	9.052
'DeepImpact'	0.9958	9.106	6.192	0.9948	10.750	6.33

Table 7.6. Wilcoxon Signed-Rank Test Results

Machine Learning Model	**P-value Statistic**
Random Forest	0.012
Artificial Neural Network	0.038
k-Nearest Neighbors	0.007
Support Vector Machine	0.016

The kNN algorithm demonstrated a clear case of model overfitting as it performed best during the training and model development phase with perfect accuracy results. However, similar performance was not achieved during the model validation phase, thus exhibiting a lack of generalization ability. A shallow artificial neural network did not

perform well as its learning ability was confined to a single hidden layer, which was not enough, considering the problem complexity.

It was ascertained, through the analysis of model performance evaluation results, that the deep learning model 'DeepImpact' with three fully-connected hidden layers exhibited a state-of-art performance in terms of predicting and monitoring impact force generation during the high impact shovel loading operation. The ML model closest to the deep learning model, in terms of performance, was the RF algorithm. The RF model displayed its learning and prediction power for a real world operation. The complete order of model performance in terms of accuracy are as follows: DL > RF > SVM > kNN > ANN. Table 7.5 shows the p-value computed by comparing the performance results of each of these ML models with the DL-based 'DeepImpact' model using the Wilcoxon signed-rank test. It can be seen that each of the computed p-values, through the statistical testing, dropped below the set threshold value of 0.05 (5%) which indicates the rejection of null hypothesis. Thus, it can be concluded with confidence that the DL model's exceptional performance is significantly reliable with regards to predicting and monitoring impact force for any shovel dumping operation.

7.4. SUMMARY

This section presented the results along with detailed analysis and discussion for the experimentation conducted through mathematical model and 3D virtual prototype. The section also presented and discussed the results for the development of intelligence-based framework for real-time impact force monitoring using deep learning, AI, and ML algorithms, for HISLO process.

The mathematical model developed in Section 3, was tested through detailed experimentation. The experiment involved HISLO process involving the CAT 793D truck being loaded by the P&H 4100XPC shovel. A displacement vector was obtained by solving the EOMs for the complete vibration system, which was then further used to model the final impact force model for multi-shovel pass HISLO operation.

The virtual prototype for CAT 793D truck and P&H 4100XPC cable shovel, in Section 4, was used to conduct detailed experiments. Experiments were used to capture the impact force generated at the truck bed due to the gravity dumping of material during a HISLO process. The coupled FEA-DEM methodology was used to maintain proper continuous flow dynamics for the HISLO process, thus accurately capturing the dynamic impact force. The maximum impact forces magnitudes of 571 kN and 422 kN, for the first and second shovel passes, respectively, at the truck bed surface were recorded during the experiments. The vibration levels were reduced by 35.96% and 55.90%, during the first and second shovel passes, respectively, at the operator's seat. Based on the ISO [4, 5, 22, 23] standards, the RMS acceleration levels fall under 'Uncomfortable' category, which is an improvement from the previous 'Extremely Uncomfortable' level. This has been accomplished through the accurate representation of the shovel loading process using proper continuous flow dynamics.

The work also involved new knowledge and understanding into the whole body vibration exposure problem, which has impacted operator health and safety issues. A deep learning model was developed for impact force progression monitoring, thus intelligently implementing the process optimization in real-time. The developed state-of-the-art DL model 'DeepImpact' gave an R^2 value of 0.9948, and RMSE and MAE values of 10.750

and 6.33, respectively, during the testing phase. Thus, this outperformed the four ML algorithms including ANN, SVM, kNN, and RF models. With the implementation of such a smart system within a shovel control system, whole body vibration exposure to the truck operator could be effectively minimized, which would result in a safe working environment at every mine site.

8. SUMMARY, CONCLUSIONS, AND RECOMMENDATIONS

This section summarizes the research work carried out along with the conclusions drawn from this study. The section also includes the contributions from this research study to the existing body of knowledge, and the recommendations for advancing this research frontier.

8.1. SUMMARY

High impact shovel loading operations are fairly common in large scale surface mining operations due to significant economic advantages. Large impact forces are generated during material dumping from an ultra-large shovel dipper (in excess of 100 tons per pass under gravity) into the bed of ultra-large dump trucks due to the high frequency shock waves developed in the process. These shockwaves propagate through the body of the truck and chassis to an operator's cabin and seat. As a result, the operator's legs, lower back, shoulders, hands, spine, and neck are exposed to the high frequency shockwaves. This experience is referred to as whole body vibration (WBV). Under HISLO, WBV levels that exceed the recommended ISO safe limits, within the ISO 2631: Sections 1,2,4,5 [4, 5, 22, 23], generally exposes operators to safety and health risks.

Significant research on WBV phenomenon and its control solutions has been carried out in the area of military applications. While dump trucks are stationary elements, the external excitation force generated during HISLO operations is dynamic. Thus, military applications are starkly different from mining in terms of HISLO WBV phenomenon. Fundamental research for modelling HISLO impact force was carried out by Ali and Frimpong [9]. They developed a mathematical model to capture the dynamic impact force

for the first shovel pass of material under gravity into a truck. The research advanced the frontier of the existing knowledge. However, the model has significant limitations, including its inability to (i) model impact forces for subsequent passes after the first shovel pass; (ii) capture the cushioning effect of material from previous passes; and (iii) capture truck physical properties, which can have significant effect on the behavior of generated impact force.

Ali and Frimpong [6] presented the idea of controlling the WBVs by optimizing the shovel dumping operation. They showed that a reduction of 17.34% could be achieved during the first shovel pass by optimizing the dumping height during truck loading. That reduction in the impact force resulted in the reduction of vibrations levels at the operator's seat by 19.61% [8]. The solution framework from Ali and Frimpong [6] reduces the vibrations levels at the operator's seat from 3.56 m/s^2 to 2.86 m/s^2. However, based on the specified ISO safety limits, this value still exceeds the upper limit of the 'Extremely Uncomfortable Zone'. Thus, the current optimized process could still expose operators to high WBV levels that could cause permanent and life threatening injuries to mining truck operators. Therefore, there was a strong need to develop improved solutions to bring the vibration levels to within the comfortable category.

Comprehensive mathematical and virtual prototype models have been developed in this study to capture the generation and progression of dynamic impact force during the HISLO process. The study also developed a novel algorithm and framework to achieve the real-time monitoring and optimization of the HISLO process. The primary objective was to address the WBV problem under HISLO conditions and provide safe and healthy working environments for the shovel-truck operations in large scale surface mining

operations. This research was a pioneering effort towards improving the existing knowledge and advancing the frontiers for HISLO process. Following is the summary of the methods and procedures used in this study to achieve the objectives of this study:

1. The introduction provided the background of the HISLO problem with WBV exposure and its effect on the operator's health and safety. The study properly defined the research focus and the aims, objectives, and the scope for executing the research tasks. It also explained the adopted methodologies for achieving the stated objectives. The research novelty, along with its contributions to the body of knowledge, frontier advances, and to industry have been included in this section.
2. An in-depth critical review of all the relevant literature was carried out to examine the contributions, frontier advances, and the key limitations of the existing body of knowledge in relevant research areas. These areas include whole body vibrations, impact force modeling, discrete element analysis, dynamic virtual simulation systems, and smart solutions using artificial intelligence and machine learning. It was established through the literature review, that the fundamental work in HISLO vibration control was carried out by Ali and Frimpong [6]. It was established that the external impact force is the major cause of WBV, and then it was demonstrated, with shovel dumping height optimization, that the impact force can be reduced by 17.34% for the first shovel pass according to Ali and Frimpong [6] and that the resulting vibration levels at the operator's seat are reduced by 19.61% [8]. The solution framework provided by Ali and Frimpong [6] reduced the vibrations levels at the operator's seat from 3.56 m/s^2 to 2.86 m/s^2. However, based on the specified ISO safety limits, this value still exceeds the maximum limit of the 'Extremely

Uncomfortable Zone', which can still cause permanent and life endangering injuries to operators. Therefore, advanced research initiatives were required to provide solutions to the HISLO problems and their impact on operator safety and health.

3. A rigorous and a generalized mathematical model was developed for capturing the dynamic impact force on truck bed surface during any multi-pass shovel loading process. Multi-body Lagrangian mechanics was used to develop the governing equations of the complete system from which the mathematical model of the resulting forces was developed primarily for the truck body surface. The model provides the capability of capturing the cushioning effect of the existing material from previous shovel pass(es) on the subsequent shovel passes. The model can be used to understand the generation and propagation of impact force for any HISLO process.

4. Detailed experimentation was done using both mathematical model and the 3D virtual prototype. The experiments were conducted to investigate the generation and progression of dynamic impact force at the truck bed surface during a shovel dumping process. A thorough analysis was conducted for the case of CAT 793D dump truck getting loaded by a large cable shovel, i.e., P&H 4100 XPC. The cushioning effect for subsequent passes was observed and examined for multi-pass HISLO process.

5. An intelligence-based framework for real-time impact force monitoring during any high impact shovel loading operation was developed using deep learning and artificial intelligence. The framework required extensive operational data for

development. Therefore, all the data collected through virtual simulation experimentation was used to develop the deep learning, AI, and machine learning models. The novel deep learning architecture was introduced, developed, trained, and evaluated against four of the most widely used state-of-the-art machine learning algorithms, namely, artificial neural network (ANN), random forest, support vector machine (SVM), and k-Nearest neighbors (kNN), for impact force monitoring during a HILSO operation.

8.2. CONCLUSIONS

The following conclusions were drawn through a critical review of the relevant literature:

1. Significant research has been carried out into the WBV phenomenon and its control solutions in the area of military applications. Considering the fact that a dump truck is stationary and the excitation force introduced by the dumped material into the truck body is dynamic, the WBV phenomenon in HISLO is very much different from those in military applications. Vibrational levels for a dump truck were quantified by Aouad and Frimpong [24] through a detailed study of HISLO dynamic vibration by using a virtual simulator. Ali and Frimpong [6, 9] used mathematical and virtual models to optimize the shovel dumping operations. To the best of author's knowledge, no other study has developed solutions for HISLO vibration problem.
2. The existing mathematical model, provided by Ali and Frimpong [9], lacks critical parameters, which are essential for an accurate estimate of the impact force during

any HISLO scenario. Furthermore, the model was limited to a single shovel pass, and thus, it lacked practicality and widespread application.

3. The solution framework provided by Ali and Frimpong [6] reduced the vibrations levels on the operator's seat from 3.56 m/s^2 to 2.86 m/s^2. However, according to the specified ISO safety limits, this value still falls under the category of 'Highly Uncomfortable'.

4. Machine learning and artificial intelligence have been used previously in a variety of fields in the mining sector, including mineral resource mapping/exploration, mineral processing, and rock mechanics, for intelligence-based solution development. However, no work has been done for developing a framework for intelligent monitoring of impact force generation and progression at the truck bed surface.

5. Therefore, the present study was designed to achieve the following objectives: (i) develop a rigorous mathematical model for capturing the dynamic impact force during any multi-pass shovel loading operation; (ii) develop a 3D virtual prototype model to simulate the high impact shovel loading operation and examine the generation and progression of dynamic impact force; (iii) use artificial intelligence and machine learning algorithms to develop intelligence-based solution framework for real-time monitoring of the dynamic impact force along with optimization of the dumping process for solving the WBV problem.

The following conclusions were drawn through the development and experimentation of mathematical model:

1. A detailed mathematical modelling technique, based on multi-body Lagrangian mechanics, was used to formulate the governing system of equations that capture the impact forces during a shovel dumping process for a HISLO operation.
2. The developed model has the capability to capture the realistic impact force magnitudes for a multi-shovel pass dumping process. With the inclusion of critical truck parameters and the ability to capture the cushioning effect for any subsequent pass after prior shovel pass(es), the model captured the most accurate HISLO scenario and the resulting forces on a truck body surface.
3. The model was tested with detailed experimentation on a HISLO scenario involving the loading of the CAT 793D by P&H 4100XPC cable shovel.
4. A set of displacement vectors was obtained by solving the EOMs for the complete vibration system, which was further used to model the final impact force model for multi-shovel pass HISLO operation.
5. The captured profile of dynamic impact force showed that the development and the progression of the force followed the same trajectory for both shovel passes. However, the maximum absolute magnitude of the force for the second shovel pass was significantly reduced, as compared to that of the first shovel pass. The maximum amplitude of 623 kN was recorded during the first shovel pass, whereas a magnitude of 478 kN was observed during the second shovel pass.
6. The model has the capability to capture the cushioning effect introduced by the material from the first shovel pass over the truck body and, thus, reducing the resulting impact for the subsequent pass. As a result of the cushioning effect, the

maximum magnitude of the resulting force for the second shovel pass was reduced by 23.27%.

The virtual prototype model was designed to conduct detailed experiments with CAT 793D truck and P&H 4100XPC cable shovel. Proper dimensions were used for creating the CAD geometry of the model under SOLIDWORKS for the actual CAT 793D haul truck and P&H 4100 XPC shovel bucket. The discrete element method (DEM) was used, along with finite element method (FEM), for an accurate representation of the HISLO process since the dumping process involves loose rock/soil material dropping under gravity from the shovel bucket onto the truck bed surface. ABAQUS was employed as the prototyping platform using the coupled FEA-DEM methodology. Impact force at the truck bed surface generated due to the gravity dropping of material into the truck body during a high impact shovel loading operation was captured through those experiments. An improved representation of the HISLO process with continuous flow dynamics ensured through FEA-DEM coupled methodology allowed an accurate capturing of impact force.

Through the development of virtual prototype model, detailed experimentation, and a thorough analysis of the results, following conclusions were drawn:

1. The maximum impact force magnitudes recorded during the HISLO experiments were 571 kN and 422 kN, for the first and second shovel passes, respectively, at the truck bed surface.
2. The results showed that the vibration levels were reduced by 35.96% and 55.90%, during the first and second shovel passes, respectively, at the operator's seat.
3. With an accurate representation of shovel loading process with proper continuous flow dynamics, based on the ISO [4, 5, 22, 23] standards, the RMS acceleration

levels fall under 'Uncomfortable' category, which is an improvement from the previous 'Extremely Uncomfortable' zone.

A novel deep learning architecture referred to as 'DeepImpact' was introduced for impact force monitoring during a HISLO operation. Four of the most widely used state-of-the-art machine learning algorithms, namely, artificial neural network (ANN), random forest (RF), support vector machine (SVM), and k-nearest neighbors (kNN), were developed and used for testing and evaluation of the deep learning model. The results from the detailed experiments conducted using the virtual prototype model for varying material properties and operating conditions during the HISLO process were used for the development of data-driven intelligence-based models.

Through the development and implementation of intelligence-based framework for real-time impact force monitoring, following conclusions were drawn:

1. The experimental data was divided into two sections, i.e., training and testing with 80-20 proportion. Training dataset was used for model development and the testing dataset, was used to carry out the model evaluation.
2. The final novel 'DeepImpact' model consisted of an architecture with an input layer connected to three hidden layers with 35, 20, and 12 neurons, respectively, and an output layer.
3. Three of the most widely used performance indicators, R-squared, MAE (mean absolute error), and RMSE (root mean square error) were used to evaluate the model performance.

4. The complete order of model performance in terms of accuracy was as follows: deep learning (DL) > random forest (RF) > support vector machine (SVM) > k-nearest neighbors (kNN) > artificial neural network (ANN).
5. As the deep learning network architecture got deeper and wider, in terms of both the number of fully-connected hidden layers and/or the number of hidden neurons, the number of trainable model parameters increased exponentially, thus required more computational time during model development.
6. The purpose of dropout layer in a deep learning architecture is to avoid overfitting. However, it was observed in this study that the addition of the dropout layer to any given network architecture, resulted in an increase in error loss during model validation.
7. A clear case of overfitting was demonstrated by the kNN algorithm as it showed an exceptional performance during the training and model development phase with perfect accuracy results. However, during the model validation phase, similar performance was not achieved, thus exhibiting a lack of generalization ability.
8. A shallow artificial neural network has its learning capability confined to a single hidden layer, and thus, it was not able to perform well. Considering the problem complexity, its knowledge acquisition capability was inadequate.
9. Different DL architectures were tested in this study, with different number of fully-connected hidden layers, different number of neurons in each of those hidden layers, dropout layers at different locations, and varying the degree of dropout in the model. These deep learning model variants showed varied performance for predicting the impact force at the truck bed surface.

10. The final deep learning model, referred to as 'DeepImpact', showed a state-of-the-art performance in impact force monitoring during high impact shovel loading operation exhibiting R^2, RMSE, and MAE values of 0.9948, 10.750, and 6.33, respectively, during the final model validation.

8.3. RESEARCH CONTRIBUTIONS

This research study contributed by providing a better understanding of the dynamic impact force generation and progression through an accurate modelling of high impact shovel loading operations. The study also presented the development of advanced technological means by which the WBVs can be controlled during a HISLO process. In particular, the following were the scientific contributions of the research work to the existing body of knowledge and the industry through frontier advancement:

1. This work was a pioneering effort in developing solutions for addressing WBV problem, which is a serious health and safety concern for dump truck operators during HISLO processes.
2. The developed 3D virtual prototype model in this study can be used to examine the HISLO process with continuous material flow modeling using the FEA-DEM coupled methodology.
3. The study can be used to examine the cushioning effect due to the existing material on the truck bed surface during subsequent pass(es) in HISLO process.
4. The developed deep learning model can be used for impact force progression monitoring, and thus to implement intelligent HISLO process optimization in real-time.

5. With the implementation of such a smart system, within a shovel control system, WBV exposure to the truck operator could be effectively minimized, which would result in a safe working environment at every mine site.
6. The work provided comprehensive procedural details for developing a novel intelligence-based technology using state-of-the-art machine learning and artificial intelligence techniques, which serves as a benchmark for further smart technological advancement in the mining sector.

8.4. RECOMMENDATIONS

This study was a pioneering effort in understanding the HISLO process and developing solution for addressing WBV problem, which has been a serious health and safety concern for dump truck operators during HISLO processes. To improve upon the current, the following recommendations are made for critical examination through advanced research initiatives.

1. The 3D virtual prototype model developed in this study for examining the high impact shovel loading operation can be improved. The full-scale 3D virtual model of CAT 793D dump truck was developed using SOLIDWORKS. However, a simplified version consisting of truck body was executed in the detailed experimentations. A full-scale virtual model, representing the shovel dumping operation in real world, can be adapted to simulate the HISLO process using the FEA-DEM methodology. A better representation of the HISLO process, would allow for an even more accurate modelling of the generation and progression of dynamic impact force at the truck bed surface.

2. The modelling process of the coupled FEA-DEM procedures adopted for simulating the high impact shovel loading operation can be improved. The impact forces recorded at the truck bed surface through FEA largely depends upon the rock/soil material being dumped under gravity and the precision with which it is modelled through DEM. The current work has taken an assumption on the homogeneity and uniformity of particle shape and size distribution. That assumption can be relaxed by modelling the rock/soil particles with different shapes and sizes in an attempt to improve the overall accuracy of the HISLO process representation which would lead to an improved approximation of the impact force profile.
3. The deep learning model needs to train on an improved dataset. Detailed experiments needs to be conducted for a wider and a dense range of material properties and operating conditions. Noise could be added to the training dataset. Moreover, haul truck type and the corresponding suspension system properties need to be included as explanatory variables in the dataset. Training of the intelligence-based model, with such an enhanced dataset would improve the general applicability for any HISLO process.
4. The whole training and development process of the deep learning algorithm could also be improved. More advanced variants of deep learning architecture needs to be tested by either making the network deeper or by adding more complex layers to the model. This will enhance the model performance by ensuring robustness with an improved knowledge acquisition ability.

5. Validation of the AI and machine learning model is an important procedure and requires improvement. The deep learning model developed in this study was trained and validated using the simulated dataset. Simulation experiments are carried out in a controlled environment which may oversimplify the model testing. The validation of the deep learning model using the real-world field dataset would reflect on its generalization ability and would improve its wide-range applicability.
6. Performance evaluation of the deep learning and machine learning model is a key component during model development and testing procedure which can be improved. For evaluating the performance of AI models, the choice of the evaluation metrics (error estimate formulation) is of vital importance. The present study have used R-squared, RMSE, and MAE as the main performance evaluation metrics during the model evaluation phase. Further studies can be conducted using improved composite metrics such as mean absolute scaled error (MASE), relative mean absolute scaled error (RelMAE), and relative root mean square error (RelRMSE). This will improve the overall evaluation process and will strengthen the state-of-the-art performance claim for the deep learning model.

BIBLIOGRAPHY

1. DOE (2019) Mining Industry Profile. https://www.energy.gov/eere/amo/mining-industry-profile. Accessed 10 Jul 2019

2. Ramani R V. (2012) Surface mining technology: progress and prospects. Procedia Eng 46:9–21

3. Frimpong S (2020) Course Notes on MIN Eng. 4933, "Surface Mining Methods and Equipment,." Missouri University of Science & Technology, Rolla MO, USA

4. ISO 2631 – 1 (1997) Mechanical Vibration and Shock – Evaluation of Human Exposure to Whole Body Vibration – Part 1: General Requirements. Int Organ Stand Switz

5. ISO 2631 – 5 (2004) Mechanical Vibration and Shock – Evaluation of Human Exposure to Whole Body Vibration – Part 5: Method for Evaluation of Vibration containing Multiple Shocks. Int Organ Stand Switz

6. Ali D, Frimpong S (2017) Virtual Simulation of High Impact Shovel Loading Operation for Optimum Dumping Characterization. J Powder Metall Min 06:1–9. https://doi.org/10.4172/2168-9806.1000149

7. Ali D (2016) Mechanics of impulse force reduction for mitigating dump truck vibrations under HISLO conditions. Missouri University of Science and Technology, Rolla MO, USA

8. Ali D, Frimpong S (2019) Virtual Prototype Simulation for Vibration Analysis with Optimum Dumping Characterization under High Impact Shovel Loading Conditions. Int J Min Sci 5:14–22

9. Ali D, Frimpong S (2018) Impulse force reductions and their effects on WBV exposures in high impact shovel loading operations. Int J Min Sci Technol 28:423–435. https://doi.org/10.1016/j.ijmst.2018.03.007

10. Dindarloo SR (2016) Dynamic impact of ageing dump truck suspension systems on whole-body vibrations in high-impact shovel loading operations. Missouri University of Science and Technology, Rolla MO

11. McManus SJ, St. Clair KA, Boileau PE, et al (2002) Evaluation of Vibration and Shock Attenuation Performance of a Suspension Seat with a Semi-Active Magnetorheological Fluid Damper. J Sound Vib 253:313–327

12. Friedmann PP (1997) A Fundamental Study of Active Vibration Control in Rotorcraft using the ACSR Approach. In: US Army Research Office, Engineering and Environmental Science Division. Research Triangle Park, NC 27709-2211

13. Law SS, Wu ZM, Chan SL (2004) Vibration Control Study of a Suspension Footbridge Using Hybrid Slotted Bolted Connection Elements. Eng Struct 26:107–116

14. Choi YT, Wereley NM (2003) Vibration Control of a Landing Gear System Featuring Electrorheologicai!Magnetorheological Fluids. J Aircr 40:432–439

15. Wickramasinghe, V.; Zimcik, D.; Chen Y (2004) A Novel Adaptive Structural Impedance Control Approach to Suppress Aircraft Vibration and Noise. Pap Present RTO AVT

16. Moses RW (1997) Vertical-Tail-Buffeting Alleviation using Piezoelectric Actuators: Some results of the Actively Controlled Response of Buffet-Affected Tails (ACROBAT) program. In: SPIE. pp 87 – 98

17. Wang KW (2006) Piezoelectric Tailoring with Enhanced Electromechanical Coupling for Concurrent Vibration Control of Mistuned Periodic Structures. Arlington, VA

18. Ruff T (2002) Hazard Detection and Warning Devices: Safety Enhancement for Off-Highway Dump Trucks. A Compend NIOSH Min Res Washingt DC

19. Aldinger JA, Kenny JM, Keran CM (1995) Mobile Equipment Accidents in Surface Coal Mines. US Bur Mines, Inf Circ 9428 51

20. Ruff T, Coleman P, Martini L (2011) Machine-related injuries in the US mining industry and priorities for safety research. Int J Inj Contr Saf Promot 18:11–20. https://doi.org/10.1080/17457300.2010.487154

21. MSHA (2019) Mine Injury and Worktime

22. ISO 2631 – 2 (2003) Mechanical Vibration and Shock – Evaluation of Human Exposure to Whole Body Vibration – Part 2: Vibrations in buildings (1 Hz to 80 Hz). Int Organ Stand Switz

23. ISO 2631 – 4 (2001) Mechanical Vibration and Shock – Evaluation of Human Exposure to Whole Body Vibration – Part 4: Guidelines for the evaluation of the effects of Vibration and Rotational Motion on Passenger and Crew Comfort in Fixed guide way Transport Systems. Int Organ Stand Switz

24. Aouad N, Frimpong S (2013) Virtual Prototype Simulation of Truck Vibrations in High-Impact Shovel Loading Operations. J Powder Met Min S1:004: https://doi.org/10.4172/2168-9806.S1-004

25. Cowings PS, Toscano WB, DeRoshia C, Tauson RA (2001) Effects of command and control vehicle (C2V) operational environment on soldier health and performance. Hum Perf Extrem Env 5:66–91

26. Rozali A, Rampal KG, Shamsul Bahri MT, et al (2009) Low back pain and association with whole body vibration among military armoured vehicle drivers in Malaysia. Med J Malaysia 64:197–204

27. Khan M, Gani A, Ab Aziz SA, Hassan AH (2010) Determination of whole body vIbration (WBV) of Main Battle Tank (MBT) PT-91M. Def S T Tech Bull 3:29–35

28. Ha SH, Seong MS, Choi SB (2013) Design and vibration control of military vehicle suspension system using magnetorheological damper and disc spring. Smart Mater Struct 22:065006

29. Iverson S, Jung SJ, Biswas K (2003) Comparison of Ore Pass Computer Simulations for Designs Against Dynamic Load. In: Annual meeting of the Society for Mining, Metallurgical, and Exploration, Inc. 24–26 February 2003. Cincinnati, OH, USA

30. Metz R (2007) Impact and drop testing with ICP® force sensors. . J Sound Vib 41:18–20

31. Yan-hua S, Min X, Chun J, et al (2015) Operator Health Risk Evaluation of Off-Highway Dump Truck under Shovel Loading Condition. J Cent South Univ 22:2655 – 2664

32. Miller RE, Boman P, Walden J, et al (2000) Acceleration and GPS Data Monitor Truck-Haulage Jolts. Min Eng 58:20–22

33. Kittusamy NK (2002) Ergonomic Risk Factors – A study of Heavy Earthmoving Machinery Operators. ASSE Found Res 38 – 45

34. Kittusamy NK (2004) A checklist for evaluating cab design of construction equipment. Appl Occup Environ Hyg 18:721– 723

35. Kittusamy NK, Mayton AG, Jobes CC, Ambrose DH (2003) N361 A Systematic Comparison of Different Seats on Shuttle Cars Used in Underground Coal Mines. In: The 32nd International Congress and Exposition on Noise Control Engineering. Seogwipo, Korea

36. Kittusamy NK (2003) Self-Reported Musculoskeletal Symptoms among Operators of Heavy Construction Equipment. In: XVth Triennial Congress, International Ergonomics Association. Seoul, Korea

37. Kittusamy NK, Viswanathan M, Jorgensen MJ (2005) Field Study to Evaluate the Effectiveness of a Continuous Passive Lumbar Motion System. In: XIX Annual International Occupational Ergonomics and Safety Conference. Las Vegas, Nevada, USA

38. Eger T, Smets M, Grenier S (2005) Whole-Body-Vibration Exposure Experienced During the Operation of Small and Large Load-Haul-Dump Vehicles. In: 5th Canadian Rural Health Research Society Conference and the Fourth International Rural Nurses Congress. Sudbury, ON

39. Hoy J, Mubarak N, Nelson S, et al (2005) Whole body vibration and posture as risk factors for low back pain among forklift truck drivers. J Sound Vib 284:933–946. https://doi.org/10.1016/J.JSV.2004.07.020

40. Wenzhang Z, Yi L, Guobiao S, Ligong W (2000) Study on Non-Linear Dynamic Characteristic of Vehicle Suspension Rubber Component. In: 2000 North American ADAMS User Conference. Orlando, FL, USA, pp 19 – 21

41. Kim W, Lee J-W, Kim H-K, Doo M-S (2001) Handling Analysis of Active Height Control System using ADAMS. In: North American MDI Users' Conference. Novi, Michigan, USA, pp 18–20

42. Chang MK, Li YF, Huang HW (2011) Hazard of Vibration and Healthy Risk Assessment for Domestic Dump Truck Driver in Taiwan. Appl Mech Mater 52–54:186–191. https://doi.org/10.4028/www.scientific.net/AMM.52-54.186

43. Frimpong S, Galecki G, Chang Z (2011) Dump truck operator vibration control in high-impact shovel loading operations. Int J Mining, Reclam Environ 25:213–225

44. Aouad N, Frimpong S (2014) Lagrangian Formulation and Numerical Solutions to Dump Truck Vibrations Under HISLO Conditions. J Vib Acoust 136:021020. https://doi.org/10.1115/1.4026479

45. Doktan M (2001) Impact of Blast Fragmentation on Truck Shovel Fleet Performance. In: 17th International Mining Congress and Exhibition of Turkey, Antalya. pp 375–379

46. Teufelsbauer H, Wang Y, Pudasaini SP, et al (2011) DEM simulation of impact force exerted by granular flow on rigid structures. Acta Geotech 6:119–133. https://doi.org/10.1007/s11440-011-0140-9

47. Hosseininia ES (2012) Discrete element modeling of inherently anisotropic granular assemblies with polygonal particles. Particuology 10:542–552. https://doi.org/10.1016/J.PARTIC.2011.11.015

48. Law RPH, Lam AYT, Choi KY (2013) A Numerical Study of Granular Surge Flow through a Row of Baffles. In: Proceedings of the 18th International Conference on Soil Mechanics and Geotechnical Engineering. Paris

49. Albaba A, Lambert S, Nicot F, Chareye B (2014) DEM simulation of dry granular flow impacting a rigid wall. Comput Methods Recent Adv Geomech – Oka, Murakami, Uzuoka Kimoto (Eds), Taylor Fr Group, London 1869–1874. https://doi.org/10.1201/b17435-331

50. Bruno AC, Schifini R, Khüner GS, et al (2001) New magnetic techniques for inspection and metal-loss assessment of oil pipelines. J Magn Magn Mater 226:2061–2062

51. Bobaru F, Rattanadit K, Promratana K, Turner JA (2009) Force Chains and Resonant Behavior in Bending of a Granular Layer on an Elastic Support. Fac Publ from Dep Eng Mech Publ Mech Mater 41:691–706. https://doi.org/10.1016/j.mechmat.2009.01.023

52. Leonardi A, Wittel FK, Mendoza M, et al (2014) Particle-fluid-structure interaction for debris flow impact on flexible barriers. Zurich, Switzerland

53. Ur Rehman A, Awuah-Offei K, Sherizadeh T (2020) Discrete Element Modeling of Scaled Bucket Excavation. In: 54th U.S. Rock Mechanics/Geomechanics Symposium. American Rock Mechanics Association

54. Rehman AU, Awuah-Offei K (2020) Understanding How Speed, Tractive Effort, Digging Height, and Rake Angle Affect Bucket Penetration and Resistive Forces for Rubber Tire Loaders. Mining, Metall Explor 37:1423–1435

55. Narendran TV, Weinelt B (2017) Digital Transformation Initiative Mining and Metals Industry. In: World Econ. Forum. http://reports.weforum.org/digital-transformation/wp-content/blogs.dir/94/mp/files/pages/files/wef-dti-mining-and-metals-white-paper.pdf. Accessed 10 Jun 2019

56. Bellamy D, Pravica L (2011) Assessing the Impact of Driverless Haul Trucks in Australian Surface Mining. Resour Policy 36:149–158

57. Bartos PJ (2007) Is Mining a High-Tech Industry? Investigations into Innovation and Productivity Advance. Resour Policy 32:149–158

58. Al-Alawi SM, Tawo EE (1998) Application of artificial neural networks in mineral resource evaluation. J King Saud Univ Sci 10:127–138

59. Brown WM, Gedeon TD, Groves DI, Barnes RG (2000) Artificial neural networks: a new method for mineral prospectivity mapping. Aust J earth Sci 47:757–770

60. Brown WM, Groves DI, Gedeon TD (2003) An artificial neural network method for mineral prospectivity mapping: a comparison with fuzzy logic and Bayesian probability methods. Springer, Dordrecht

61. Rigol-Sanchez JP, Chica-Olmo M, Abarca-Hernandez F (2003) Artificial neural networks as a tool for mineral potential mapping with GIS. Int J Remote Sens 24:1151–1156

62. Nykänen V, Groves DI, Ojala VJ, et al (2008) Reconnaissance-scale conceptual fuzzy-logic prospectivity modelling for iron oxide copper–gold deposits in the northern Fennoscandian Shield, Finland. Aust J earth Sci 55:25–38

63. Bokhari AA, Hu GD, Al-Mokredi M, et al (2010) Fuzzy Logic Plateful Mineral Exploration and Development in Southwestern China. In: 2010 2nd International Conference on Information Engineering and Computer Science. IEEE, pp 1–4

64. Lee S, Oh HJ (2011) Application of Artificial Neural Network for Mineral Potential Mapping. IntechOpen

65. Setyadi H, Widodo LE, Notosiswoyo S, et al (2016) GIS modeling using fuzzy logic approach in mineral prospecting based on geophysical data. In: AIP Conference Proceedings. p 1711(1)

66. Kashani SBM, Abedi M, Norouzi GH (2016) Fuzzy logic mineral potential mapping for copper exploration using multi-disciplinary geo-datasets, a case study in seridune deposit, Iran. Earth Sci Informatics 9:167–181

67. Zhang N, Zhou K (2015) Mineral prospectivity mapping with weights of evidence and fuzzy logic methods. J Intell Fuzzy Syst 29:2639–2651

68. Tabaei M, Esfahani MM, Rasekh P, Esna-ashari A (2017) Mineral prospectivity mapping in GIS using fuzzy logic integration in Khondab area, western Markazi province, Iran. J Tethys 5:367–379

69. Karadogan A, Kahriman A, Ozer U (2008) Application of fuzzy set theory in the selection of underground mining method. J South African Inst Min Metall 108:73–79

70. Bascetin A, Oztas O, Kanli AI (2006) EQS: a computer software using fuzzy logic for equipment selection in mining engineering. Journal-South African Inst Min Metall 106:63

71. Aghajani Bazzazi ABBAS, Osanloo M, Karimi B (2011) A new fuzzy multi criteria decision making model for open pit mines equipment selection. Asia-Pacific J Oper Res 28:279–300

72. Hosseini SAA, Ataei M, Hosseini SM, Akhyani M (2012) Application of fuzzy logic for determining of coal mine mechanization. J Coal Sci Eng 18:225–230

73. Ozkan E, Iphar M, Konuk A (2019) Fuzzy logic approach in resource classification. Int J Mining, Reclam Environ 33:183–205

74. Bandopadhyay S, Chattopadhyay A (1986) Selection of Post-Mining Uses of Land Via Fuzzy Algorithm. In: 19th International Symposium on the Application of Computers in Mine Planning. pp 321– 332

75. Kommadath B, Sarkar R, Rath B (2012) A fuzzy logic based approach to assess sustainable development of the mining and minerals sector. Sustain Dev 20:386–399

76. Bangian AH, Ataei M, Sayadi A, Gholinejad A (2011) Fuzzy analytical hierarchy processing to define optimum post mining land use for pit area to clarify reclamation costs. Gospod Surowcami Miner 27:145–168

77. Anis M, Idrus A, Amijaya H, Subagyo S (2017) Fuzzy Logic Approach For Post-Mining Land Use Planning: A Case Study On Coal Mine Of Pt. Adaro Indonesia-South Kalimantan. Indones Min J 20:81–91

78. Ur Rehman A, Lyche T, Awuah-Offei K, Nadendla VSS (2020) Effect of text message alerts on miners evacuation decisions. Saf Sci 130:104875. https://doi.org/https://doi.org/10.1016/j.ssci.2020.104875

79. Iphar M, Cukurluoz AK (2018) Fuzzy risk assessment for mechanized underground coal mines in Turkey. Int J Occup Saf Ergon 1–18

80. Monjezi M, Singh TN, Khandelwal M, et al (2006) Prediction and analysis of blast parameters using artificial neural network. Noise Vib Worldw 37:8–16

81. Khandelwal M, Singh TN (2009) Prediction of blast-induced ground vibration using artificial neural network. Int J Rock Mech Min Sci 46:1214–1222

82. Khandelwal M, Kumar DL, Yellishetty M (2011) Application of soft computing to predict blast-induced ground vibration. Eng Comput 27:117–125

83. Zhongya Z, Xiaoguang J (2018) Prediction of peak velocity of blasting vibration based on artificial neural network optimized by dimensionality reduction of FA-MIV. Math Probl Eng 1–12

84. Bahrami A, Monjezi M, Goshtasbi K, Ghazvinian A (2011) Prediction of rock fragmentation due to blasting using artificial neural network. Eng Comput 27:177–181

85. Sayadi A, Monjezi M, Talebi N, Khandelwal M (2013) A comparative study on the application of various artificial neural networks to simultaneous prediction of rock fragmentation and backbreak. J Rock Mech Geotech Eng 5:318–324

86. Ebrahimi E, Monjezi M, Khalesi MR, Armaghani DJ (2016) Prediction and optimization of back-break and rock fragmentation using an artificial neural network and a bee colony algorithm. Bull Eng Geol Environ 75:27–36

87. Tiile RN (2018) Artificial neural network approach to predict blast-induced ground vibration, airblast and rock fragmentation vibration, airblast and rock fragmentation. Missouri University of Science & Technology

88. Ghasemi E, Ataei M, Hashemolhosseini H (2013) Development of a fuzzy model for predicting ground vibration caused by rock blasting in surface mining. J Vib Control 19:755–770

89. Monjezi M, Rezaei M, Varjani AY (2009) Prediction of rock fragmentation due to blasting in Gol-E-Gohar iron mine using fuzzy logic. Int J Rock Mech Min Sci 46:1273–1280

90. Monjezi M, Rezaei M, Yazdian A (2010) Prediction of backbreak in open-pit blasting using fuzzy set theory. Expert Syst Appl 37:2637–2643

91. Rezaei M, Monjezi M, Varjani AY (2011) Development of a fuzzy model to predict flyrock in surface mining. Saf Sci 49:298–305

92. Shams S, Monjezi M, Majd VJ, Armaghani DJ (2015) Application of fuzzy inference system for prediction of rock fragmentation induced by blasting. Arab J Geosci 8:10819–10832

93. Karri V (1999) RBF neural network for thrust and torque predictions in drilling operations. In: Proceedings Third International Conference on Computational Intelligence and Multimedia Applications. ICCIMA'99 (Cat. No. PR00300). IEEE, pp 55–59

94. Desai CK, Shaikh AA (2006) Drill wear monitoring using artificial neural network with differential evolution learning. In: 2006 IEEE International Conference on Industrial Technology. IEEE, pp 2019–2022

95. Torno S, Toraño J, Menéndez M, et al (2011) Mathematical and fuzzy logic models in prediction of geological and geomechanical properties of rock mass by excavation data on underground works. J Civ Eng Manag 17:197–206

96. Jang H, Topal E (2013) Optimizing overbreak prediction based on geological parameters comparing multiple regression analysis and artificial neural network. Tunn Undergr Sp Technol 38:161–169

97. Elkatatny S, Tariq Z, Mahmoud M (2016) Real time prediction of drilling fluid rheological properties using Artificial Neural Networks visible mathematical model (white box). J Pet Sci Eng 146:1202–1210

98. Lashari S e Z, Takbiri-Borujeni A, Fathi E, et al (2019) Drilling performance monitoring and optimization: a data-driven approach. J Pet Explor Prod Technol 9:2747–2756

99. Ali D, Frimpong S (2020) Artificial intelligence, machine learning and process automation: existing knowledge frontier and way forward for mining sector. Artif Intell Rev 1–18. https://doi.org/https://doi.org/10.1007/s10462-020-09841-6

100. Ali D, Frimpong S (2018) Artificial intelligence models for predicting the performance of hydro-pneumatic suspension struts in large capacity dump trucks. Int J Ind Ergon 67:283–295. https://doi.org/10.1016/j.ergon.2018.06.005

101. Rao SS (1995) Mechanical Vibrations, Third. Addison - Wesley Publishing Company, World Student Series

102. Cundall P, Strack O (1979) A discrete Element Method for granular assemblies. geotechnique 29:47–65

103. SIMULIA (2017) Discrete Element Method. ABAQUS Docs.

104. Itasca (2016) PFC 5.0 Documentation

105. Ali D, Frimpong S, Mayton AG (2020) Intelligent Tracking of Impulse Force for Surface Mine Haul Trucks During High Impact Shovel Loading Operations. In: ASME 2020 International Design Engineering Technical Conferences and Computers and Information in Engineering Conference

106. Abaqus Analysis User's Guide Session 15.1

107. Kisabo AB, Uchenna NC, Adebimpe FA Newton's method for solving non-linear system of algebraic equations (NLSAEs) with MATLAB/Simulink® and MAPLE®. Am J Math Comput Model 2:117–131

108. Kovács Z (2011) Understanding convergence and stability of the Newton-Raphson method

109. Lakshmanan S (2019) How, When, and Why Should You Normalize / Standardize / Rescale Your Data?

110. Brownlee J (2017) How to One Hot Encode Sequence Data in Python. In: Long Short-Term Mem. Networks. https://machinelearningmastery.com/how-to-one-hot-encode-sequence-data-in-python/. Accessed 10 Sep 2020

111. Dobbin, K.K., Simon RM (2011) Optimally splitting cases for training and testing high dimensional classifiers. BMC Med Genomics 4:31

112. LeCun Y, Bengio Y, Hinton G (2015) Deep Learning. Nature 521:436–444

113. Nassif AB, Shahin I, Attili I, et al (2019) Speech recognition using deep neural networks: A systematic review. In: IEEE Access, 7. pp 19143–19165

114. Szegedy C, Liu W, Jia Y, et al (2015) Going deeper with convolutions. In: Proceedings of the IEEE conference on computer vision and pattern recognition. pp 1–9

115. Zhang X, Zou J, He K, Sun J (2015) Accelerating very deep convolutional networks for classification and detection. IEEE Trans Pattern Anal Mach Intell 38:1943–1955

116. Shin HC, Roth HR, Gao M, et al (2016) Deep convolutional neural networks for computer-aided detection: CNN architectures, dataset characteristics and transfer learning. IEEE Trans Med Imaging 35:1285–1298

117. Ting DSW, Yi PH, Hui F (2018) Clinical applicability of deep learning system in detecting tuberculosis with chest radiography. Radiology 286:729–31

118. Bejnordi E., Veta M, van Diest P. (2017) Diagnostic assessment of deep learning algorithms for detection of lymph node metastases in women with breast cancer. JAMA 318:2199–210

119. Lee CS, Tyring AJ, Deruyter NP, et al (2017) Deep-learning based, automated segmentation of macular edema in optical coherence tomography. Biomed Opt Express 8:3440–3448

120. Poplin R, Varadarajan A V., Blumer K, et al (2018) Prediction of cardiovascular risk factors from retinal fundus photographs via deep learning. Nat Biomed Eng 2:158

121. Gulshan V, Peng L, Coram M, et al (2016) Development and validation of a deep learning algorithm for detection of diabetic retinopathy in retinal fundus photographs. JAMA 316:2402–2410

122. Kalchbrenner N, Grefenstette E, Blunsom P (2014) A convolutional neural network for modelling sentences. arXiv Prepr arXiv14042188

123. Kim Y (2014) Convolutional neural networks for sentence classification. arXiv Prepr arXiv14085882

124. Palaz D, Collobert R (2015) Analysis of cnn-based speech recognition system using raw speech as input. Idiap

125. Tu Z, Hu B, Lu Z, Li H (2015) Context-dependent translation selection using convolutional neural network. arXiv Prepr arXiv150302357

126. Hinton G, Deng L, Yu D, et al (2012) Deep neural networks for acoustic modeling in speech recognition. IEEE Signal Process Mag 29:

127. Liu Z, Yan S, Luo P, et al (2016) Fashion landmark detection in the wild. In: European Conference on Computer Vision. Springer, Cham, pp 229–245

128. Belagiannis V, Rupprecht C, Carneiro G, Navab N (2015) Robust optimization for deep regression. In: IEEE international conference on computer vision. pp 2830–2838

129. Lathuilière S, Juge R, Mesejo P, et al (2017) Deep mixture of linear inverse regressions applied to head-pose estimation. In: IEEE Conference on Computer Vision and Pattern Recognition. pp 4817–4825

130. Sun Y, Wang X, Tang X (2013) Deep convolutional network cascade for facial point detection. In: IEEE conference on computer vision and pattern recognition. pp 3476–3483

131. Bulat A, Tzimiropoulos G (2017) How far are we from solving the 2d & 3d face alignment problem?(and a dataset of 230,000 3d facial landmarks). In: IEEE International Conference on Computer Vision. pp 1021–1030

132. Abdel-Hamid O, Mohamed AR, Jiang H, Penn G (2012) Applying convolutional neural networks concepts to hybrid NN-HMM model for speech recognition. In: 2012 IEEE international conference on Acoustics, speech and signal processing (ICASSP). IEEE, pp 4277–4280

133. Wang S-C (2003) Artificial neural network. Springer US, Boston, MA

134. Sheela KG, Deepa SN (2013) Review on Methods to Fix Number of Hidden Neurons in Neural Networks. Math Probl Eng 2013:1–11. https://doi.org/10.1155/2013/425740

135. Ali D, Hayat MB, Alagha L, Molatlhegi O (2018) An evaluation of machine learning and artificial intelligence models for predicting the flotation behavior of fine high-ash coal. Adv Powder Technol 29:3493–3506

136. Breiman L (2001) Random Forests. Mach Learn 45:5–32. https://doi.org/10.1023/A:1010933404324

137. Kuhn M, Johnson K (2013) Regression Trees and Rule-Based Models. In: Applied Predictive Modeling. Springer, New York, NY

138. Breiman L, Friedman J, Stone C, Olshen R (1984) Classification and regression trees

139. Strobl C, Malley J, Tutz G (2009) An introduction to recursive partitioning: rationale, application, and characteristics of classification and regression trees, bagging, and random forests. Psychol Methods 14:323

140. Vapnik VN, Vapnik V (1998) Statistical learning theory. Wiley, New York, N.Y., USA

141. Syaliman KU, Nababan EB, Sitompul OS (2018) Improving the accuracy of k-nearest neighbor using local mean based and distance weight. In: Journal of Physics: Conference Series (Vol. 978, No. 1, p. 012047). IOP Publishing

142. Bhatia N (2010) Survey of nearest neighbor techniques. arXiv Prepr arXiv10070085

143. Deekshatulu BL, Chandra P (2013) Classification of heart disease using k-nearest neighbor and genetic algorithm. Procedia Technol 10:85–94

144. Sánchez AS, Iglesias-Rodríguez FJ, Fernández PR, de Cos Juez FJ (2016) Applying the K-nearest neighbor technique to the classification of workers according to their risk of suffering musculoskeletal disorders. Int J Ind Ergon 52:92–99

145. Pan Z, Wang Y, Ku W (2017) A new general nearest neighbor classification based on the mutual neighborhood information. Knowledge-Based Syst 121:142–152

146. García-Pedrajas N, Ortiz-Boyer D (2009) Boosting k-nearest neighbor classifier by means of input space projection. Expert Syst Appl 36:10570–10582

147. Wang J, Neskovic P, Cooper LN (2007) Improving nearest neighbor rule with a simple adaptive distance measure. Pattern Recognit Lett 28:207–213

148. Ougiaroglou S, Evangelidis G (2012) Fast and accurate k-nearest neighbor classification using prototype selection by clustering. In: 2012 16th Panhellenic Conference on Informatics. IEEE, pp 168–173

149. Yunsheng S, Jiye L, Jing L, Xingwang Z (2017) An efficient instance selection algorithm for k nearest neighbor regression. Neurocomputing 251:26–34

150. Kramer O (2011) Dimensionality reduction by unsupervised k-nearest neighbor regression. In: 2011 10th International Conference on Machine Learning and Applications and Workshops (Vol. 1). IEEE, pp 275–278

151. Haara A, Kangas A (2012) Comparing k nearest neighbours methods and linear regression–is there reason to select one over the other? Math Comput For Nat Sci 4:50–65

152. Greche L, Jazouli M, Es-Sbai N, et al (2017) Comparison between Euclidean and Manhattan distance measure for facial expressions classification. In: 2017 International Conference on Wireless Technologies, Embedded and Intelligent Systems (WITS). IEEE, pp 1–4

153. Kingma DP, Ba J (2014) Adam: A method for stochastic optimization. arXiv Prepr arXiv14126980

154. Srivastava N, Hinton G, Krizhevsky A, et al (2014) Dropout: a simple way to prevent neural networks from overfitting. J Mach Learn Res 15:1929–1958

155. Belayneh A, Adamowski J, Khalil B, Ozga-Zielinski B (2014) Long-term SPI drought forecasting in the Awash River Basin in Ethiopia using wavelet neural network and wavelet support vector regression models. J Hydrol 508:418–429. https://doi.org/10.1016/j.jhydrol.2013.10.052

156. Oshiro TM, Perez PS, Baranauskas JA (2012) How many trees in a random forest? P. Perner (Ed.), Machine Learning and Data Mining in Pattern Recognition, Lecture Notes in Computer Science

157. Rajasekaran S, Gayathri S, Lee TL (2008) Support vector regression methodology for storm surge predictions. Ocean Eng 35:1578–1587

158. Yang H, Huang K, King I, Lyu MR (2009) Localized support vector regression for time series prediction. Neurocomputing 72:2659–2669

159. Wu KP, Wang SD (2009) Choosing the kernel parameters for support vector machines by the inter-cluster distance in the feature space. Pattern Recognit 42:710–717

160. Aouad N (2008) Mechanics of dump truck vibrations in high-impact shovel loading. Missouri University of Science & Technology

VITA

Danish Ali was born on March 7, 1991. He obtained his Bachelor of Science (BS) in Mining Engineering from University of Engineering and Technology (UET), Lahore, Pakistan from 2010 to 2014. He received all three gold medals for his excellent academic performance during his undergrad. He worked as a Graduate Trainee Engineer (GTE) in an open pit surface coal mine for three months for Engro Corp., after finishing his bachelor's degree. He obtained his Master of Science (MS) in Mining Engineering from Missouri University of Science & Technology (S&T) in Rolla, MO, formerly known as University of Missouri Rolla (UMR) from 2014 to 2016.

In Fall 2017, he joined the doctoral program in Mining Engineering at Missouri University of Science & Technology under the mentorship of Dr. Samuel Frimpong, Professor, Robert H. Quenon Chair, and the Director of the Heavy Mining Machinery Research Group at Missouri S&T. He worked as a Research Assistant on autonomous truck operations using artificial intelligence along with impact force reduction technology as part of the Heavy Mining Machinery Research Group. In 2017 and 2018, he won the 3rd place and the best poster award in graduate poster competitions for Mining Division and the Mineral Processing Division, respectively, at SME. In 2019, he won the Outstanding Researcher award and the Dean's PhD Outstanding Scholar award at Missouri S&T. He has worked as an Engineering Material Testing Intern at ECS Mid-Atlantic in Frederick, MD from May to August in 2020 and 2019. During his Ph.D., he served as the Teaching Assistant for various undergraduate and graduate level courses. He also served as the President, Vice President, and ISC representative for S&T Cricket Club, Council of Graduate Students (CGS), and the Student Council, respectively. He received his Ph.D. in Mining Engineering from the Missouri University of Science and Technology in May, 2021.